

NORSAR Scientific Report No. 2-97/98

Semiannual Technical Summary

1 October 1997 – 31 Mars 1998

Kjeller, May 1998

APPROVED FOR PUBLIC RELEASE, DISTRIBUTION UNLIMITED

REPORT DOCUMENTATION PAGE

1a. REPORT SECURITY CLASSIFICATION Unclassified			1b. RESTRICTIVE MARKINGS Not applicable			
2a. SECURITY CLASSIFICATION AUTHORITY Not Applicable			3. DISTRIBUTION / AVAILABILITY OF REPORT Approved for public release; distribution unlimited			
2b. DECLASSIFICATION / DOWNGRADING SCHEDULE						
4. PERFORMING ORGANIZATION REPORT NUMBER(S) Scientific Rep.2-97/98			5. MONITORING ORGANIZATION REPORT NUMBER(S) Scientific Rep. 2-97/98			
6a. NAME OF PERFORMING ORGANIZATION NFR/NORSAR		6b. OFFICE SYMBOL (if applicable)	7a. NAME OF MONITORING ORGANIZATION HQ/AFTAC/TTS			
6c. ADDRESS (City, State, and ZIP Code) Post Box 51 N-2007 Kjeller, Norway			7b. ADDRESS (City, State, and ZIP Code) Patrick AFB, FL 32925-6001			
8a. NAME OF FUNDING / SPONSORING ORGANIZATION Advanced Research Projects Agency/NTPO		8b. OFFICE SYMBOL (if applicable) NMRO/NTPO	9. PROCUREMENT INSTRUMENT IDENTIFICATION NUMBER Contract No. F08650-96-C-0001			
8c. ADDRESS (City, State, and ZIP Code) 1901 N. Moore St., Suite 609 Arlington, VA 22209			10. SOURCE OF FUNDING NUMBERS			
			PROGRAM ELEMENT NO. R&D	PROJECT NO. NORSAR Phase 3	TASK NO. SOW Task 5.0	WORK UNIT ACCESSION NO. Sequence No. 004A2
11. TITLE (Include Security Classification) Semiannual Technical Summary, 1 October 1997 - 31 March 1998						
12. PERSONAL AUTHOR(S)						
13a. TYPE OF REPORT Scientific Summary		13b. TIME COVERED FROM 1 OCT97 TO 31 MAR 98		14. DATE OF REPORT (Year, Month, Day) 1998 May	15. PAGE COUNT 147	
16. SUPPLEMENTARY NOTATION						
17. COSATI CODES			18. SUBJECT TERMS (Continue on reverse if necessary and identify by block number) NORSAR, Norwegian Seismic Array			
FIELD	GROUP	SUB-GROUP				
8	11					
19. ABSTRACT (Continue on reverse if necessary and identify by block number) This Semiannual Technical Summary describes the operation, maintenance and research activities at the Norwegian Seismic Array (NORSAR), the Norwegian Regional Seismic Array (NORESS), the Arctic Regional Seismic Array (ARCESS) and the Spitsbergen Regional Array for the period 1 October 1997 - 31 March 1998. Statistics are also presented for additional seismic stations, which through cooperative agreements with institutions in the host countries provide continuous data to the NORSAR Data processing Center (NDPC). These stations comprise the Finnish Regional Seismic Array (FINESS), the German Regional Seismic Array (GERESS), the Hagfors array in Sweden and the regional seismic array in Apatity, Russia. (cont.)						
20. DISTRIBUTION / AVAILABILITY OF ABSTRACT <input type="checkbox"/> UNCLASSIFIED/UNLIMITED <input type="checkbox"/> SAME AS RPT. <input type="checkbox"/> DTIC USERS			21. ABSTRACT SECURITY CLASSIFICATION			
22a. NAME OF RESPONSIBLE INDIVIDUAL Mr. Michael C. Baker			22b. TELEPHONE (Include Area Code) (407) 494-4219		22c. OFFICE SYMBOL AFTAC/TTS	

Abstract (cont.)

The NORSAR Detection Processing system has been operated throughout the period with an average uptime of 99.77%. A total of 2196 seismic events have been reported in the NORSAR monthly seismic bulletin for October 1997 through March 1998. The performance of the continuous alarm system and the automatic bulletin transfer to AFTAC has been satisfactory. Processing of requests for full NORSAR and regional array data on magnetic tapes has progressed according to established schedules.

This Semiannual Report also presents statistics from operation of the Regional Monitoring System (RMS). The RMS has been operated in a limited capacity, with continuous automatic detection and location and with analyst review of selected events of interest for GSETT-3. Data sources for the RMS have comprised all the regional arrays processed at NORSAR. The Generalized Beamforming (GBF) program is now used as a pre-processor to RMS.

On-line detection processing and data recording at the NORSAR Data Processing Center (NDPC) of NORESS, ARCESS, FINESS and GERESS data have been conducted throughout the period. Data from two small-aperture arrays at sites in Spitsbergen and Apatity, Kola Peninsula, as well as the Hagfors array in Sweden, have also been recorded and processed. Processing statistics for the arrays as well as results of the RMS analysis for the reporting period are given.

The operation of the regional arrays has proceeded normally in the period, except for an extended outage of the NORESS array from 14 January to 5 February 1998 (power surge), and an extended outage of the Spitsbergen array from 15-31 December 1997 (failure of power supply).

Maintenance activities in the period comprise preventive/corrective maintenance in connection with all the NORSAR subarrays, NORESS and ARCESS. Other activities have involved repair of defective electronic equipment, cable splicing and work in connection with the small-aperture array in Spitsbergen.

Summaries of seven scientific and technical contributions are presented in Chapter 7 of this report.

Section 7.1 is entitled "Seismic Threshold Monitoring for Continuous Assessment of Global Detection Capability". We give examples of two main types of applications based on data from a world-wide seismic network: a) an estimated continuous *global threshold level* and b) an estimated continuous *global detection capability*. The first application provides a continuous view of the global seismic "background field" as calculated from the station data, with the purpose to assess the upper magnitude limit of any seismic event that might have occurred around the globe. The second application introduces detection thresholds for each station and provide a simplified estimate, continuously in time, of the n-station detection capability of the network. The latter approach naturally produces higher threshold values, with the difference typically being 0.5-1 magnitude unit. We show that both these approaches are useful especially during large earthquakes, where conventional capability maps based on statistical noise and signal models cannot be applied.

In order to illustrate the usefulness of combining the global monitoring with site-specific monitoring for areas of special interest, we consider a large earthquake aftershock sequence in

Kamchatka and its effect on the threshold trace in a very different region (the Novaya Zemlya nuclear test site). We demonstrate that the effects of the aftershock signals on the thresholds calculated for Novaya Zemlya are modest, partly due to the emphasis on high-frequency signals. This indicates that threshold monitoring could provide significantly improved event detection during aftershock sequences compared to conventional methods, for which the large number of detected phases tends to cause problems in the phase association process.

Section 7.2 gives a summary report of the pipeline processing part in the Operations Manual for the global Threshold Monitoring (TM) system at the Provisional International Data Center (PIDC). This processing comprises:

- Continuous calculation of short-term-averages (STAs) for all primary stations using the detection and feature extraction program (*DPX*) running in the Alpha processing pipeline.
- Continuous calculation of the three-station detection capability of the network for a set of 2562 globally distributed target areas, using the STAs calculated by *DFX*.
- Interpolation and reformatting of the three-station detection capability to facilitate map displays of the results.

Three types of products (plots) are available from the TM system. These products are designed to provide useful information to the international community on the performance and status of the primary seismic network used for CTBT monitoring. The paper describes the directory structure of the TM software and the major software modules. New utility software to assist in the Threshold Monitoring developments is documented.

Section 7.3 describes the development of a regional database for seismic event screening. These efforts involve creating a database of regional seismic recordings to be used in a subsequent research effort to study the seismic event screening problem (see the Protocol to the Comprehensive Nuclear Test-Ban Treaty for the concept of event screening). This contribution gives an account of the event and station selection criteria, the approach taken to arrive at a list of events, and the current status of the effort of compiling this database. As of the date of this report, data have been copied from the archive for about 80 of the 103 events selected for the database. The copying effort started with the oldest data, and what remains are events from the period 1993-1997.

Section 7.4 is entitled "Monitoring seismic events in the Barents/Kara Sea region". This paper, which is a joint effort between Kola Regional Seismological Centre and NORSAR, describes briefly the KRSC seismic network and the approaches to data processing and event location implemented at the KRSC data center. The paper presents accurate regionally based location estimates of past nuclear explosions, including the small ($m_b=3.8$) explosion on 26 August 1984. The paper also describes some other interesting seismic events occurring in the region in recent years. A method for site-specific monitoring is presented and applied to processing of Amderma station data.

Case studies, some of which are discussed briefly in this paper, have demonstrated that traditional regional discriminants are not effective for separating between seismic source types at low event magnitudes in this region. In particular, the authors conclude that the S/P ratio, even at high frequencies, is rather unstable and should not be relied upon for regional event discrimination.

With regard to the two Kara sea events on 16 August 1997, the authors of this paper disagree with those scientists who have claimed that these events can be positively identified as earthquakes on the basis of seismological evidence. On the other hand, neither is there any seismological evidence to confidently classify these events as explosions. In the opinion of these authors, the source type of these two events remains unresolved.

Section 7.5 is a study of the Indian nuclear explosions on 11 and 13 May 1998. The paper discusses the results from detection and location processing, with emphasis on the northern European arrays and the station NIL in Nilore, Pakistan. It is noted that the communications link from station NIL, which has been established and operated by NORSAR through a VSAT connection via Norway, operated very well, and enabled data from this key station to be provided immediately upon request by the IDC.

The paper notes that the stations in Scandinavia, in particular ARCES and SPITS, detected the first explosion with very high SNR. The second set of explosions (on 13 May), were not detectable. The NORSAR array recordings for the 11 May main event were compared to similar recordings of the 1974 PNE in India, and the waveforms show a remarkable similarity. The size of the two explosions in 1974 and 1998 is also very close, as measured at NORSAR.

Section 7.6 is entitled "Accurate location of seismic events in northern Norway using a local network, and implications for regional calibration of IMS stations". A seismic network was installed in the Ranafjord area in June 1997 as part of the NEONOR (Neotectonics in Norway) project which is a multidisciplinary research project undertaken in cooperation with several other Norwegian institutions. The purpose of the network was to monitor seismic activity along the potential neotectonic Båsmoen fault. Of the total 260 seismic events located in the first nine months of operation, 180 are probable earthquakes located within the network. The magnitudes of the local events range from M_L 0.1 to 2.8, with depths mainly in the 4-12 km. range. Eight of the events within the network were also located by the NORSAR GBF system, and these locations as well as NORSAR analyst reviewed locations have been compared to the local solutions. The analyst locations are all within 25 km of the true location, which is an excellent result taking into account the low magnitudes (mostly M_L 2.0-2.5) and the large distances to the stations (at least 500 km).

Section 7.7 summarizes the activities related to the GSETT-3 experiment and experience gained at the Norwegian NDC during the period 1 October 1997 - 31 March 1998. Norway has been contributing primary station data from three arrays: ARCESS, NORESS and NORSAR and one auxiliary array (Spitsbergen). Norway's NDC is also acting as a regional data center, forwarding data to the IDC from GSETT-3 primary and auxiliary stations in several countries. The work at the Norwegian NDC has continued to focus on operational aspects, like stable forwarding of data using the Alpha protocol, proper handling of outgoing and incoming messages, improvement to routines for dealing with failure of critical components, as well as implementation of other measures to ensure maximum reliability and robustness in providing data to the IDC. NOR_NDC will continue the efforts towards improvements and hardening of all critical data acquisition and data forwarding hardware and software components, so as to meet future requirements related to operation of IMS stations to the maximum extent possible.

The PrepCom has tasked its Working Group B with overseeing, coordinating and evaluating the GSETT-3 experiment until the end of 1998. The PrepCom has also encouraged states that operate IMS-designated stations to continue to do so on a voluntary basis and in the framework

of the GSETT-experiment until such time that the stations have been certified for formal inclusion in IMS. In line with this, and provided that adequate funding is obtained, we envisage continuing the provision of data from Norwegian IMS-designated stations without interruption to the PIDC, and later on, following certification, to the IDC in Vienna, via the new global communications infrastructure currently being elaborated by the PrepCom.

Frode Ringdal

AFTAC Project Authorization : T/6141/NORSAR
ARPA Order No. : 4138 AMD # 53
Program Code No. : 0F10
Name of Contractor : The Norwegian Research Council (NFR)
Effective Date of Contract : 1 Oct 1995
Contract Expiration Date : 30 Sep 1998
Project Manager : Frode Ringdal +47 63 80 59 00
Title of Work : The Norwegian Seismic Array
(NORSAR) Phase 3
Amount of Contract : \$ 2,958,528
Contract Period Covered by Report : 1 October 1997 - 31 March 1998

The views and conclusions contained in this document are those of the authors and should not be interpreted as necessarily representing the official policies, either expressed or implied, of the Advanced Research Projects Agency, the Air Force Technical Applications Center or the U.S. Government.

This research was supported by the Advanced Research Projects Agency of the Department of Defense and was monitored by AFTAC, Patrick AFB, FL32925, under contract no. F08650-96-C-0001.

NORSAR Contribution No. 638

Table of Contents

1	Summary.....	1
2	NORSAR Operation.....	5
2.1	Detection Processor (DP) operation.....	5
2.2	Array Communications.....	9
2.3	NORSAR Event Detection operation.....	16
3	Operation of Regional Arrays.....	21
3.1	Recording of NORESS data at NDPC, Kjeller.....	21
3.2	Recording of ARCESS data at NDPC, Kjeller.....	24
3.3	Recording of FINESS data at NDPC, Kjeller.....	27
3.4	Recording of Spitsbergen data at NDPC, Kjeller.....	30
3.5	Event detection operation.....	33
3.6	Regional Monitoring System operation.....	64
4	Improvements and Modifications.....	66
4.1	NORSAR.....	66
5	Maintenance Activities.....	67
6	Documentation Developed.....	71
7	Summary of Technical Reports / Papers Published.....	72
7.1	Seismic Threshold Monitoring for continuous assessment of global detection capability.....	72
7.2	Threshold Monitoring: Summary of pipeline processing.....	92
7.3	Development of a regional database for seismic event screening.....	102
7.4	Monitoring seismic events in the Barents/Kara Sea region.....	106
7.5	The Indian nuclear explosions of 11 and 13 May 1998.....	121
7.6	Accurate location of seismic events in northern Norway using a local network, and implications for regional calibration of IMS stations.....	131
7.7	Status Report: Norway's participation in GSETT-3.....	140



1 Summary

This Semiannual Technical Summary describes the operation, maintenance and research activities at the Norwegian Seismic Array (NORSAR), the Norwegian Regional Seismic Array (NORESS), the Arctic Regional Seismic Array (ARCESS) and the Spitsbergen Regional Array for the period 1 October 1997 - 31 March 1998. Statistics are also presented for additional seismic stations, which through cooperative agreements with institutions in the host countries provide continuous data to the NORSAR Data Processing Center (NPDC). These stations comprise the Finnish Regional Seismic Array (FINESS), the German Regional Seismic Array (GERESS), the Hagfors array in Sweden and the regional seismic array in Apatity, Russia.

The NORSAR Detection Processing system has been operated throughout the period with an average uptime of 99.77%. A total of 2196 seismic events have been reported in the NORSAR monthly seismic bulletin for October 1997 through March 1998. The performance of the continuous alarm system and the automatic bulletin transfer to AFTAC has been satisfactory. Processing of requests for full NORSAR and regional array data on magnetic tapes has progressed according to established schedules.

This Semiannual Report also presents statistics from operation of the Regional Monitoring System (RMS). The RMS has been operated in a limited capacity, with continuous automatic detection and location and with analyst review of selected events of interest for GSETT-3. Data sources for the RMS have comprised all the regional arrays processed at NORSAR. The Generalized Beamforming (GBF) program is now used as a pre-processor to RMS.

On-line detection processing and data recording at the NORSAR Data Processing Center (NDPC) of NORESS, ARCESS, FINESS and GERESS data have been conducted throughout the period. Data from two small-aperture arrays at sites in Spitsbergen and Apatity, Kola Peninsula, as well as the Hagfors array in Sweden, have also been recorded and processed. Processing statistics for the arrays as well as results of the RMS analysis for the reporting period are given.

The operation of the regional arrays has proceeded normally in the period, except for an extended outage of the NORESS array from 14 January to 5 February 1998 (power surge), and an extended outage of the Spitsbergen array from 15-31 December 1997 (failure of power supply).

Maintenance activities in the period comprise preventive/corrective maintenance in connection with all the NORSAR subarrays, NORESS and ARCESS. Other activities have involved repair of defective electronic equipment, cable splicing and work in connection with the small-aperture array in Spitsbergen.

Summaries of seven scientific and technical contributions are presented in Chapter 7 of this report.

Section 7.1 is entitled "Seismic Threshold Monitoring for Continuous Assessment of Global Detection Capability". We give examples of two main types of applications based on data from a world-wide seismic network: a) an estimated continuous *global threshold level* and b) an estimated continuous *global detection capability*. The first application provides a continuous view of the global seismic "background field" as calculated from the station data, with the purpose to assess the upper magnitude limit of any seismic event that might have occurred around the globe. The second application introduces detection thresholds for each station and provide a

simplified estimate, continuously in time, of the n-station detection capability of the network. The latter approach naturally produces higher threshold values, with the difference typically being 0.5-1 magnitude unit. We show that both these approaches are useful especially during large earthquakes, where conventional capability maps based on statistical noise and signal models cannot be applied.

In order to illustrate the usefulness of combining the global monitoring with site-specific monitoring for areas of special interest, we consider a large earthquake aftershock sequence in Kamchatka and its effect on the threshold trace in a very different region (the Novaya Zemlya nuclear test site). We demonstrate that the effects of the aftershock signals on the thresholds calculated for Novaya Zemlya are modest, partly due to the emphasis on high-frequency signals. This indicates that threshold monitoring could provide significantly improved event detection during aftershock sequences compared to conventional methods, for which the large number of detected phases tends to cause problems in the phase association process.

Section 7.2 gives a summary report of the pipeline processing part in the Operations Manual for the global Threshold Monitoring (TM) system at the Provisional International Data Center (PIDC). This processing comprises:

- Continuous calculation of short-term-averages (STAs) for all primary stations using the detection and feature extraction program (*DPX*) running in the Alpha processing pipeline.
- Continuous calculation of the three-station detection capability of the network for a set of 2562 globally distributed target areas, using the STAs calculated by *DFX*.
- Interpolation and reformatting of the three-station detection capability to facilitate map displays of the results.

Three types of products (plots) are available from the TM system. These products are designed to provide useful information to the international community on the performance and status of the primary seismic network used for CTBT monitoring. The paper describes the directory structure of the TM software and the major software modules. New utility software to assist in the Threshold Monitoring developments is documented.

Section 7.3 describes the development of a regional database for seismic event screening. These efforts involve creating a database of regional seismic recordings to be used in a subsequent research effort to study the seismic event screening problem (see the Protocol to the Comprehensive Nuclear Test-Ban Treaty for the concept of event screening). This contribution gives an account of the event and station selection criteria, the approach taken to arrive at a list of events, and the current status of the effort of compiling this database. As of the date of this report, data have been copied from the archive for about 80 of the 103 events selected for the database. The copying effort started with the oldest data, and what remains are events from the period 1993-1997.

Section 7.4 is entitled "Monitoring seismic events in the Barents/Kara Sea region". This paper, which is a joint effort between Kola Regional Seismological Centre and NORSAR, describes briefly the KRSC seismic network and the approaches to data processing and event location implemented at the KRSC data center. The paper presents accurate regionally based location estimates of past nuclear explosions, including the small ($m_b=3.8$) explosion on 26 August 1984. The paper also describes some other interesting seismic events occurring in the region in recent years.

A method for site-specific monitoring is presented and applied to processing of Amderma station data.

Case studies, some of which are discussed briefly in this paper, have demonstrated that traditional regional discriminants are not effective for separating between seismic source types at low event magnitudes in this region. In particular, the authors conclude that the S/P ratio, even at high frequencies, is rather unstable and should not be relied upon for regional event discrimination.

With regard to the two Kara sea events on 16 August 1997, the authors of this paper disagree with those scientists who have claimed that these events can be positively identified as earthquakes on the basis of seismological evidence. On the other hand, neither is there any seismological evidence to confidently classify these events as explosions. In the opinion of these authors, the source type of these two events remains unresolved.

Section 7.5 is a study of the Indian nuclear explosions on 11 and 13 May 1998. The paper discusses the results from detection and location processing, with emphasis on the northern European arrays and the station NIL in Nilore, Pakistan. It is noted that the communications link from station NIL, which has been established and operated by NORSAR through a VSAT connection via Norway, operated very well, and enabled data from this key station to be provided immediately upon request by the IDC.

The paper notes that the stations in Scandinavia, in particular ARCES and SPITS, detected the first explosion with very high SNR. The second set of explosions (on 13 May), were not detectable. The NORSAR array recordings for the 11 May main event were compared to similar recordings of the 1974 PNE in India, and the waveforms show a remarkable similarity. The size of the two explosions in 1974 and 1998 is also very close, as measured at NORSAR.

Section 7.6 is entitled "Accurate location of seismic events in northern Norway using a local network, and implications for regional calibration of IMS stations". A seismic network was installed in the Ranafjord area in June 1997 as part of the NEONOR (Neotectonics in Norway) project which is a multidisciplinary research project undertaken in cooperation with several other Norwegian institutions. The purpose of the network was to monitor seismic activity along the potential neotectonic Båsmoen fault. Of the total 260 seismic events located in the first nine months of operation, 180 are probable earthquakes located within the network. The magnitudes of the local events range from M_L 0.1 to 2.8, with depths mainly in the 4-12 km. range. Eight of the events within the network were also located by the NORSAR GBF system, and these locations as well as NORSARs analyst reviewed locations have been compared to the local solutions. The analyst locations are all within 25 km of the true location, which is an excellent result taking into account the low magnitudes (mostly M_L 2.0-2.5) and the large distances to the stations (at least 500 km).

Section 7.7 summarizes the activities related to the GSETT-3 experiment and experience gained at the Norwegian NDC during the period 1 October 1997 - 31 March 1998. Norway has been contributing primary station data from three arrays: ARCESS, NORESS and NORSAR and one auxiliary array (Spitsbergen). Norway's NDC is also acting as a regional data center, forwarding data to the IDC from GSETT-3 primary and auxiliary stations in several countries. The work at the Norwegian NDC has continued to focus on operational aspects, like stable forwarding of data using the Alpha protocol, proper handling of outgoing and incoming messages, improvement to routines for dealing with failure of critical components, as well as implementation of

other measures to ensure maximum reliability and robustness in providing data to the IDC. NOR_NDC will continue the efforts towards improvements and hardening of all critical data acquisition and data forwarding hardware and software components, so as to meet future requirements related to operation of IMS stations to the maximum extent possible.

The PrepCom has tasked its Working Group B with overseeing, coordinating and evaluating the GSETT-3 experiment until the end of 1998. The PrepCom has also encouraged states that operate IMS-designated stations to continue to do so on a voluntary basis and in the framework of the GSETT-experiment until such time that the stations have been certified for formal inclusion in IMS. In line with this, and provided that adequate funding is obtained, we envisage continuing the provision of data from Norwegian IMS-designated stations without interruption to the PIDC, and later on, following certification, to the IDC in Vienna, via the new global communications infrastructure currently being elaborated by the PrepCom.

Frode Ringdal

2 NORSAR Operation

2.1 Detection Processor (DP) operation

There was 1 break in the otherwise continuous operation of the NORSAR online system within the current 6-month reporting interval. The uptime percentage for the period is 99.77 as compared to 99.99 for the previous period.

Fig. 2.1.1 and the accompanying Table 2.1.1 both show the daily DP downtime for the days between 1 October 1997 and 31 March 1998. The monthly recording times and percentages are given in Table 2.1.2.

The breaks can be grouped as follows:

a)	Hardware failure	0
b)	Stops related to program work or error	0
c)	Hardware maintenance stops	0
d)	Power jumps and breaks	1
e)	TOD error correction	0
f)	Communication lines	0

The total downtime for the period was 10 hours and 16 minutes. The mean-time-between-failures (MTBF) was 93 days.

J. Torstveit

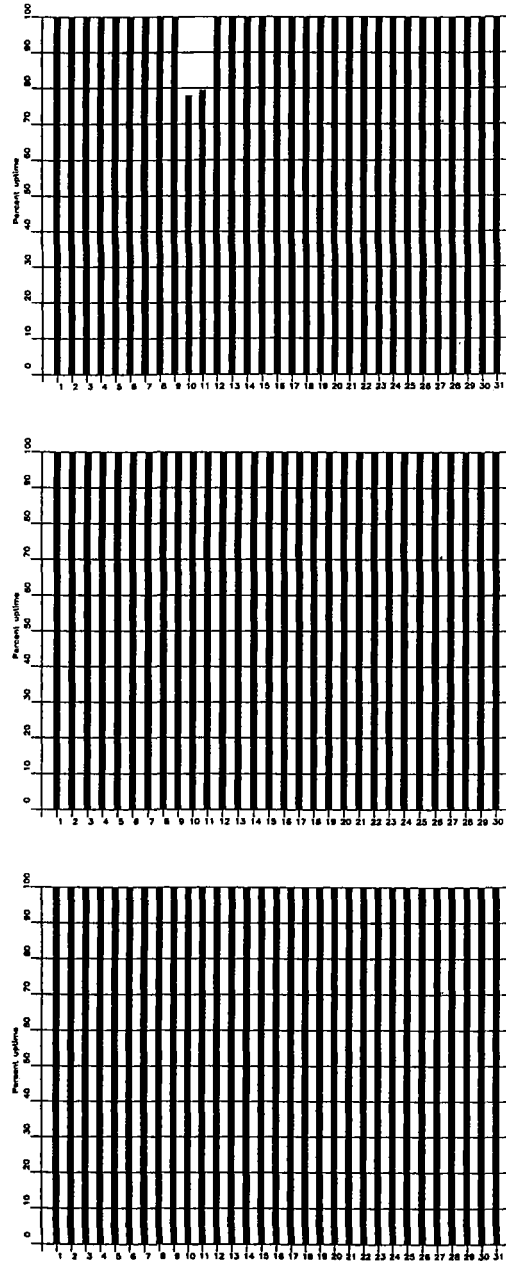


Fig. 2.1.1. Detection Processor uptime for October (top), November (middle) and December (bottom) 1997.

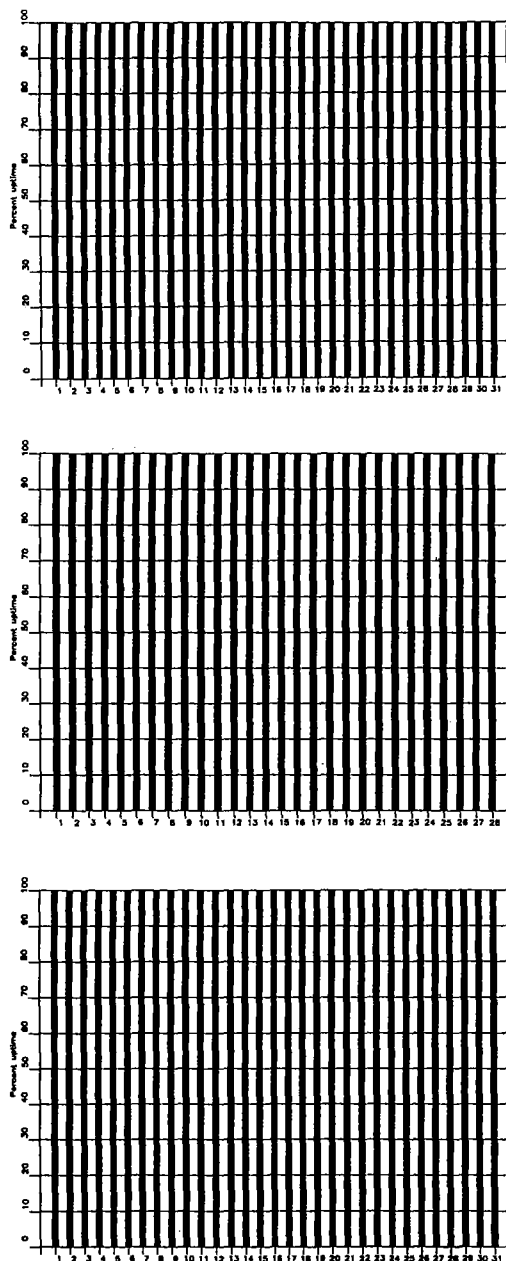


Fig. 2.1.1. Detection Processor uptime for January (top), February (middle) and March (bottom) 1998.

Date	Time	Cause
10 Oct	1841 -	Power failure
11 Oct	- 0457	

Table 2.1.1. The major downtimes in the period 1 October 1997 - 31 March 1998.

Month	DP Uptime Hours	DP Uptime %	No. of DP Breaks	No. of Days with Breaks	DP MTBF* (days)
Oct 97	733.75	98.62	1	2	15.3
Nov	720.00	100	0	0	30.0
Dec	744.00	100	0	0	31.0
Jan 98	744.00	100	0	0	31.0
Feb	672.00	100	0	0	28.0
Mar	744.00	100	0	0	31.0
		99.77	1	2	

*Mean-time-between-failures = total uptime/no. of up intervals.

Table 2.1.2. Online system performance, 1 October 1997 - 31 March 1998.

2.2 Array Communications

After completion of the NORSAR refurbishment project, the operation of the subarray communication lines has proceeded normally.

For a complete description of the NORSAR refurbishment project, reference is made to Section 4.1 of the NORSAR Semiannual Technical Summary, 1 April - 30 September 1995.

From October 1997 through March 1998, there were no significant communications outages at any of the NORSAR subarrays.

A simplified daily summary of the communications performance for the seven individual subarray lines is summarized, on a month-by-month basis, in Table 2.2.1.

F. Ringdal

Table 1
NORSAR Communication Status Report
Month: October 1997

Day	Subarray						
	01A	01B	02B	02C	03C	04C	06C
01	X	X	X	X	X	X	X
02	X	X	X	X	X	X	X
03	X	X	X	X	X	X	X
04	X	X	X	X	X	X	X
05	X	X	X	X	X	X	X
06	X	X	X	X	X	X	X
07	X	X	X	X	X	X	X
08	X	X	X	X	X	X	X
09	X	X	X	X	X	X	X
10	X	X	X	X	X	X	X
11	X	X	X	X	X	X	X
12	X	X	X	X	X	X	X
13	X	X	X	X	X	X	X
14	X	X	X	X	X	X	X
15	X	X	X	X	X	X	X
16	X	X	X	X	X	X	X
17	X	X	X	X	X	X	X
18	X	X	X	X	X	X	X
19	X	X	X	X	X	X	X
20	X	X	X	X	X	X	X
21	X	X	X	X	X	X	X
22	X	X	X	X	X	X	X
23	X	X	X	X	X	X	X
24	X	X	X	X	X	X	X
25	X	X	X	X	X	X	X
26	X	X	X	X	X	X	X
27	X	X	X	X	X	X	X
28	X	X	X	X	X	X	X
29	X	X	X	X	X	X	X
30	X	X	X	X	X	X	X
31	X	X	X	X	X	X	X
Total hours normal operation	733.73	733.73	733.73	733.73	733.73	733.73	733.73
% normal operation	98.62	98.62	98.62	98.62	98.62	98.62	98.62

Legend:

- X : Normal operations
- A : All channels masked for more than 12 hours that day
- B : All SP channels masked for more than 12 hours that day
- C : All LP channels masked for more than 12 hours that day
- I : Communication outage for more than 12 hours

Table 1
NORSAR Communication Status Report
Month: November 1997

Day	Subarray						
	01A	01B	02B	02C	03C	04C	06C
01	X	X	X	X	X	X	X
02	X	X	X	X	A	X	X
03	X	X	X	X	A	X	X
04	X	X	X	X	X	X	X
05	X	X	X	X	X	X	X
06	X	X	X	X	X	X	X
07	X	X	X	X	X	X	X
08	X	X	X	X	X	X	X
09	X	X	X	X	X	X	X
10	X	X	X	X	X	X	X
11	X	X	X	X	X	X	X
12	X	X	X	X	X	X	X
13	X	X	X	X	X	X	X
14	X	X	X	X	X	X	X
15	X	X	X	X	X	X	X
16	X	X	X	X	X	X	X
17	X	X	X	X	X	X	X
18	X	X	X	X	X	X	X
19	X	X	X	X	X	X	X
20	X	X	X	X	X	X	X
21	X	X	X	X	X	X	X
22	X	X	X	X	X	X	X
23	X	X	X	X	X	X	X
24	X	X	X	X	X	X	X
25	X	X	X	X	X	X	X
26	X	X	X	X	X	X	X
27	X	X	X	X	X	X	X
28	X	X	X	X	X	X	X
29	X	X	X	X	X	X	X
30	X	X	X	X	X	X	X
31	-	-	-	-	-	-	-
Total hours normal operation	720	720	720	720	676	720	720
% normal operation	100	100	100	100	93.89	100	100

Legend:

- X : Normal operations
- A : All channels masked for more than 12 hours that day
- B : All SP channels masked for more than 12 hours that day
- C : All LP channels masked for more than 12 hours that day
- I : Communication outage for more than 12 hours

Table 1
NORSAR Communication Status Report
Month: December 1997

Day	Subarray						
	01A	01B	02B	02C	03C	04C	06C
01	X	X	X	X	X	X	X
02	X	X	X	X	X	X	X
03	X	X	X	X	X	X	X
04	X	X	X	X	X	X	X
05	X	X	X	X	X	X	X
06	X	X	X	X	X	X	X
07	X	X	X	X	X	X	X
08	X	X	X	X	X	X	X
09	X	X	X	X	X	X	X
10	X	X	X	X	X	X	X
11	X	X	X	X	X	X	X
12	X	X	X	X	X	X	X
13	X	X	X	X	X	X	X
14	X	X	X	X	X	X	X
15	X	X	X	X	X	X	X
16	X	X	X	X	X	X	X
17	X	X	X	X	X	X	X
18	X	X	X	X	X	X	X
19	X	X	X	X	X	X	X
20	X	X	X	X	X	X	X
21	X	X	X	X	X	X	X
22	X	X	X	X	X	X	X
23	X	X	X	X	X	X	X
24	X	X	X	X	X	X	X
25	X	X	X	X	X	X	X
26	X	X	X	X	X	X	X
27	X	X	X	X	X	X	X
28	X	X	X	X	X	X	X
29	X	X	X	X	X	X	X
30	X	X	X	X	X	X	X
31	X	X	X	X	X	X	X
Total hours normal operation	744	744	744	744	744	744	744
% normal operation	100	100	100	100	100	100	100

Legend:

- X : Normal operations
- A : All channels masked for more than 12 hours that day
- B : All SP channels masked for more than 12 hours that day
- C : All LP channels masked for more than 12 hours that day
- I : Communication outage for more than 12 hours

Table 1
NORSAR Communication Status Report
Month: January 1998

Day	Subarray						
	01A	01B	02B	02C	03C	04C	06C
01	X	X	X	X	X	X	X
02	X	X	X	X	X	X	X
03	X	X	X	X	X	X	X
04	X	X	X	X	X	X	X
05	X	X	X	X	X	X	X
06	X	X	X	X	X	X	X
07	X	X	X	X	X	X	X
08	X	X	X	X	X	X	X
09	X	X	X	X	X	X	X
10	X	X	X	X	X	X	X
11	X	X	X	X	X	X	X
12	X	X	X	X	X	X	X
13	X	X	X	X	X	X	X
14	X	X	X	X	X	X	X
15	X	X	X	X	X	X	X
16	X	X	X	X	X	X	X
17	X	X	X	X	X	X	X
18	X	X	X	X	X	X	X
19	X	X	X	X	X	X	X
20	X	X	X	X	X	X	X
21	X	X	X	X	X	X	X
22	X	X	X	X	X	X	X
23	X	X	X	X	X	X	X
24	X	X	X	X	X	X	X
25	X	X	X	X	X	X	X
26	X	X	X	X	X	X	X
27	X	X	X	X	X	X	X
28	X	X	X	X	X	X	X
29	X	X	X	X	X	X	X
30	X	X	X	X	X	X	X
31	X	X	X	X	X	X	X
Total hours normal operation	744	744	744	744	744	744	744
% normal operation	100	100	100	100	100	100	100

Legend:

- X : Normal operations
- A : All channels masked for more than 12 hours that day
- B : All SP channels masked for more than 12 hours that day
- C : All LP channels masked for more than 12 hours that day
- I : Communication outage for more than 12 hours

Table 1
NORSAR Communication Status Report
Month: February 1998

Day	Subarray						
	01A	01B	02B	02C	03C	04C	06C
01	X	X	X	X	X	X	X
02	X	X	X	X	X	X	X
03	X	X	X	X	X	X	X
04	X	X	X	X	X	X	X
05	X	X	X	X	X	X	X
06	X	X	X	X	X	X	X
07	X	X	X	X	X	X	X
08	X	X	X	X	X	X	X
09	X	X	X	X	X	X	X
10	X	X	X	X	X	X	X
11	X	X	X	X	X	X	X
12	X	X	X	X	X	X	X
13	X	X	X	X	X	X	X
14	X	X	X	X	X	X	X
15	X	X	X	X	X	X	X
16	X	X	X	X	X	X	X
17	X	X	X	X	X	X	X
18	X	X	X	X	X	X	X
19	X	X	X	X	X	X	X
20	X	X	X	X	X	X	X
21	X	X	X	X	X	X	X
22	X	X	X	X	X	X	X
23	X	X	X	X	X	X	X
24	X	X	X	X	X	X	X
25	X	X	X	X	X	X	X
26	X	X	X	X	X	X	X
27	X	X	X	X	X	X	X
28	X	X	X	X	X	X	X
29	-	-	-	-	-	-	-
30	-	-	-	-	-	-	-
31	-	-	-	-	-	-	-
Total hours normal operation	668	672	672	672	672	628	672
% normal operation	99.4	100	100	100	100	93.45	100

Legend:

- X : Normal operations
- A : All channels masked for more than 12 hours that day
- B : All SP channels masked for more than 12 hours that day
- C : All LP channels masked for more than 12 hours that day
- I : Communication outage for more than 12 hours

Table 1
NORSAR Communication Status Report
Month: March 1998

Day	Subarray						
	01A	01B	02B	02C	03C	04C	06C
01	X	X	X	X	X	X	X
02	X	X	X	X	X	X	X
03	X	X	X	X	X	X	X
04	X	X	X	X	X	X	X
05	X	X	X	X	X	X	X
06	X	X	X	X	X	X	X
07	X	X	X	X	X	X	X
08	X	X	X	X	X	X	X
09	X	X	X	X	X	X	X
10	X	X	X	X	X	X	X
11	X	X	X	X	X	X	X
12	X	X	X	X	X	X	X
13	X	X	X	X	X	X	X
14	X	X	X	X	X	X	X
15	X	X	X	X	X	X	X
16	X	X	X	X	X	X	X
17	X	X	X	X	X	X	X
18	X	X	X	X	X	X	X
19	X	X	X	X	X	X	X
20	X	X	X	X	X	X	X
21	X	X	X	X	X	X	X
22	X	X	X	X	X	X	X
23	X	X	X	X	X	X	X
24	X	X	X	X	X	X	X
25	X	X	X	X	X	X	X
26	X	X	X	X	X	X	X
27	X	X	X	X	X	X	X
28	X	X	X	X	X	X	X
29	X	X	X	X	X	X	X
30	X	X	X	X	X	X	X
31	X	X	X	X	X	X	X
Total hours normal operation	744	744	744	744	744	740	744
% normal operation	100	100	100	100	100	99.46	100

Legend:

- X : Normal operations
- A : All channels masked for more than 12 hours that day
- B : All SP channels masked for more than 12 hours that day
- C : All LP channels masked for more than 12 hours that day
- I : Communication outage for more than 12 hours

2.3 NORSAR Event Detection operation

In Table 2.3.1 some monthly statistics of the Detection and Event Processor operation are given. The table lists the total number of detections (DPX) triggered by the on-line detector, the total number of detections processed by the automatic event processor (EPX) and the total number of events accepted after analyst review (teleseismic phases, core phases and total).

	Total DPX	Total EPX	Accepted events		Sum	Daily
			P-phases	Core Phases		
Oct 97	9999	800	229	52	281	9.1
Nov 97	9849	986	404	64	468	15.6
Dec 97	10602	1137	642	43	685	22.1
Jan 98	10077	792	213	59	272	8.8
Feb 98	9729	740	192	38	230	8.2
Mar 98	9578	737	209	51	260	8.4
	59834	5192	1889	307	2196	12.0

Table 2.3.1. Detection and Event Processor statistics, 1 October 1997 - 31 March 1998.

NORSAR Detections

The number of detections (phases) reported by the NORSAR detector during day 275, 1997, through day 090, 1998, was 59,834, giving an average of 331 detections per processed day (181 days processed). Table 2.3.2 shows daily and hourly distribution of detections for NORSAR.

B. Paulsen

NOA .FKX Hourly distribution of detections

Day	00	01	02	03	04	05	06	07	08	09	10	11	12	13	14	15	16	17	18	19	20	21	22	23	Sum	Date
274	17	17	16	31	13	7	10	13	6	15	3	5	11	8	19	12	4	12	3	8	6	2	5	11	254	Oct 01 Wednesday
275	3	14	16	6	6	5	6	3	11	9	5	19	12	12	15	18	19	16	25	19	21	26	19	13	318	Oct 02 Thursday
276	19	22	21	14	22	5	12	9	9	6	5	14	10	10	12	7	16	17	25	21	22	24	31	19	372	Oct 03 Friday
277	24	21	20	33	27	26	24	18	11	17	13	15	19	22	16	30	27	15	21	20	23	18	12	20	492	Oct 04 Saturday
278	16	14	17	19	24	19	15	20	15	11	12	11	7	19	7	12	6	15	18	23	7	13	6	9	335	Oct 05 Sunday
279	20	9	7	15	7	4	1	1	0	3	1	19	18	10	14	4	17	7	9	7	6	66	12	42	299	Oct 06 Monday
280	13	13	8	15	28	11	8	5	7	5	5	4	19	15	9	18	12	8	9	9	16	19	7	17	280	Oct 07 Tuesday
281	14	14	15	12	5	5	7	13	7	11	1	13	10	9	10	7	5	13	10	6	4	17	8	4	220	Oct 08 Wednesday
282	7	2	13	13	14	0	1	9	7	2	6	4	4	2	5	2	4	4	9	7	9	1	4	8	137	Oct 09 Thursday
283	6	10	8	9	8	4	4	2	6	11	5	3	1	4	6	2	9	7	8	0	0	0	0	0	113	Oct 10 Friday
284	0	0	0	0	12	17	12	17	6	14	7	6	10	7	9	7	11	23	33	43	18	24	28	19	323	Oct 11 Saturday
285	19	24	34	36	29	24	19	27	13	19	14	25	24	11	17	17	22	17	22	46	24	29	12	26	550	Oct 12 Sunday
286	23	24	31	26	21	16	8	6	7	10	11	22	13	16	8	4	20	19	9	14	8	14	19	15	364	Oct 13 Monday
287	12	20	20	14	11	7	7	5	2	2	35	11	30	22	10	9	14	6	11	2	8	11	10	14	293	Oct 14 Tuesday
288	10	57	9	25	7	8	2	5	2	2	3	19	26	18	20	4	5	3	5	2	15	16	14	13	290	Oct 15 Wednesday
289	9	11	15	8	7	3	3	4	13	3	7	21	13	1	9	13	5	17	15	18	15	17	18	17	262	Oct 16 Thursday
290	13	25	23	22	19	12	11	9	20	14	10	13	13	23	13	17	15	28	16	21	18	22	19	17	413	Oct 17 Friday
291	16	21	36	16	31	30	14	19	25	28	22	18	14	13	17	14	13	18	17	23	17	20	18	17	477	Oct 18 Saturday
292	22	28	29	23	19	18	20	21	11	17	17	14	15	16	29	17	34	24	17	34	16	17	16	24	498	Oct 19 Sunday
293	27	19	18	19	14	19	17	15	11	19	13	5	18	25	12	12	15	17	26	10	15	15	17	397	Oct 20 Monday	
294	9	11	13	22	16	10	12	3	7	11	16	7	12	10	16	11	4	7	18	11	11	12	13	16	278	Oct 21 Tuesday
295	15	20	30	26	14	8	6	8	5	8	12	8	21	16	11	5	14	13	24	22	13	16	17	20	352	Oct 22 Wednesday
296	13	21	18	26	23	9	12	13	14	6	18	10	18	14	25	7	9	23	17	11	9	18	16	16	366	Oct 23 Thursday
297	22	18	19	27	26	7	12	12	6	13	9	14	23	24	24	22	26	18	19	17	27	26	13	24	448	Oct 24 Friday
298	19	21	26	22	11	24	15	14	15	14	18	10	21	18	9	12	14	21	19	22	18	21	19	21	424	Oct 25 Saturday
299	18	17	19	29	16	19	27	18	19	22	17	15	19	15	11	12	17	15	20	29	11	21	13	18	437	Oct 26 Sunday
300	16	16	13	9	20	4	3	8	2	6	1	10	0	3	5	12	6	7	4	6	16	11	11	15	204	Oct 27 Monday
301	13	15	22	18	10	13	25	9	12	4	8	11	9	3	14	11	12	8	9	14	14	9	10	9	282	Oct 28 Tuesday
302	12	12	15	11	13	17	5	5	12	2	3	2	18	6	7	13	8	4	7	10	12	6	9	7	216	Oct 29 Wednesday
303	9	14	14	12	26	15	12	7	17	5	3	7	17	15	6	10	14	18	18	18	23	23	14	18	335	Oct 30 Thursday
304	19	20	15	11	19	16	9	7	9	8	12	4	15	23	8	20	11	28	11	18	16	24	14	32	369	Oct 31 Friday
305	22	22	19	23	28	18	18	10	10	21	14	14	14	27	19	15	19	18	12	30	19	18	18	14	442	Nov 01 Saturday
306	19	15	16	24	18	11	23	18	21	20	19	11	21	17	19	20	21	35	29	29	25	27	17	20	495	Nov 02 Sunday
307	20	13	28	28	22	24	8	22	24	8	14	9	5	3	18	24	13	17	17	31	16	25	20	13	422	Nov 03 Monday
308	20	21	19	17	25	16	11	8	11	6	15	12	5	13	8	16	3	8	11	16	21	26	23	25	356	Nov 04 Tuesday
309	25	31	29	26	24	23	13	10	11	19	31	8	18	14	17	12	21	17	9	15	21	24	17	25	460	Nov 05 Wednesday
310	15	21	22	20	12	17	13	2	22	10	17	15	7	16	17	16	17	13	9	13	12	10	17	12	345	Nov 06 Thursday
311	14	15	18	16	28	14	4	4	11	10	7	13	12	6	11	11	3	18	10	8	8	8	13	13	275	Nov 07 Friday
312	8	10	5	4	9	6	6	6	2	9	34	18	38	9	10	27	6	12	18	14	12	22	15	19	319	Nov 08 Saturday
313	25	15	18	16	15	26	9	12	21	20	20	8	16	13	16	13	21	19	19	17	20	19	20	27	425	Nov 09 Sunday
314	18	15	22	8	14	12	9	6	7	3	8	15	11	10	7	14	12	16	10	16	13	22	17	20	305	Nov 10 Monday
315	12	10	13	27	15	10	3	5	6	4	14	2	7	12	9	14	2	13	11	7	19	8	16	20	259	Nov 11 Tuesday
316	14	10	10	26	10	11	7	4	3	7	18	13	6	7	18	12	8	6	6	5	6	6	22	10	245	Nov 12 Wednesday
317	19	13	17	22	7	14	11	6	8	18	42	4	14	11	16	2	5	13	12	10	9	15	19	14	321	Nov 13 Thursday
318	11	8	12	2	16	14	4	9	1	8	11	8	18	4	6	26	18	13	10	15	18	21	19	24	296	Nov 14 Friday
319	17	15	25	20	17	22	22	14	12	11	11	17	15	16	10	31	20	15	36	19	14	24	20	443	Nov 15 Saturday	
320	20	22	21	32	23	21	15	28	22	25	19	23	17	25	14	17	14	16	16	16	15	13	19	11	464	Nov 16 Sunday
321	25	19	14	7	9	29	14	15	8	8	17	8	8	7	17	7	13	15	14	13	12	15	13	11	318	Nov 17 Monday
322	12	40	11	16	12	15	8	4	9	11	4	33	16	53	42	17	42	23	17	15	24	19	13	21	477	Nov 18 Tuesday
323	15	21	22	9	13	8	15	2	11	15	6	20	18	16	12	14	17	15	13	13	11	14	22	22	344	Nov 19 Wednesday
324	19	24	17	17	22	23	23	7	5	15	6	9	7	8	7	7	22	7	13	14	13	18	10	20	333	Nov 20 Thursday
325	9	5	10	11	19	14	12	5	7	16	7	17	8	22	3	14	18	17	15	14	19	11	11	9	293	Nov 21 Friday
326	12	14	19	10	21	11	28	16	18	7	11	11	2	10	5	8	16	16	7	10	13	7	11	15	298	Nov 22 Saturday
327	20	10	12	14	23	15	16	26	17	13	16	10	7	19	14	14	16	25	10	13	15	16	13	14	368	Nov 23 Sunday
328	17	25	26	6	23	11	5	1	2	0	2	19	3	4	6	2	3	0	1	7	3	5	1	8	180	Nov 24 Monday
329	16	9	6	7	4	3	9	1	11	0	8	8	44	24	24	10	3	11	17	0	6	13	18	17	269	Nov 25 Tuesday

Table 2.3.2 (Page 1 of 4)

NOA .FKX Hourly distribution of detections

Day	00	01	02	03	04	05	06	07	08	09	10	11	12	13	14	15	16	17	18	19	20	21	22	23	Sum	Date
330	8	12	6	16	9	4	4	6	1	4	17	5	21	7	13	11	5	14	10	8	6	7	5	8	207	Nov 26 Wednesday
331	12	8	17	8	19	9	13	7	2	7	5	9	19	1	8	9	15	26	12	34	9	8	17	4	278	Nov 27 Thursday
332	15	14	9	14	9	9	17	7	6	9	9	43	17	16	5	15	10	6	21	8	14	8	11	39	331	Nov 28 Friday
333	22	8	17	25	11	15	13	7	15	18	25	8	20	12	13	11	8	16	9	7	31	27	9	18	365	Nov 29 Saturday
334	16	17	12	7	9	9	11	20	11	7	14	14	12	9	9	14	19	13	18	16	16	20	22	18	333	Nov 30 Sunday
335	24	9	20	19	14	11	6	12	10	9	2	5	6	8	15	14	2	11	14	17	7	13	6	7	261	Dec 01 Monday
336	22	11	11	16	11	9	5	3	2	2	1	7	33	5	21	5	7	4	4	10	5	7	6	7	214	Dec 02 Tuesday
337	8	11	7	10	9	8	5	2	3	0	7	7	22	18	4	6	6	6	9	6	9	10	14	15	202	Dec 03 Wednesday
338	6	23	15	26	9	7	25	13	6	5	13	5	9	4	9	17	6	5	10	8	14	9	35	14	293	Dec 04 Thursday
339	23	28	15	12	11	25	16	9	25	9	8	40	68	48	58	50	49	48	70	51	73	55	33	31	855	Dec 05 Friday
340	49	27	38	41	34	39	43	26	25	27	21	23	44	28	25	12	11	34	29	32	18	25	11	27	689	Dec 06 Saturday
341	16	37	28	35	23	33	24	24	38	16	30	33	21	27	29	22	29	23	25	15	31	29	16	34	638	Dec 07 Sunday
342	18	29	37	25	25	24	17	9	11	14	14	3	8	13	27	17	18	12	20	15	8	14	19	27	424	Dec 08 Monday
343	23	21	26	28	15	9	16	18	15	9	11	9	12	15	19	8	10	4	11	16	6	13	12	11	337	Dec 09 Tuesday
344	12	14	17	16	14	18	10	4	20	4	9	19	16	9	7	16	9	16	10	6	11	18	9	8	292	Dec 10 Wednesday
345	15	9	9	13	18	11	0	5	9	1	16	15	9	2	6	9	9	2	8	8	13	9	8	10	214	Dec 11 Thursday
346	8	14	13	16	22	4	13	5	4	6	7	14	16	4	22	13	10	16	7	5	8	16	5	14	262	Dec 12 Friday
347	5	13	10	16	44	23	25	34	8	16	21	13	11	16	19	17	21	22	28	20	26	13	19	11	451	Dec 13 Saturday
348	13	13	21	12	23	11	6	8	10	22	14	6	15	13	9	9	13	18	13	16	16	16	16	24	337	Dec 14 Sunday
349	15	18	20	22	16	16	7	12	13	19	9	17	13	6	16	20	12	22	22	22	14	15	14	18	378	Dec 15 Monday
350	16	18	21	17	10	11	5	4	8	3	12	5	8	3	18	5	9	7	5	6	13	11	11	15	241	Dec 16 Tuesday
351	18	10	12	15	17	20	14	6	5	9	4	12	10	5	12	6	8	11	12	14	10	13	9	10	262	Dec 17 Wednesday
352	16	9	10	6	6	16	15	8	8	13	2	25	9	6	5	13	6	5	18	12	12	13	11	11	255	Dec 18 Thursday
353	16	21	10	22	14	18	10	10	2	18	7	12	25	21	6	5	8	4	10	13	5	14	14	4	289	Dec 19 Friday
354	26	22	15	9	15	12	12	8	15	10	17	14	15	21	15	6	11	10	10	12	13	52	11	12	363	Dec 20 Saturday
355	23	15	15	14	18	38	14	20	13	19	9	15	13	16	14	18	25	20	25	12	20	19	16	18	429	Dec 21 Sunday
356	20	14	37	14	14	20	6	6	2	4	19	7	21	15	4	2	10	15	6	15	9	5	8	15	288	Dec 22 Monday
357	7	12	6	9	13	4	9	7	1	14	24	9	6	12	15	6	13	12	14	16	29	20	22	16	296	Dec 23 Tuesday
358	25	16	29	30	21	22	16	12	16	33	23	12	21	19	12	20	24	14	19	28	23	27	18	20	500	Dec 24 Wednesday
359	21	20	14	20	15	19	20	20	17	11	17	20	13	15	19	15	19	16	5	15	13	10	23	18	395	Dec 25 Thursday
360	23	24	17	15	14	32	19	21	15	13	14	16	18	16	21	14	20	20	14	18	15	21	16	16	432	Dec 26 Friday
361	17	15	11	16	14	14	10	11	8	10	7	13	11	13	7	18	10	14	11	14	10	13	4	9	280	Dec 27 Saturday
362	11	12	6	24	8	18	9	10	11	14	8	6	13	8	13	15	9	7	8	8	8	6	8	16	256	Dec 28 Sunday
363	10	14	14	5	9	6	3	6	5	8	1	11	23	3	4	6	9	4	2	5	7	4	6	3	168	Dec 29 Monday
364	8	8	3	7	9	7	2	5	4	9	11	17	27	19	6	10	20	9	11	7	19	14	20	13	265	Dec 30 Tuesday
365	17	26	11	30	14	15	14	20	21	21	15	14	20	15	14	26	18	22	22	11	24	14	23	18	445	Dec 31 Wednesday
1	14	16	16	22	16	17	24	20	10	15	15	24	11	17	12	24	19	16	19	14	22	21	14	19	417	Jan 01 Thursday
2	39	17	17	10	13	19	15	14	10	13	12	19	19	14	10	12	14	14	20	17	11	27	16	21	393	Jan 02 Friday
3	19	21	16	20	17	15	26	18	9	23	15	19	19	7	13	16	16	14	17	14	37	12	20	24	427	Jan 03 Saturday
4	21	17	16	27	19	19	30	12	20	8	12	19	11	9	13	19	16	16	12	18	32	19	18	21	424	Jan 04 Sunday
5	15	24	25	20	11	14	5	1	3	4	4	1	13	0	0	1	10	13	4	3	11	9	11	4	206	Jan 05 Monday
6	8	8	2	10	14	2	3	0	3	1	3	0	6	3	7	5	4	1	2	3	1	7	2	2	97	Jan 06 Tuesday
7	8	11	9	8	5	3	5	3	6	5	12	3	7	5	15	11	7	8	18	19	13	5	10	12	208	Jan 07 Wednesday
8	19	15	20	22	11	12	11	17	9	5	5	10	10	13	7	6	7	4	6	4	15	5	14	7	254	Jan 08 Thursday
9	17	4	14	24	17	6	8	2	4	6	17	18	25	3	14	8	16	13	13	36	21	8	26	23	343	Jan 09 Friday
10	22	13	22	24	37	18	23	14	25	22	19	23	19	21	15	21	17	25	21	23	22	13	18	14	491	Jan 10 Saturday
11	20	19	28	14	25	19	18	11	25	24	8	14	14	6	6	11	13	15	14	27	13	17	21	15	397	Jan 11 Sunday
12	22	16	21	23	22	13	10	3	7	12	13	4	7	22	2	9	10	5	7	11	10	18	14	15	296	Jan 12 Monday
13	16	27	13	27	13	8	10	7	5	4	14	3	31	13	13	7	6	18	5	10	14	12	10	12	298	Jan 13 Tuesday
14	9	12	8	11	15	16	6	9	1	3	7	10	13	5	8	5	3	17	19	13	24	15	11	22	262	Jan 14 Wednesday
15	16	12	8	17	17	12	11	8	6	10	8	14	21	1	10	14	9	21	12	19	11	29	18	13	317	Jan 15 Thursday
16	19	12	18	17	12	14	7	5	3	7	9	9	4	22	13	5	8	12	18	17	18	25	17	16	307	Jan 16 Friday
17	20	23	17	19	21	22	30	15	18	24	23	22	19	18	22	17	21	22	26	21	27	24	30	27	528	Jan 17 Saturday
18	22	23	33	27	22	32	9	14	25	10	14	11	6	13	10	16	12	16	11	14	18	18	16	16	408	Jan 18 Sunday
19	21	12	18	19	13	21	13	9	18	7	7	12	13	9	9	7	7	10	10	9	6	13	21	8	292	Jan 19 Monday
20	15	14	13	14	15	11	7	6	6	10	6	11	6	5	8	19	18	11	13	15	13	10	11	11	268	Jan 20 Tuesday

Table 2.3.2. (Page 2 of 4)

NQA .FKX Hourly distribution of detections

Day	00	01	02	03	04	05	06	07	08	09	10	11	12	13	14	15	16	17	18	19	20	21	22	23	Sum	Date
21	28	18	12	17	19	20	17	8	4	4	8	10	16	6	13	11	9	4	6	7	8	10	1	15	271	Jan 21 Wednesday
22	15	15	8	12	14	17	11	9	8	10	9	5	16	19	9	30	22	11	17	20	19	20	22	23	361	Jan 22 Thursday
23	12	11	23	21	23	12	11	11	11	23	12	10	23	21	20	13	14	14	8	18	29	17	16	14	387	Jan 23 Friday
24	23	21	20	26	15	22	18	13	18	15	15	21	11	25	17	27	25	15	17	15	22	21	23	31	476	Jan 24 Saturday
25	19	16	21	14	11	26	19	15	21	13	19	15	10	10	13	13	16	17	12	14	18	17	16	27	392	Jan 25 Sunday
26	19	20	22	14	15	13	4	10	4	7	9	2	4	8	7	14	18	5	12	16	14	21	10	20	288	Jan 26 Monday
27	24	28	22	19	24	27	22	20	17	15	13	23	9	14	17	14	7	20	8	27	32	26	19	22	469	Jan 27 Tuesday
28	19	23	12	19	12	15	7	1	6	6	3	5	9	22	7	9	12	10	4	9	7	4	13	7	241	Jan 28 Wednesday
29	14	11	9	11	14	11	4	2	37	1	0	12	16	5	12	14	11	15	18	13	17	18	16	11	292	Jan 29 Thursday
30	21	21	22	19	18	19	9	15	8	15	4	13	39	9	15	20	21	16	15	20	8	11	10	5	373	Jan 30 Friday
31	8	21	9	14	10	8	7	10	13	10	12	9	8	14	15	15	6	27	17	17	19	19	21	22	331	Jan 31 Saturday
32	26	27	28	15	17	25	29	23	24	22	20	13	16	15	13	19	15	25	22	9	15	14	19	15	466	Feb 01 Sunday
33	10	12	16	19	20	15	13	9	6	8	15	8	9	14	18	34	11	9	16	15	11	20	13	16	337	Feb 02 Monday
34	23	18	19	19	20	24	6	15	17	11	7	11	8	14	9	16	8	12	24	19	28	20	21	29	398	Feb 03 Tuesday
35	14	20	28	17	19	25	18	14	12	10	17	17	9	38	22	14	20	13	15	10	10	17	23	27	429	Feb 04 Wednesday
36	35	20	16	14	16	17	11	10	14	6	21	20	14	10	26	7	6	6	13	22	14	9	13	11	351	Feb 05 Thursday
37	8	17	20	15	15	10	10	2	8	11	19	12	19	16	8	12	18	10	14	16	23	15	25	8	331	Feb 06 Friday
38	21	29	23	24	14	22	22	22	19	22	14	15	20	16	20	15	6	7	21	24	24	15	24	18	457	Feb 07 Saturday
39	20	18	15	13	21	15	15	21	20	10	18	17	27	13	13	19	23	11	22	22	25	29	25	19	451	Feb 08 Sunday
40	29	17	22	29	21	20	14	11	12	11	18	11	32	50	29	17	13	14	15	18	13	22	19	19	476	Feb 09 Monday
41	16	23	18	16	21	16	8	14	16	9	10	7	7	6	8	11	21	10	15	17	13	14	22	15	333	Feb 10 Tuesday
42	18	16	24	19	18	15	8	8	3	7	11	10	17	20	9	17	22	12	15	19	29	17	13	24	371	Feb 11 Wednesday
43	21	20	24	14	16	17	7	11	13	3	13	24	10	6	23	7	9	24	7	11	13	24	16	24	357	Feb 12 Thursday
44	17	12	13	25	10	10	5	15	6	14	2	27	15	23	19	19	18	21	9	19	8	23	10	16	356	Feb 13 Friday
45	19	19	12	12	17	17	21	31	10	26	10	15	13	15	19	13	13	14	18	19	16	15	12	18	394	Feb 14 Saturday
46	21	24	20	19	16	22	12	15	9	13	8	13	13	7	11	9	13	14	6	14	8	14	12	9	322	Feb 15 Sunday
47	15	19	20	12	16	12	16	15	6	8	8	19	13	29	13	11	20	9	16	21	16	15	13	28	370	Feb 16 Monday
48	9	28	12	14	10	9	4	4	3	5	7	3	7	20	10	18	14	15	18	19	10	16	15	25	295	Feb 17 Tuesday
49	21	36	20	17	24	21	14	22	16	34	11	9	23	9	6	13	14	7	9	9	10	10	13	12	380	Feb 18 Wednesday
50	15	15	13	13	14	15	9	8	7	11	6	9	3	13	36	10	18	14	7	9	7	19	14	16	301	Feb 19 Thursday
51	14	13	18	18	24	10	6	10	13	13	19	9	18	11	14	8	12	11	12	15	17	12	10	18	325	Feb 20 Friday
52	12	21	20	10	21	13	22	13	11	26	14	15	24	16	18	11	16	5	17	9	19	8	15	23	379	Feb 21 Saturday
53	17	11	20	23	19	18	13	18	22	15	14	16	19	21	11	19	20	26	20	18	15	21	27	18	441	Feb 22 Sunday
54	21	9	21	18	26	21	12	16	9	7	20	15	12	11	18	10	21	11	15	18	15	16	16	8	366	Feb 23 Monday
55	13	18	13	16	11	18	13	7	2	3	8	13	9	7	7	16	8	13	9	8	20	22	18	12	284	Feb 24 Tuesday
56	22	21	19	10	16	19	20	14	11	33	17	10	17	21	4	18	26	16	8	25	14	9	11	14	395	Feb 25 Wednesday
57	10	15	21	13	10	10	20	9	5	7	10	10	19	7	10	14	5	13	13	8	10	7	16	11	273	Feb 26 Thursday
58	12	10	15	9	5	9	5	6	13	6	10	7	7	12	13	19	12	8	14	19	14	8	19	23	275	Feb 27 Friday
59	21	17	12	8	8	12	13	3	5	5	8	11	0	5	3	3	2	8	4	4	8	8	11	11	190	Feb 28 Saturday
60	6	16	12	11	11	15	16	28	16	17	21	10	18	18	21	14	14	15	23	18	12	18	11	11	372	Mar 01 Sunday
61	23	17	21	16	14	13	4	13	11	3	10	20	19	10	11	9	9	6	20	10	22	10	7	7	315	Mar 02 Monday
62	17	14	23	5	9	5	14	5	5	6	5	10	16	11	11	13	18	13	15	11	17	10	17	279	Mar 03 Tuesday	
63	26	16	16	17	19	13	6	7	4	10	2	17	5	8	12	9	20	10	10	20	12	18	13	8	298	Mar 04 Wednesday
64	16	21	23	19	14	7	5	11	14	7	2	6	10	20	13	7	7	11	14	8	15	8	19	284	Mar 05 Thursday	
65	27	28	19	21	27	20	18	12	12	15	16	15	14	21	14	13	10	11	15	14	19	21	9	19	410	Mar 06 Friday
66	10	11	16	22	11	15	17	13	12	13	13	18	7	11	12	9	20	17	18	17	11	22	10	19	344	Mar 07 Saturday
67	30	16	17	12	16	15	13	19	12	13	15	20	9	14	19	11	9	20	18	18	18	17	20	16	387	Mar 08 Sunday
68	14	16	13	13	14	21	6	8	10	7	18	18	12	9	28	9	10	4	2	10	8	8	6	12	276	Mar 09 Monday
69	12	7	13	6	13	11	6	3	5	11	3	10	7	11	12	13	13	12	20	18	26	22	21	12	287	Mar 10 Tuesday
70	22	21	27	26	19	20	17	19	13	3	16	18	8	18	10	13	12	15	24	17	14	19	19	13	403	Mar 11 Wednesday
71	13	14	14	21	17	12	9	3	10	5	6	17	14	9	12	17	14	15	21	15	10	11	18	31	328	Mar 12 Thursday
72	29	19	8	15	11	23	8	7	12	8	6	6	12	32	10	17	9	11	11	15	18	22	18	21	348	Mar 13 Friday
73	20	20	14	18	16	15	14	16	11	10	18	19	16	12	17	15	13	26	28	27	9	24	11	18	407	Mar 14 Saturday
74	12	17	19	16	13	14	17	7	14	11	19	8	14	10	15	18	16	17	9	11	24	17	17	11	346	Mar 15 Sunday
75	17	14	20	22	18	19	8	7	11	6	4	7	7	2	17	5	12	5	6	9	7	8	9	6	246	Mar 16 Monday
76	12	15	8	16	10	8	3	7	4	11	9	14	16	23	20	12	16	14	14	11	18	17	25	15	318	Mar 17 Tuesday

Table 2.3.2. (Page 3 of 4)

NOA .FKX Hourly distribution of detections

Day	00	01	02	03	04	05	06	07	08	09	10	11	12	13	14	15	16	17	18	19	20	21	22	23	Sum	Date	
77	24	15	13	25	14	16	14	10	3	19	13	8	22	15	13	14	9	13	14	10	10	14	10	16	334	Mar 18 Wednesday	
78	15	21	17	12	14	8	7	6	22	11	12	9	7	10	16	6	16	13	18	20	12	11	8	4	295	Mar 19 Thursday	
79	19	6	5	7	10	8	8	7	6	5	11	9	11	11	9	7	13	4	11	7	18	19	9	6	226	Mar 20 Friday	
80	7	12	8	13	13	20	16	9	15	8	12	18	10	10	4	10	16	14	22	9	13	9	11	8	287	Mar 21 Saturday	
81	12	23	12	17	11	11	14	6	10	7	4	5	5	11	6	6	6	6	2	4	7	3	7	3	198	Mar 22 Sunday	
82	9	9	14	3	19	9	2	2	3	10	17	4	15	15	16	9	13	10	12	43	66	20	14	16	350	Mar 23 Monday	
83	14	10	20	19	11	13	12	8	6	7	17	15	11	6	14	17	16	7	19	14	13	13	17	9	308	Mar 24 Tuesday	
84	13	21	13	37	10	11	3	4	8	1	6	1	20	20	12	19	12	8	14	6	12	20	8	15	294	Mar 25 Wednesday	
85	25	37	23	18	19	20	19	5	4	7	6	7	4	9	16	7	20	19	11	12	12	9	18	12	339	Mar 26 Thursday	
86	24	16	14	23	22	18	12	11	15	11	14	21	17	10	14	14	16	16	13	23	19	16	16	8	383	Mar 27 Friday	
87	14	18	16	18	20	17	20	13	14	15	16	11	8	17	14	18	15	24	18	27	26	23	33	13	428	Mar 28 Saturday	
88	24	19	23	29	28	28	22	26	13	18	10	7	11	7	2	9	11	3	8	8	34	5	8	20	373	Mar 29 Sunday	
89	10	11	10	7	9	11	4	1	1	1	8	17	5	6	10	12	7	7	8	9	11	8	8	17	198	Mar 30 Monday	
90	13	13	9	6	3	0	1	3	7	27	31	3	10	10	12	10	11	17	14	10	16	13	15	22	276	Mar 31 Tuesday	
NOA	00	01	02	03	04	05	06	07	08	09	10	11	12	13	14	15	16	17	18	19	20	21	22	23			
Sum	3140	3152	2726	1960	2023	2296	2467	2372	2520	2836	2969	2925															
	3091	3099	2962	2220	1972	2184	2637	2466	2467	2573	2843	2720	62620	Total sum													
182	17	17	17	17	16	15	12	11	11	11	11	12	13	14	14	14	13	14	14	14	16	16	16	15	16	344	Total average
127	16	17	16	16	15	13	10	8	9	9	10	12	14	13	13	12	12	12	13	14	14	15	14	15	314	Average workdays	
55	18	18	18	19	19	19	18	17	15	16	15	15	15	15	14	15	16	17	17	19	18	18	16	18	405	Average weekends	

Table 2.3.2. Daily and hourly distribution of NORSAR detections. For each day is shown number of detections within each hour of the day and number of detections for that day. The end statistics give total number of detections distributed for each hour and the total sum of detections during the period. The averages show number of processed days, hourly distribution and average per processed day. (Page 4 of 4)

3 Operation of Regional Arrays

3.1 Recording of NORESS data at NDPC, Kjeller

The average recording time was 87.33% as compared to 99.83% during the previous reporting period.

Table 3.1.1 lists the main outage times and reasons.

Date	Time	Cause
10 Oct	1841 - 2255	Power failure
14 Jan	2100 -	A power surge damaged the clock
06 Feb	- 1305	

Table 3.1.1. Interruptions in recording of NORESS data at NDPC, 1 October 1997 - 31 March 1998.

Monthly uptimes for the NORESS on-line data recording task, taking into account all factors (field installations, transmissions line, data center operation) affecting this task were as follows:

October 97	:	99.42
November	:	99.99
December	:	99.99
January 98	:	44.75
February	:	80.12
March	:	99.99

Fig. 3.1.1 shows the uptime for the data recording task, or equivalently, the availability of NORESS data in our tape archive, on a day-by-day basis, for the reporting period.

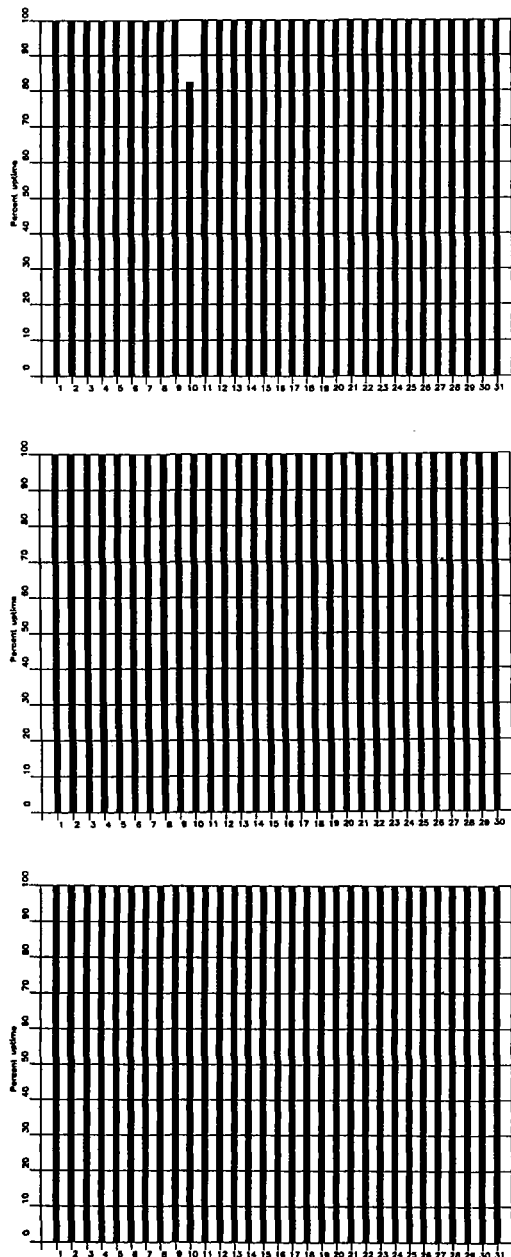


Fig. 3.1.1. NORESS data recording uptime for October (top), November (middle) and December (bottom) 1997.

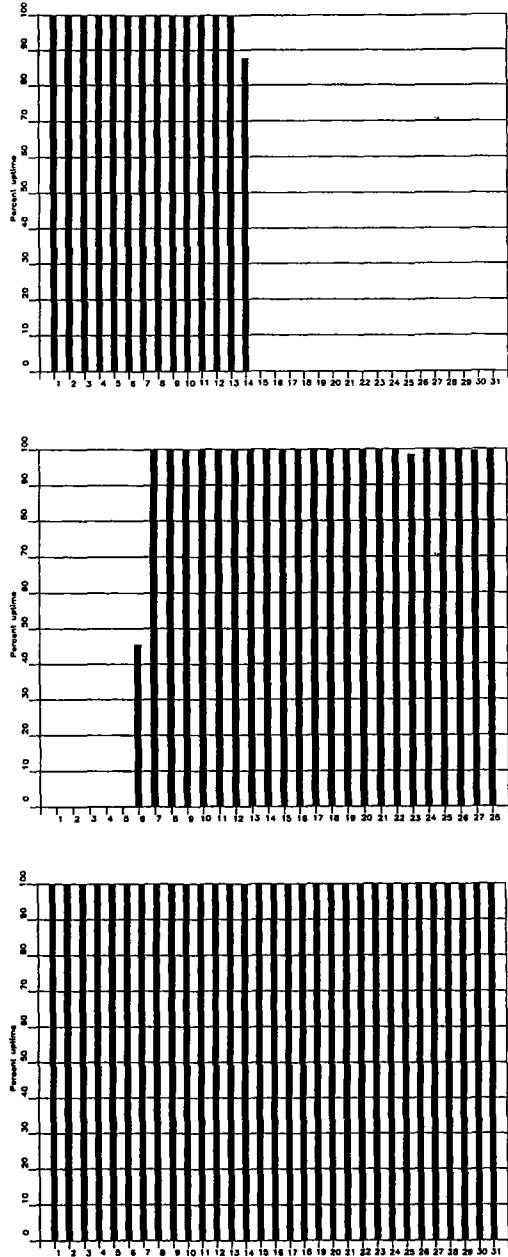


Fig. 3.1.1. (cont.) NORESS data recording uptime for January (top), February (middle) and March (bottom) 1998.

3.2 Recording of ARCESS data at NDPC, Kjeller

The average recording time was 99.68% as compared to 53.53% for the previous reporting period.

Table 3.2.1 lists the main outage times and reasons.

Date	Time	Cause
10 Oct	1841 -	Power break NDPC
11 Oct	- 0512	

Table 3.2.1. The main interruptions in recording of ARCESS data at NDPC, 1 October 1997 - 31 March 1998.

Monthly uptimes for the ARCESS on-line data recording task, taking into account all factors (field installations, transmissions line, data center operation) affecting this task were as follows:

October 97	:	98.53%
November	:	99.99%
December	:	99.97%
January 98	:	99.95%
February	:	99.73%
March	:	99.89%

Fig. 3.2.1. shows the uptime for the data recording task, or equivalently, the availability of ARCESS data in our tape archive, on a day-by-day basis, for the reporting period.

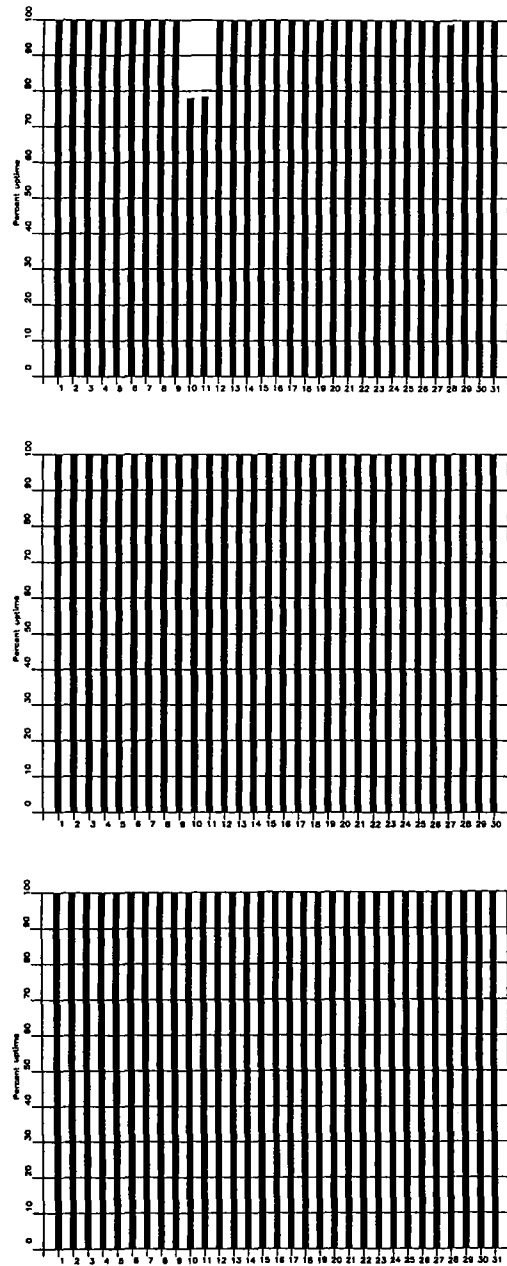


Fig. 3.2.1. ARCESS data recording uptime for October (top), November (middle) and December (bottom) 1997.

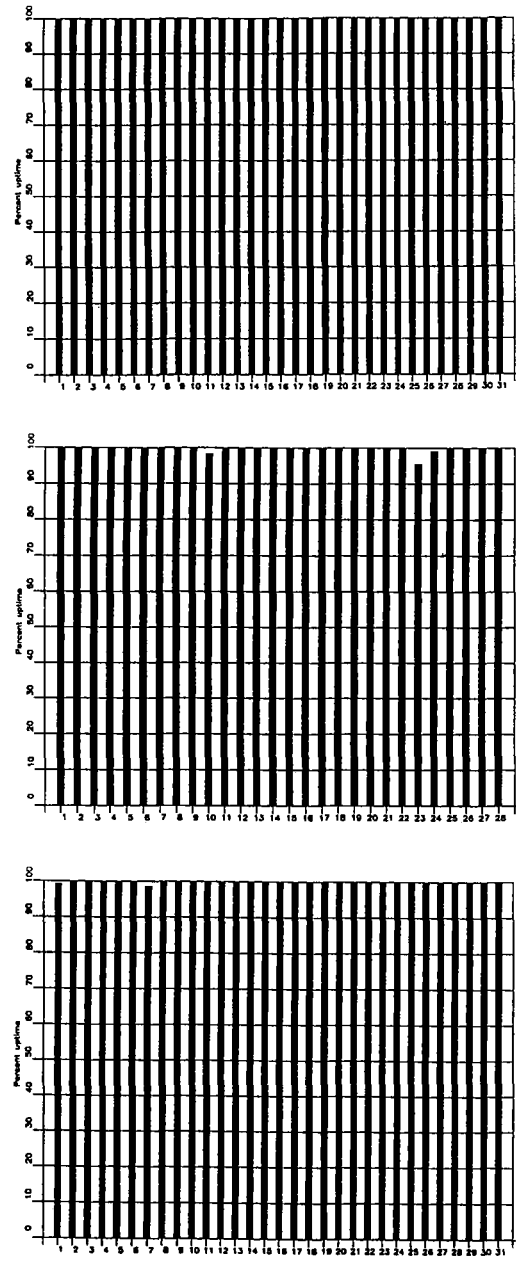


Fig. 3.2.1. (cont.) ARCESS data recording uptime for January (top), February (middle) and March (bottom) 1998.

3.3 Recording of FINESS data at NDPC, Kjeller

The average recording time was 99.81% as compared to 99.44% for the previous reporting period.

Date	Time	Cause
30 Oct	2254 -	Stop in Helsinki
31 Oct	- 0707	

Table 3.3.1. The main interruptions in recording of FINESS data at NDPC, 1 October 1997-31 March 1998.

Monthly uptimes for the FINESS on-line data recording task, taking into account all factors (field installations, transmission lines, data center operation) affecting this task were as follows:

October 97	:	98.87%
November	:	100.00%
December	:	100.00%
January 98	:	100.00%
February	:	100.00%
March	:	100.00%

Fig. 3.3.1 shows the uptime for the data recording task, or equivalently, the availability of FINESS data in our tape archive, on a day-by-day basis, for the reporting period.

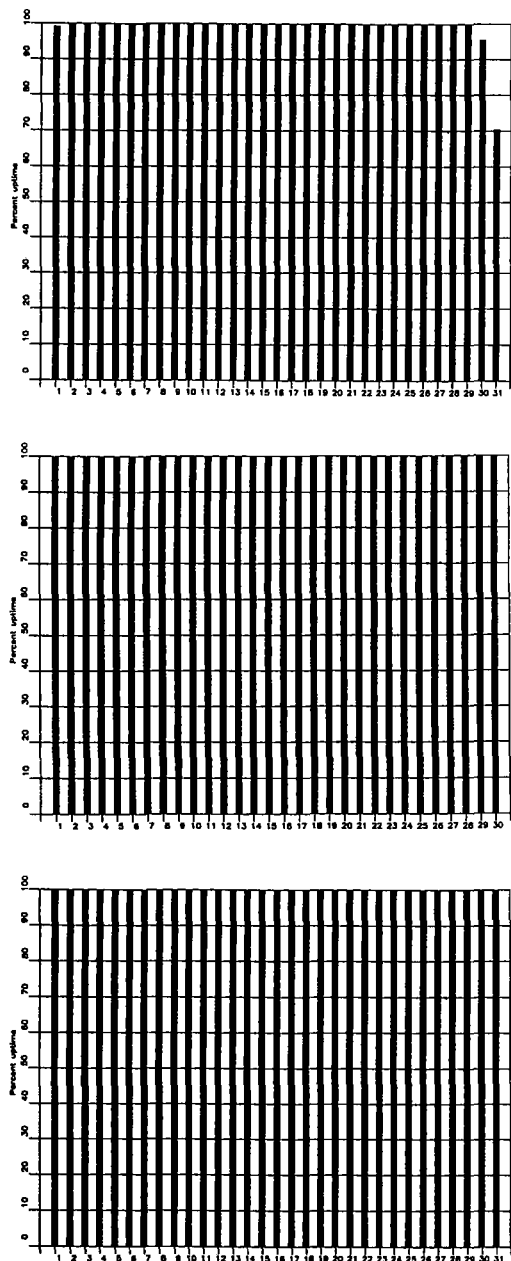


Fig. 3.3.1. FINESS data recording uptime for October (top), November (middle) and December (bottom) 1997.

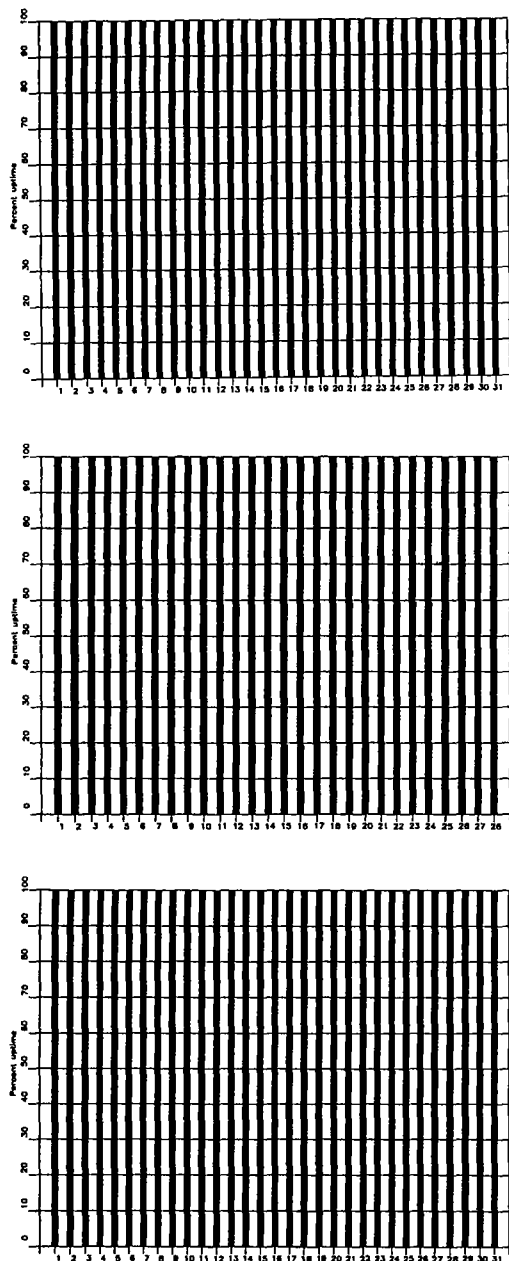


Fig. 3.3.1. (cont.) FINESS data recording uptime for January (top), February (middle) and March (bottom) 1998.

3.4 Recording of Spitsbergen data at NDPC, Kjeller

The average recording time was 91.06% as compared to 98.66% for the previous reporting period.

The main reasons for downtime follow:

Date	Time	Cause
15 Dec	1930 -	Power supply failed
30 Dec	- 1504	

Table 3.4.1. The main interruptions in recording of Spitsbergen data at NDPC, 1 October 1997 - 31 March 1998.

Monthly uptimes for the Spitsbergen online data recording task, taking into account all factors (field installations, transmission line, data center operation) affecting this task were as follows:

October 97	:	97.86%
November	:	99.41%
December	:	52.04%
January 98	:	99.59%
February	:	99.72%
March	:	97.77%

Fig. 3.4.1 shows the uptime for the data recording task, or equivalently, the availability of Spitsbergen data in our tape archive, on a day-by-day basis for the reporting period.

J. Torstveit

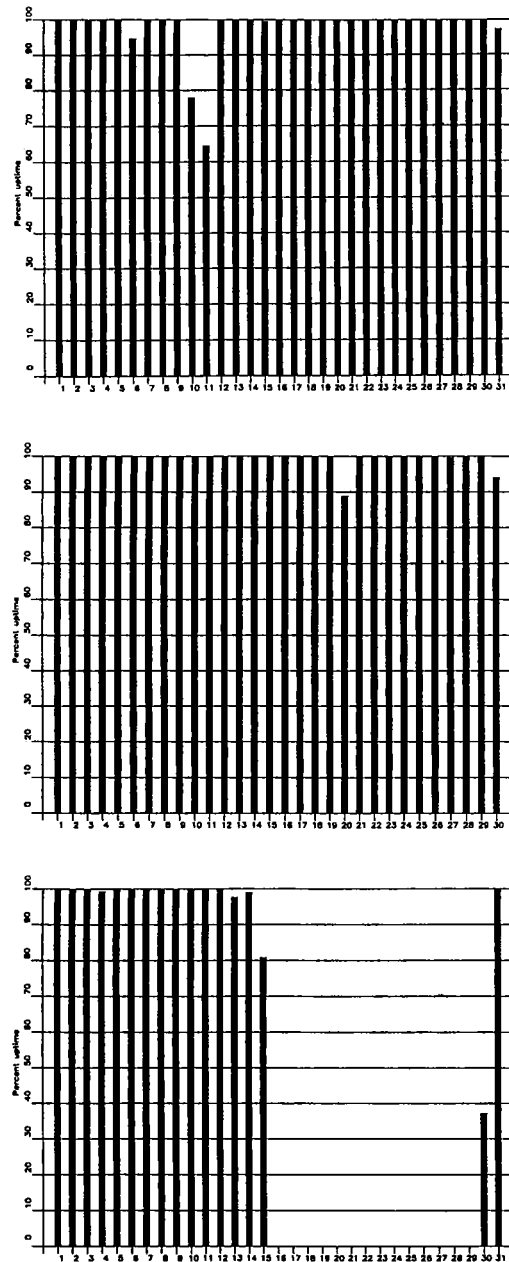


Fig. 3.4.1. Spitsbergen data recording uptime for October (top), November (middle) and December (bottom) 1997.

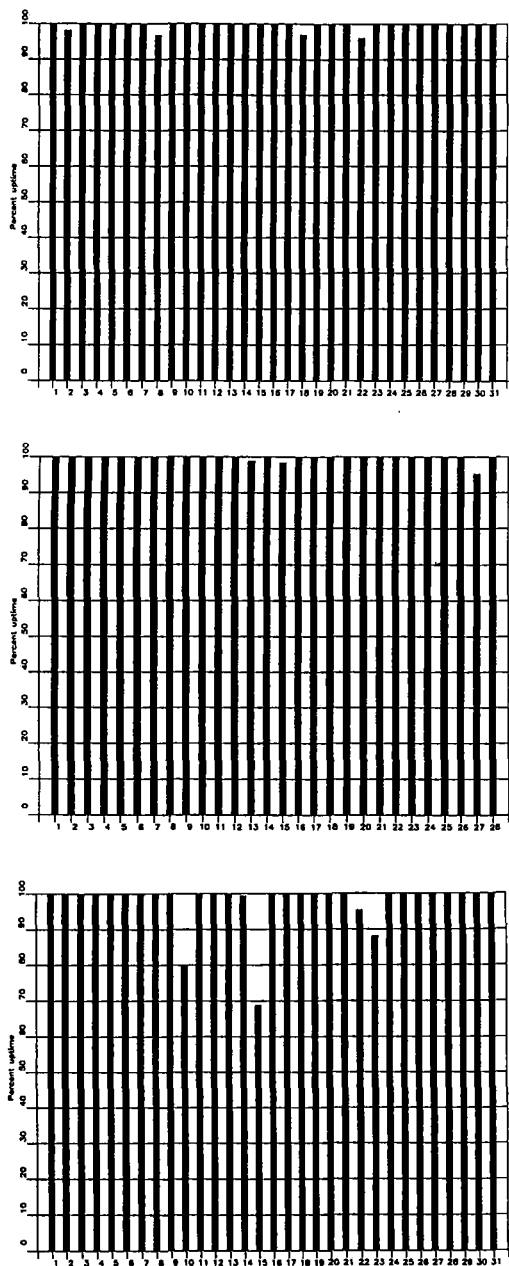


Fig. 3.4.1. (cont.) Spitsbergen data recording uptime for January (top), February (middle) and March (bottom) 1998.

3.5 Event detection operation

This section reports results from one-array automatic processing using signal processing recipes and "ronapp" recipes for the ep program (NORSAR Sci. Rep. No 2-8889).

Three systems are in parallel operation to associate detected phases and locate events:

1. The ep program with "ronapp" recipes is operated independently on each array to obtain simple one-array automatic solutions.
2. The Generalized Beamforming method (GBF) (see F. Ringdal and T. Kværna (1989), A multichannel processing approach to real time network detection, phase association and threshold monitoring, BSSA Vol 79, no 6, 1927-1940) processes the four arrays jointly and presents locations of regional events.
3. The RMS system (Regional Monitoring System; previously referred to as the IMS system (Intelligent Monitoring System) system) is operated on the same set of arrivals as ep and GBF and reports also teleseismic events in addition to regional ones.

RMS results are reported in section 3.6.

NORESS detections

The number of detections (phases) reported from day 274, 1997, through day 090, 1998, was 78,443, giving an average of 490 detections per processed day (160 days processed).

Table 3.5.1 shows daily and hourly distribution of detections for NORESS.

Events automatically located by NORESS

During days 274, 1997, through 090, 1998, 3803 local and regional events were located by NORESS, based on automatic association of P- and S-type arrivals. This gives an average of 23.6 events per processed day (161 days processed). 41% of these events are within 300 km, and 74% of these events are within 1000 km.

ARCESS detections

The number of detections (phases) reported during day 274, 1997, through day 090, 1998, was 95,915, giving an average of 527 detections per processed day (182 days processed).

Table 3.5.2 shows daily and hourly distribution of detections for ARCESS.

Events automatically located by ARCESS

During days 274, 1997, through 090, 1998, 5642 local and regional events were located by ARCESS, based on automatic association of P- and S-type arrivals. This gives an average of 30.8 events per processed day (182 days processed). 53.95% of these events are within 300 km, and 86% of these events are within 1000 km.

FINESS detections

The number of detections (phases) reported during day 274, 1997, through day 090, 1998, was 48,247, giving an average of 265 detections per processed day (182 days processed).

Table 3.5.3 shows daily and hourly distribution of detections for FINESS.

Events automatically located by FINESS

During days 274, 1997, through 090, 1998, 2998 local and regional events were located by FINESS, based on automatic association of P- and S-type arrivals. This gives an average of 16.5 events per processed day (182 days processed). 80% of these events are within 300 km, and 90% of these events are within 1000 km.

GERESS detections

The number of detections (phases) reported from day 274, 1997, through day 090, 1998, was 37,187, giving an average of 185 detections per processed day (180 days processed).

Table 3.5.4 shows daily and hourly distribution of detections for GERESS.

Events automatically located by GERESS

During days 274, 1997, through 090, 1998, 3986 local and regional events were located by GERESS, based on automatic association of P- and S-type arrivals. This gives an average of 20.6 events per processed day (181 days processed). 66% of these events are within 300 km, and 88% of these events are within 1000 km.

Apatity array detections

The number of detections (phases) reported from day 274, 1997, through day 090, 1998, was 46,665, giving an average of 256 detections per processed day (182 days processed).

As described in earlier reports, the data from the Apatity array are transferred by one-way (simplex) radio links to Apatity city. The transmission suffers from radio disturbances that occasionally result in a large number of small data gaps and spikes in the data. In order for the communication protocol to correct such errors by requesting retransmission of data, a two-way radio link would be needed (duplex radio). However, it should be noted that noise from cultural activities and from the nearby lakes cause most of the unwanted detections. These unwanted detections are "filtered" in the signal processing, as they give seismic velocities that are outside accepted limits for regional and teleseismic phase velocities.

Table 3.5.5 shows daily and hourly distribution of detections for the Apatity array.

Events automatically located by the Apatity array

During days 274, 1997, through 090, 1998, 804 local and regional events were located by the Apatity array, based on automatic association of P- and S-type arrivals. This gives an average

of 4.6 events per processed day (182 days processed). 58% of these events are within 300 km, and 78% of these events are within 1000 km.

Spitsbergen array detections

The number of detections (phases) reported from day 274, 1997, through day 090, 1998, was 149,612, giving an average of 891 detections per processed day (168 days processed).

Table 3.5.6 shows daily and hourly distribution of detections for the Spitsbergen array.

Events automatically located by the Spitsbergen array

During days 274, 1997, through 090, 1998, 12,839 local and regional events were located by the Spitsbergen array, based on automatic association of P- and S-type arrivals. This gives an average of 76.0 events per processed day (169 days processed). 49% of these events are within 300 km, and 75% of these events are within 1000 km.

Hagfors array detections

The number of detections (phases) reported from day 274, 1997, through day 090, 1998, was 70,006, giving an average of 391 detections per processed day (179 days processed).

Table 3.5.7 shows daily and hourly distribution of detections for the Hagfors array

Events automatically located by the Hagfors array

During days 274, 1997, through 090, 1998, 2199 local and regional events were located by the Hagfors array, based on automatic association of P- and S-type arrivals. This gives an average of 12.2 events per processed day (180 days processed). 30% of these events are within 300 km, and 72% of these events are within 1000 km

U. Baadshaug

NRS .FKX Hourly distribution of detections

Day	00	01	02	03	04	05	06	07	08	09	10	11	12	13	14	15	16	17	18	19	20	21	22	23	Sum	Date
77	10	3	5	13	16	24	1	9	9	12	8	8	21	24	40	24	27	35	40	22	21	26	27	17	442	Mar 18 Wednesday
78	16	8	7	11	26	7	4	5	8	6	28	10	13	21	13	13	18	16	15	11	5	8	4	2	275	Mar 19 Thursday
79	12	5	4	5	16	11	4	4	3	6	42	13	3	9	6	7	5	5	14	23	7	16	9	9	238	Mar 20 Friday
80	2	2	8	19	22	19	7	6	5	23	19	14	6	28	4	2	13	19	17	6	2	6	7	7	263	Mar 21 Saturday
81	6	13	2	7	4	6	2	4	5	4	2	11	13	8	4	1	5	7	6	0	2	2	5	3	122	Mar 22 Sunday
82	3	3	11	3	13	10	2	1	7	9	19	13	20	19	26	15	13	13	15	23	24	11	3	4	280	Mar 23 Monday
83	14	12	7	11	18	9	9	8	7	13	13	16	10	12	14	12	5	7	12	6	2	16	16	56	305	Mar 24 Tuesday
84	50	19	17	39	46	17	13	14	26	15	9	18	24	15	17	14	13	12	15	14	10	22	13	14	466	Mar 25 Wednesday
85	18	19	21	10	28	12	8	11	10	9	38	22	82	56	25	20	31	35	64	57	65	75	57	67	840	Mar 26 Thursday
86	44	27	92	51	36	8	12	5	13	10	46	41	45	27	22	17	29	12	26	15	28	14	7	17	644	Mar 27 Friday
87	10	4	9	21	28	15	17	20	25	22	11	24	28	21	8	9	36	27	38	39	33	17	12	22	496	Mar 28 Saturday
88	27	40	33	27	45	18	26	22	24	20	47	29	14	19	68	97	107	116	71	34	95	37	67	66	1149	Mar 29 Sunday
89	41	16	15	81	73	79	55	20	47	41	55	67	85	63	65	71	94	103	56	40	63	77	47	61	1415	Mar 30 Monday
90	75	36	18	14	24	6	13	6	17	32	26	43	24	52	65	98	52	58	112	106	132	139	92	65	1305	Mar 31 Tuesday
NRS	00	01	02	03	04	05	06	07	08	09	10	11	12	13	14	15	16	17	18	19	20	21	22	23		
Sum	3209	3269	3302	2609	2761	3060	3530	3412	3575	3635	3127	3391														
	3184	3342	3792	2817	2567	3013	3421	3350	3887	3473	3636	3081	78443	Total sum												
160	20	20	21	20	24	21	18	16	16	17	19	19	21	22	21	21	24	22	22	23	23	20	19	21	490	Total average
111	19	20	23	20	24	19	14	13	14	16	16	18	22	23	21	21	24	23	22	24	23	20	18	20	476	Average workdays
49	21	19	17	21	22	24	27	24	21	21	24	22	20	21	20	22	24	22	21	20	23	18	22	24	522	Average weekends

Table 3.5.1. (Page 4 of 4) Daily and hourly distribution of NORESS detections. For each day is shown number of detections within each hour of the day, and number of detections for that day. The end statistics give total number of detections distributed for each hour and the total sum of detections during the period. The averages show number of processed days, hourly distribution and average per processed day.

ARC .FKX Hourly distribution of detections

Day	00	01	02	03	04	05	06	07	08	09	10	11	12	13	14	15	16	17	18	19	20	21	22	23	Sum	Date
77	15	6	7	8	7	15	7	5	14	24	19	15	18	29	13	13	18	11	14	6	7	3	8	11	293	Mar 18 Wednesday
78	16	6	4	4	22	14	11	7	10	15	21	21	19	29	7	19	11	9	5	10	12	9	6	7	294	Mar 19 Thursday
79	25	9	8	15	6	9	6	17	23	12	16	35	33	26	15	13	25	10	8	9	8	23	15	12	378	Mar 20 Friday
80	12	2	15	10	10	4	0	4	3	7	7	17	8	16	22	11	15	7	20	14	15	6	4	11	240	Mar 21 Saturday
81	9	8	9	10	14	7	4	10	11	10	3	13	24	9	12	15	3	11	12	14	3	9	9	13	242	Mar 22 Sunday
82	7	9	9	5	12	7	4	4	6	19	17	7	23	25	10	17	15	12	10	26	21	14	9	22	310	Mar 23 Monday
83	19	9	5	11	8	7	9	12	13	14	17	23	31	24	27	23	12	10	18	23	12	14	5	8	354	Mar 24 Tuesday
84	19	6	10	29	12	25	18	19	14	21	18	24	24	19	22	18	17	13	14	16	11	14	11	13	407	Mar 25 Wednesday
85	22	9	9	12	16	24	21	16	8	35	21	18	33	22	18	33	26	16	5	9	18	20	25	22	458	Mar 26 Thursday
86	30	16	18	13	10	16	16	5	13	30	7	27	16	18	21	22	14	12	13	22	20	20	13	10	402	Mar 27 Friday
87	25	9	22	10	17	9	7	10	3	13	13	23	24	14	6	13	7	15	7	8	15	8	11	27	316	Mar 28 Saturday
88	25	15	16	31	19	26	26	33	27	12	25	29	19	29	22	23	21	24	26	38	51	31	24	31	623	Mar 29 Sunday
89	27	15	15	23	19	15	12	17	28	19	26	25	30	22	24	26	14	15	10	23	21	19	20	11	476	Mar 30 Monday
90	16	15	20	10	17	11	18	18	16	17	25	27	23	6	19	25	41	34	19	30	37	26	11	26	507	Mar 31 Tuesday
ARC	00	01	02	03	04	05	06	07	08	09	10	11	12	13	14	15	16	17	18	19	20	21	22	23		
Sum	3466	3621	3800	3714	4104	5000	4542	4106	3383	4129	3757	4845														
	4801	3427	3731	3526	3935	4498	5008	4074	4019	3319	3544	3566	95915	Total sum												
182	26	19	19	20	21	21	19	20	22	23	25	27	28	25	22	23	22	19	18	23	19	21	20	27	527	Total average
127	27	20	19	20	20	21	19	19	22	23	25	27	28	26	22	22	22	18	16	22	18	20	19	26	521	Average workdays
55	25	17	19	20	21	21	19	23	21	22	24	27	26	23	22	23	21	19	22	25	22	22	20	28	531	Average weekends

Table 3.5.2.(Page 4 of 4) Daily and hourly distribution of ARCESS detections. For each day is shown number of detections within each hour of the day, and number of detections for that day. The end statistics give total number of detections distributed for each hour and the total sum of detections during the period. The averages show number of processed days, hourly distribution and average per processed day.

FIN .FKX Hourly distribution of detections

Day	00	01	02	03	04	05	06	07	08	09	10	11	12	13	14	15	16	17	18	19	20	21	22	23	Sum	Date	
77	2	4	7	7	5	10	2	3	9	15	18	9	13	22	12	7	22	11	7	3	7	8	5	7	215	Mar 18 Wednesday	
78	3	3	5	4	4	5	3	7	17	10	25	21	10	20	7	7	22	7	9	14	8	5	15	10	241	Mar 19 Thursday	
79	17	10	15	12	18	9	17	17	21	29	33	26	25	15	6	5	9	7	2	6	8	11	12	3	333	Mar 20 Friday	
80	11	12	7	11	6	4	13	8	3	5	11	15	3	3	17	18	26	13	19	15	16	13	17	9	275	Mar 21 Saturday	
81	5	21	16	36	43	45	48	48	41	48	60	41	17	20	8	5	10	6	24	25	23	23	24	15	652	Mar 22 Sunday	
82	9	14	19	24	24	22	22	18	29	49	19	22	15	24	15	27	26	27	19	13	20	16	11	19	503	Mar 23 Monday	
83	8	11	9	18	15	21	13	23	26	35	20	30	24	18	11	13	7	11	10	16	9	11	5	9	373	Mar 24 Tuesday	
84	10	8	11	23	10	8	9	9	16	17	13	13	25	23	26	28	36	28	37	25	22	35	27	40	499	Mar 25 Wednesday	
85	35	31	30	28	25	17	14	13	17	33	37	33	35	39	43	38	36	26	17	20	9	13	6	10	605	Mar 26 Thursday	
86	10	10	6	10	6	5	4	6	10	12	19	14	13	9	15	18	24	9	6	15	8	8	8	11	256	Mar 27 Friday	
87	9	10	11	9	11	12	17	25	27	47	21	7	9	18	27	26	21	11	17	8	6	3	12	6	370	Mar 28 Saturday	
88	10	12	11	20	23	32	29	62	75	63	39	33	38	41	42	37	44	39	26	12	26	15	11	18	758	Mar 29 Sunday	
89	7	8	6	7	11	5	4	11	9	31	32	45	32	36	11	14	13	24	23	36	37	38	44	45	529	Mar 30 Monday	
90	48	41	32	36	33	37	30	30	24	43	34	19	34	32	34	36	22	5	6	3	12	7	7	7	612	Mar 31 Tuesday	
FIN	00	01	02	03	04	05	06	07	08	09	10	11	12	13	14	15	16	17	18	19	20	21	22	23			
Sum	1795	1959	1665	1784	2448	2934	2693	1736	1725	1807	1726	1695															
	1665	1873	1900	1773	2096	2768	2955	2137	1846	1843	1748	1676	48247	Total sum													
182	9	10	10	11	10	9	10	10	12	13	15	16	16	15	12	10	10	9	10	10	10	9	9	9	9	265	Total average
127	9	10	10	10	10	8	8	8	11	14	16	18	18	17	13	10	10	9	9	9	9	9	9	9	9	263	Average workdays
55	8	10	10	13	12	12	13	13	13	11	12	11	11	10	8	9	10	11	11	11	11	11	10	10	10	260	Average weekends

Table 3.5.3. (Page 4 of 4) Daily and hourly distribution of FINESS detections. For each day is shown number of detections within each hour of the day, and number of detections for that day. The end statistics give total number of detections distributed for each hour and the total sum of detections during the period. The averages show number of processed days, hourly distribution and average per processed day.

GER .FKX Hourly distribution of detections

Day	00	01	02	03	04	05	06	07	08	09	10	11	12	13	14	15	16	17	18	19	20	21	22	23	Sum	Date	
77	8	5	1	7	4	5	0	1	27	5	36	10	13	17	8	7	4	7	2	8	6	5	3	6	195	Mar 18	Wednesday
78	3	3	10	2	3	5	1	0	16	7	18	25	15	3	12	10	7	7	10	3	10	7	7	5	189	Mar 19	Thursday
79	6	1	5	11	17	3	5	7	19	23	27	14	17	13	10	4	4	3	5	2	0	11	7	3	217	Mar 20	Friday
80	4	6	4	5	1	8	3	1	7	1	4	12	5	3	7	1	16	14	11	8	7	5	10	3	146	Mar 21	Saturday
81	2	4	1	7	2	2	2	3	5	8	3	2	7	7	5	1	5	1	1	5	1	4	6	5	89	Mar 22	Sunday
82	6	7	8	6	15	4	2	3	5	15	19	19	28	17	7	11	5	2	9	5	13	1	2	4	213	Mar 23	Monday
83	6	7	4	4	5	6	5	3	7	16	11	21	11	14	11	5	8	10	9	7	3	4	2	9	188	Mar 24	Tuesday
84	4	2	4	28	13	10	11	12	16	25	20	30	41	20	17	5	11	11	11	4	6	9	6	3	319	Mar 25	Wednesday
85	3	13	2	4	10	2	11	1	8	18	13	27	19	14	14	15	9	3	4	2	4	2	3	6	207	Mar 26	Thursday
86	7	10	12	9	11	1	2	2	10	28	8	25	19	5	16	0	6	8	3	4	6	9	6	1	208	Mar 27	Friday
87	6	2	5	7	11	4	8	6	11	5	4	10	1	11	2	9	4	2	4	13	3	2	4	2	136	Mar 28	Saturday
88	0	3	1	1	1	8	3	8	4	2	6	4	8	5	2	0	6	0	0	7	16	13	11	12	121	Mar 29	Sunday
89	7	15	12	6	10	5	4	6	20	20	18	21	14	8	8	3	2	10	11	7	12	8	1	0	228	Mar 30	Monday
90	2	9	6	5	0	0	2	5	20	26	18	23	25	19	11	3	5	14	19	13	4	12	5	12	258	Mar 31	Tuesday
GER	00	01	02	03	04	05	06	07	08	09	10	11	12	13	14	15	16	17	18	19	20	21	22	23			
Sum	1058	1225	1117	1280	2506	3128	2417	1454	1111	1059	1021	987															
	1027	1096	1251	1049	1825	3088	3336	2003	1121	1074	1040	914	37187	Total sum													
180	6	6	6	7	7	6	6	7	10	14	17	17	19	13	11	8	6	6	6	6	6	6	5	5	207	Total average	
127	5	6	7	7	7	6	6	7	11	17	20	21	22	16	13	9	6	7	6	6	6	6	5	5	228	Average workdays	
53	6	5	5	6	7	6	5	6	7	7	9	9	11	7	7	6	6	5	5	5	4	5	5	6	150	Average weekends	

Table 3.5.4. (Page 4 of 4) Daily and hourly distribution of GERESS detections. For each day is shown number of detections within each hour of the day, and number of detections for that day. The end statistics give total number of detections distributed for each hour and the total sum of detections during the period. The averages show number of processed days, hourly distribution and average per processed day.

APA .FKX Hourly distribution of detections

Day	00	01	02	03	04	05	06	07	08	09	10	11	12	13	14	15	16	17	18	19	20	21	22	23	Sum	Date	
77	6	5	2	2	2	4	9	5	6	8	9	19	11	14	6	12	4	4	1	4	6	0	0	1	140	Mar 18	Wednesday
78	0	5	1	1	7	3	3	1	7	7	11	8	4	8	4	7	5	6	2	1	7	4	1	2	105	Mar 19	Thursday
79	11	9	4	1	1	1	3	6	11	9	8	4	20	10	10	3	18	3	1	5	1	17	3	0	159	Mar 20	Friday
80	2	3	4	3	4	2	0	8	3	2	2	23	15	2	23	3	12	0	9	2	1	1	4	4	132	Mar 21	Saturday
81	1	6	10	4	2	0	3	4	6	1	0	0	6	2	0	2	3	0	0	0	1	2	0	1	54	Mar 22	Sunday
82	0	3	2	1	5	0	8	0	1	3	7	4	9	9	11	8	3	4	3	9	7	6	8	2	113	Mar 23	Monday
83	0	2	2	3	2	4	6	12	10	6	12	38	32	16	9	3	4	4	3	9	6	3	0	4	190	Mar 24	Tuesday
84	3	1	4	30	6	9	9	8	20	12	10	8	10	17	5	6	11	4	2	4	16	2	0	3	200	Mar 25	Wednesday
85	0	1	5	5	9	6	22	3	9	4	9	15	11	8	13	13	20	11	3	2	2	12	4	2	189	Mar 26	Thursday
86	7	4	2	2	5	8	15	6	12	13	8	16	8	9	10	9	4	9	1	0	0	8	4	0	160	Mar 27	Friday
87	1	5	5	5	1	5	9	7	8	5	19	21	9	6	5	3	7	1	6	4	3	5	8	0	148	Mar 28	Saturday
88	2	1	2	26	9	4	4	7	5	1	4	5	9	6	4	5	7	10	9	5	18	6	2	8	159	Mar 29	Sunday
89	3	5	4	8	4	10	10	7	9	14	4	9	14	7	6	4	4	4	4	2	3	7	12	5	159	Mar 30	Monday
90	6	14	15	11	5	17	9	15	2	6	13	11	6	11	6	21	4	2	10	6	3	2	1	0	196	Mar 31	Tuesday
APA	00	01	02	03	04	05	06	07	08	09	10	11	12	13	14	15	16	17	18	19	20	21	22	23			
Sum	1193	1641	1868	3074	2459	3885	2064	1563	1230	1375	1381	1169	1167	1411	1749	2474	3264	3435	3271	1747	1458	1354	1349	1084	46665	Total sum	
182	6	7	8	9	10	10	14	17	18	14	19	21	18	11	10	9	8	7	7	8	7	8	6	6	256	Total average	
127	8	8	9	10	11	12	16	20	22	15	22	26	21	13	10	9	8	7	8	8	8	8	6	7	292	Average workdays	
55	4	4	6	6	6	6	8	10	9	9	10	11	10	7	8	8	7	5	6	7	6	6	5	5	170	Average weekends	

Table 3.5.5.(Page 4 of 4) Daily and hourly distribution of Apatity array detections. For each day is shown number of detections within each hour of the day, and number of detections for that day. The end statistics give total number of detections distributed for each hour and the total sum of detections during the period. The averages show number of processed days, hourly distribution and average per processed day.

SPI .FKX Hourly distribution of detections

Day	00	01	02	03	04	05	06	07	08	09	10	11	12	13	14	15	16	17	18	19	20	21	22	23	Sum	Date
77	26	24	18	32	25	16	24	24	28	27	10	23	36	23	25	16	14	19	26	14	21	13	8	16	508	Mar 18 Wednesday
78	23	11	5	15	27	16	16	18	32	27	33	29	23	19	26	35	37	40	24	22	27	20	28	23	576	Mar 19 Thursday
79	35	32	19	31	28	34	29	39	8	21	9	25	25	21	22	16	43	24	29	24	27	35	36	24	636	Mar 20 Friday
80	38	27	43	11	26	33	19	13	12	16	14	39	24	25	30	10	62	136	113	120	107	70	77	68	1133	Mar 21 Saturday
81	54	55	76	57	48	1	56	41	39	48	48	34	32	27	22	30	31	17	31	22	32	27	23	16	867	Mar 22 Sunday
82	29	31	26	14	21	3	0	33	25	57	21	27	16	33	20	23	26	22	28	57	83	60	62	39	756	Mar 23 Monday
83	49	53	51	40	52	25	47	48	48	35	40	40	30	23	31	36	32	29	28	25	12	24	25	24	847	Mar 24 Tuesday
84	16	26	22	65	18	14	11	25	8	21	12	17	16	30	28	10	18	10	14	22	7	9	8	18	445	Mar 25 Wednesday
85	9	13	21	18	21	12	10	21	9	18	31	13	18	29	24	27	54	37	33	13	34	22	8	18	513	Mar 26 Thursday
86	38	19	27	19	25	7	30	15	18	21	11	7	19	6	7	10	16	16	19	36	18	19	14	14	431	Mar 27 Friday
87	28	22	23	14	20	17	21	15	17	10	13	17	15	14	10	17	12	14	7	19	24	10	26	12	397	Mar 28 Saturday
88	17	7	17	11	16	9	8	21	13	10	20	7	11	18	25	22	11	43	9	22	29	5	15	33	399	Mar 29 Sunday
89	19	20	12	17	14	22	17	12	12	7	19	12	14	8	11	7	21	20	21	20	23	9	32	16	385	Mar 30 Monday
90	10	30	26	16	14	27	26	30	36	28	23	22	18	18	29	52	29	53	39	35	65	50	40	50	766	Mar 31 Tuesday
SPI	00	01	02	03	04	05	06	07	08	09	10	11	12	13	14	15	16	17	18	19	20	21	22	23		
Sum	6248	6570	6216	6212	5925	6131	6103	6134	6202	6290	6434	6362														
	6289	6302	6471	6439	6068	5941	6299	6030	6249	6243	6209	6245	149612	Total sum												
168	37	37	38	39	39	37	38	37	36	35	35	36	37	36	36	37	37	37	37	37	37	38	37	38	891	Total average
119	36	36	35	39	37	36	36	36	36	35	35	36	37	36	37	36	37	36	38	37	36	38	36	36	871	Average workdays
49	40	40	42	40	41	40	43	40	37	35	37	38	38	38	34	38	37	40	36	38	39	38	41	42	932	Average weekends

Table 3.5.6. (Page 4 of 4) Daily and hourly distribution of Spitsbergen array detections. For each day is shown number of detections within each hour of the day, and number of detections for that day. The end statistics give total number of detections distributed for each hour and the total sum of detections during the period. The averages show number of processed days, hourly distribution and average per processed day.

HFS .FKX Hourly distribution of detections

Day	00	01	02	03	04	05	06	07	08	09	10	11	12	13	14	15	16	17	18	19	20	21	22	23	Sum	Date
77	3	0	2	2	2	7	2	6	5	14	4	8	20	6	6	15	18	13	7	13	10	23	17	26	229	Mar 18 Wednesday
78	35	22	41	42	70	66	72	15	16	13	11	53	8	21	6	3	18	6	10	18	9	28	19	46	648	Mar 19 Thursday
79	76	63	85	77	82	63	19	8	4	3	8	5	4	11	4	8	6	3	7	16	15	26	28	47	668	Mar 20 Friday
80	44	52	77	52	61	63	30	11	10	8	4	16	11	9	8	7	18	5	8	14	6	20	11	22	567	Mar 21 Saturday
81	10	24	36	32	22	5	31	6	5	15	7	13	8	18	11	3	4	3	1	6	7	6	11	5	289	Mar 22 Sunday
82	14	24	50	33	17	7	9	1	1	9	18	6	13	8	18	14	10	5	18	32	53	29	30	33	452	Mar 23 Monday
83	66	70	47	12	16	8	20	5	4	4	15	14	6	10	10	13	3	7	3	10	3	0	5	3	354	Mar 24 Tuesday
84	2	2	1	23	3	5	8	9	5	4	4	7	25	7	15	7	12	3	9	7	3	6	4	2	173	Mar 25 Wednesday
85	13	10	3	6	4	5	4	2	4	6	5	12	11	7	20	8	16	16	3	3	5	4	4	2	173	Mar 26 Thursday
86	6	6	2	4	7	0	12	3	3	1	13	9	17	1	15	4	9	5	0	13	3	5	4	2	144	Mar 27 Friday
87	4	4	5	2	5	2	11	7	5	6	13	11	6	18	9	5	12	6	3	1	8	2	8	10	163	Mar 28 Saturday
88	1	3	12	10	6	9	8	15	4	3	6	8	5	6	7	8	5	2	7	4	25	3	6	11	174	Mar 29 Sunday
89	6	7	3	4	7	7	3	5	3	3	6	10	4	16	9	10	2	4	6	2	4	7	1	3	132	Mar 30 Monday
90	3	4	4	2	3	7	13	4	13	23	31	12	5	21	22	12	15	10	1	3	8	12	3	8	239	Mar 31 Tuesday
HFS	00	01	02	03	04	05	06	07	08	09	10	11	12	13	14	15	16	17	18	19	20	21	22	23		
Sum	2835	3255	3390	2604	3217	2981	3018	2751	2409	2864	2835	2589														
	2735	3087	3422	3262	3012	2891	2832	3084	2445	2999	2713	2776	70006	Total sum												
179	15	16	17	18	19	19	18	15	17	18	16	17	16	17	17	15	14	13	17	16	15	16	16	14	391	Total average
127	16	16	17	18	19	19	16	13	16	17	15	15	17	19	19	16	14	14	18	17	16	16	16	14	393	Average workdays
52	14	16	17	18	19	19	24	18	17	20	19	20	12	12	11	13	11	10	13	13	12	15	14	15	370	Average weekends

Table 3.5.7. (Page 4 of 4) Daily and hourly distribution of Hagfors array detections. For each day is shown number of detections within each hour of the day, and number of detections for that day. The end statistics give total number of detections distributed for each hour and the total sum of detections during the period. The averages show number of processed days, hourly distribution and average per processed day

3.6 Regional Monitoring System operation

The Regional Monitoring System (RMS) was installed at NORSAR in December 1989 and was operated at NORSAR from 1 January 1990 for automatic processing of data from ARCESS and NORESS. A second version of RMS that accepts data from an arbitrary number of arrays and single 3-component stations was installed at NORSAR in October 1991, and regular operation of the system comprising analysis of data from the 4 arrays ARCESS, NORESS, FINESS and GERESS started on 15 October 1991. As opposed to the first version of RMS, the one in current operation also has the capability of locating events at teleseismic distance.

Data from the Apatity array were included on 14 December 1992, and from the Spitsbergen array on 12 January 1994. Detections from the Hagfors array were available to the analysts and could be added manually during analysis from 6 December 1994. After 2 February 1995, Hagfors detections were also used in the automatic phase association.

The operational stability of RMS has been very good during the reporting period. In fact the RMS event processor (pipeline) has had no downtime of its own; i.e., all data available to RMS have been processed by RMS.

Phase and event statistics

Table 3.6.1 gives a summary of phase detections and events declared by RMS. From top to bottom the table gives the total number of detections by the RMS, the number of detections that are associated with events automatically declared by the RMS, the number of detections that are not associated with any events, the number of events automatically declared by the RMS, the total number of events defined by the analyst, and finally the number of events accepted by the analyst without any changes (i.e., from the set of events automatically declared by the RMS).

Due to reductions in the FY94 funding for RMS activities (relative to previous years), new criteria for event analysis were introduced from 1 January 1994. Since that date, only regional events in areas of special interest (e.g, Spitsbergen, since it is necessary to acquire new knowledge in this region) or other significant events (e.g, felt earthquakes and large industrial explosions) were thoroughly analyzed. Teleseismic events were analyzed as before.

To further reduce the workload on the analysts and to focus on regional events in preparation for Gamma-data submission during GSETT-3, a new processing scheme was introduced on 2 February 1995. The GBF (Generalized Beamforming) program is used as a pre-processor to RMS, and only phases associated to selected events in northern Europe are considered in the automatic RMS phase association. All detections, however, are still available to the analysts and can be added manually during analysis.

There is one exception to the new rule for automatic phase association: all detections from the Spitsbergen array are passed directly on to the RMS. This allows for thorough analysis of all events in the Spitsbergen region.

	Oct 97	Nov 97	Dec 97	Jan 98	Feb 98	Mar 98	Total
Phase detections	79166	98079	8493	76725	90213	97726	526845
- Associated phases	7740	7058	4322	5905	6264	6727	38016
- Unassociated phases	71426	91021	80614	70820	83949	90999	488829
Events automatically declared by RMS	1912	1790	1035	1748	1619	1714	9818
No. of events defined by the analyst	407	258	168	200	206	264	1503
No. of events accepted without modifications	0	0	0	1	0	0	1

Table 3.6.1. RMS phase detections and event summary.

U. Baadshaug
B.Kr. Hokland
B. Paulsen

4 Improvements and Modifications

4.1 NORSAR

NORSAR instrumentation

During this reporting period, 1 AIM24 digitizer, 3 Brick amplifiers and 2 KS54000P power supplies have been repaired and reinstalled. The previously reported lightning problems have been significantly reduced by the installation of new protection units.

A block diagram of the remote sensor site components can be found in NORSAR Sci. Rep. No. 1-95/96.

NORSAR data acquisition

The Science Horizons XAVE data acquisition system has been operating satisfactorily during the reporting period. A block diagram of the digitizer and communication controller components is found in NORSAR Sci. Rep No 2-94/95.

NORSAR detection processing and feature extraction

The NORSAR detection processor has been running satisfactorily. To maintain consistent detection capability, the NORSAR beam tables have remained unchanged.

Detection statistics for the NORSAR array are given in section 2.

A description of the NORSAR beamforming techniques can be found in NORSAR Sci. Rep. 2-95/96.

NORSAR event processing

The automatic routine processing of NORSAR events as described in NORSAR Sci. Rep. No. 2-93/94, has been running satisfactorily. The analyst tools for reviewing and updating the solutions have been continuously modified to simplify operations and improve results.

NOA processing at the PIDC

On 5 December 1997 the CCB report for including NOA in the GSETT-3 primary station network was reviewed and approved. Since 13 December 1997, the DFX has processed NOA data and arrivals have been associated and included in the REB.

J. Fyen

5 Maintenance Activities

Activities in the field and at the Maintenance Center

This section summarizes the activities at the Maintenance Center (NMC) Hamar, and includes activities related to monitoring and control of the NORSAR teleseismic array, as well as the NORESS, ARCESS, FINESS, GERESS, Apatity, Spitsbergen and Hagfors small-aperture arrays.

Activities also involve preventive and corrective maintenance, planning and activities related to the refurbishment of the NORSAR teleseismic array.

NORSAR

Visits to subarrays in connection with:

- Cable splicing
- Repair of broken power supply cards in BB seismometers
- Control of power outage due to damage caused by heavy snowfall

NORESS

- Removal, repair and replacement of GPS time receiver
- Removal, repair and replacement of hub power supply unit which had been damaged by lightning
- Repair of remote site electronics
- Replacement of fiber optical transmitter at remotes sites C2 and D4

NMC

- Repair of defective electronic equipment

Additional details for the reporting period are provided in Table 5.1.

P.W. Larsen

K.A. Løken

Subarray/ area	Task	Date
<i>October 1997</i>		
NORSAR		October
01B	Cable splicing at SP01 and SP05.	1-3/10
04C	Cable splicing at SP03.	6/10
02B	Reset 48 VDC power supply	7/10
01B	Cable splicing at SP01, SP02 and SP05	8-9/10
01B	Reinstalled SP05	13/10
04C	Cable splicing at SP01	15-16/10
NMC	Repair of defective electronic equipment.	October
<i>November 1997</i>		
NORSAR		November
02C	Removed the BB seismometer from the borehole. Repaired the broken power supply card. Air and moisture was removed from the seismometer which was then backfilled with one atmosphere of helium before it was reinstalled in the borehole.	5/11
02C	Installed dc/dc converter card and power modification unit at SP00.	6/11
01B	Removed the BB seismometer from the borehole. Repaired the broken power supply card. Air and moisture was removed from the seismometer which was then backfilled with helium before it was reinstalled in the borehole.	7/11
NMC	Repair of defective electronic equipment.	November
<i>December 1997</i>		
NORSAR		December
03C	Disconnected data cable from remote site SP05 at the CIM port. The GPS output is framed incorrectly.	20/12

Subarray/ area	Task	Date
02B	The data output from the digitizer at SP03 had a lot of gaps due to a bad communications cable. Disconnected transmit line at the remote site.	22/12
NMC	Repair of defective electronic equipment.	December
<i>January 1998</i>		
NORSAR		January
01A	Visited site due to power outage. The main power line was found to have been cut by falling trees caused by heavy snowfall.	2/1
02B	The main power line was found to have been damaged by heavy snowfall	7/1
NORESS	The GPS time receiver was found to be out of lock and not working properly. The unit had to be taken to NMC for repair.	15/1
NMC	Repair of defective electronic equipment. Repair and testing of Hub unit from ARCESS	January
<i>February 1998</i>		
NORESS	Reinstalled the GPS time receiver after repair at NMC. The Hub power supply unit was found to have been damaged by lightning and had to be take to NMC for repair	4/2
	Reinstalled the Hub power supply unit. With the power unit running again, we found that lightning had damaged more of the installation. The KS-36000 broadband seismometer and the remote sites C2, C4, C5, C7, and D4 were not working.	6/2
	Repair of remote site electronics at sites C2, C4, C5, C7, and D4.	9-12/2

Subarray/ area	Task	Date
NMC	The down-hole power supply for the KS-36000 seismometer was found to be defective. The seismometer has to be removed from the 60 m deep borehole before it can be repaired.	16-18/2
	Replaced the remote sites 32 VDC power supply.	23/2
	Repair of defective electronic equipment.	February
<i>March 1998</i>		
NORESS	Replaced power supply at remote site A0. Replaced fiber optical transmitter at remote sites C2 and D4.	20/3
NMC	Repair of defective electronic equipment	March

Table 5.1. Activities in the field and the NORSAR Maintenance Center during 1 October 1997 - 31 March 1998.

6 Documentation Developed

Asming, V.E., E.O. Kremenetskaya & F. Ringdal (1998): Monitoring seismic events in the Barents/Kara Sea region, *Semiannual Technical Summary, 1 October 1997 - 31 March 1998*, NORSAR Sci. Rep. 2-97/98, Kjeller, Norway.

Baadshaug, U., S. Mykkeltveit & J. Fyen (1998): Status Report: Norway's participation in GSETT-3, *Semiannual Technical Summary, 1 October 1997 - 31 March 1998*, NORSAR Sci. Rep. 2-97/98, Kjeller, Norway.

Hicks, E. (1998): Accurate location of seismic events in northern Norway using a local network, and implications for regional calibration of IMS stations, *Semiannual Technical Summary, 1 October 1997 - 31 March 1998*, NORSAR Sci. Rep. 2-97/98, Kjeller, Norway.

Kværna, T. & F. Ringdal (1997): Event magnitudes, capability maps and magnitude thresholds. Expanded Abstract, Proc. 19th Annual Seismic Research Symposium on Monitoring a Comprehensive Test Ban Treaty, September 1997.

Kværna, T. & F. Ringdal (1998): Seismic Threshold Monitoring for continuous assessment of global detection capability, *Semiannual Technical Summary, 1 October 1997 - 31 March 1998*, NORSAR Sci. Rep. 2-97/98, Kjeller, Norway.

Mykkeltveit, S., B.Kr. Hokland & B. Paulsen (1998): Development of a regional database for seismic event screening, *Semiannual Technical Summary, 1 October 1997 - 31 March 1998*, NORSAR Sci. Rep. 2-97/98, Kjeller, Norway.

Schweitzer, J., F. Ringdal and J. Fyen (1998): The Indian nuclear explosions of 11 and 13 May 1998, *Semiannual Technical Summary, 1 October 1997 - 31 March 1998*, NORSAR Sci. Rep. 2-97/98, Kjeller, Norway.

Semiannual Technical Summary, 1 April - 30 September 1997, NORSAR Sci. Rep. 1-97/98, Kjeller, Norway.

Taylor, L. (1998): Threshold Monitoring: Summary of pipeline processing, *Semiannual Technical Summary, 1 October 1997 - 31 March 1998*, NORSAR Sci. Rep. 2-97/98, Kjeller, Norway.

7 Summary of Technical Reports / Papers Published

7.1 Seismic Threshold Monitoring for continuous assessment of Global detection capability

Summary

Continuous seismic threshold monitoring is a technique that has been developed over the past several years to use a seismic network for monitoring a geographical area continuously in time. The method provides, at a given confidence level, a continuous assessment of the upper magnitude limit of possible seismic events that might have occurred in the target area. In this paper we expand upon previous work to apply the method to a global network of seismic stations, and give examples of application from a prototype system which will eventually be installed at the International Data Center for monitoring the comprehensive nuclear test ban treaty.

Using a global grid of 2562 geographical aiming points, we compute site-specific threshold traces for each grid point, and apply spatial interpolation to obtain full global coverage. For each grid point, the procedure is in principle to "focus" the network by tuning the frequency filters and array beams using available information on signal and noise characteristics at each station-site combination. Generic phase attenuation relationships and standard travel-time tables are used in this initial implementation, but the system lends itself easily to applying station-site specific corrections (magnitudes, travel-times, etc.) to each seismic phase.

We give examples of two main types of applications based on data from a world-wide seismic network: a) an estimated continuous *global threshold level* and b) an estimated continuous *global detection capability*. The first application provides a continuous view of the global seismic "background field" as calculated from the station data, with the purpose to assess the upper magnitude limit of any seismic event that might have occurred around the globe. The second application introduces detection thresholds for each station and provide a simplified estimate, continuously in time, of the n-station detection capability of the network. The latter approach naturally produces higher threshold values, with the difference typically being 0.5-1 magnitude unit. We show that both these approaches are useful especially during large earthquakes, where conventional capability maps based on statistical noise and signal models cannot be applied.

In order to illustrate the usefulness of combining the global monitoring with site-specific monitoring for areas of special interest, we consider a large earthquake aftershock sequence in Kamchatka and its effect on the threshold trace in a very different region (the Novaya Zemlya nuclear test site). We demonstrate that the effects of the aftershock signals on the thresholds calculated for Novaya Zemlya are modest, partly due to the emphasis on high-frequency signals. This indicates that threshold monitoring could provide significantly improved event detection during aftershock sequences compared to conventional methods, for which the large number of detected phases tends to cause problems in the phase association process.

Introduction

Traditionally, assessments of seismic network detection capabilities are based upon assuming statistical models for the noise and signal distributions. These models include station correc-

tions for signal attenuation and a combinational procedure to determine the detection threshold as a function of the number of phase detections required for reliable location (Sykes & Evernden 1982; Harjes, 1985; Hannon 1985; Ringdal 1986; Sereno & Bratt, 1989).

In general, it is implicitly understood that any network will have a detection threshold that varies with time. It is important to retain such information along with the information on the average capability. However, with methods being used in practical operation today, no attempt is made to specify the time-dependency of the calculated threshold. For example, the noise models used in these capability assessments are not able to accommodate the effect of interfering signals, such as the coda of large earthquakes, which may cause the estimated thresholds to be significantly degraded at times. Furthermore, only a statistical capability assessment is achieved, and no indication is given as to particular time intervals when the possibility of undetected seismic events is particularly high, for example during unusual background noise conditions or outages of key stations.

The continuous threshold monitoring technique has been developed to address these problems. The basic principles were described by Ringdal & Kväerna (1989, 1992), who showed that this method could be useful as a supplement to event detection analysis. In this paper we expand further on the utility of this method, with particular emphasis on seismic threshold monitoring on a global scale, using a world-wide network. Some examples are given on how such monitoring could be achieved in a practical system, which will eventually be implemented at the International Data Center for monitoring a Comprehensive Test Ban Treaty (CTBT).

Approaches to threshold monitoring

The capability achieved by the threshold monitoring method is in general dependent upon the size of the target area, and it is convenient to consider three basic approaches:

Site-specific threshold monitoring: A seismic network is focused on a small area, such as a known test site. This narrow focusing enables a high degree of optimization, using site-station specific calibration parameters and sharply focused array beams.

Regional threshold monitoring: Using a dense geographical grid, and applying site-specific monitoring to each grid point, threshold contours for an extended region are computed through interpolation. In contrast to the site-specific approach, it is usually necessary to apply generic attenuation relations, and the monitoring capability will therefore not be quite as optimized.

Global threshold monitoring: This is a natural extension of the regional monitoring approach, but requires a somewhat different strategy for effective implementation. Using a global network, and taking into account that phase propagation time is up to several tens of minutes, it is necessary to establish elaborate global travel-time and attenuation tables, and to use a much coarser geographical grid than in the regional approach.

The regional and global monitoring techniques provide geographical threshold maps that have several advantages over standard network capability maps. They are far more accurate during time intervals when interfering seismic events occur. They can also more easily reflect special conditions such as a particularly favorable source-station propagation paths, and have the advantage of not being tied to specific event detection criteria.

In this paper, an overview is given of the underlying principles for continuous threshold monitoring on a global scale.

Method description

Generating the threshold trace

Let us assume that a network of seismic stations are available for monitoring a specified target site. For simplicity of presentation, we will assume that these are all array stations, able to provide phase velocity and azimuth information for detected signals. Extension to the single-station case is straightforward. The stations can be located either at regional or teleseismic distances.

Following Ringdal & Kværna (1992), let us consider a network of seismic stations ($i=1,2,\dots,N$) and a number of seismic phases ($j=1,2,\dots,M$). For a seismic event of magnitude $m_b=m$ an estimate \hat{m}_{ij} of m is given by

$$\hat{m}_{ij} = \log S_{ij} + b_j(\Delta, h) \quad (1)$$

where S_{ij} is the measured signal power of the j -th phase at the i -th station

$b_j(\Delta, h)$ is a distance-depth correction factor for the j -th phase.

In standard formulas for magnitude, the signal power S_{ij} is usually estimated as A/T , i.e., amplitude divided by dominant signal period. In our case, we will assume that S_{ij} is the measurement of signal power (e.g., short term average, STA) at the expected signal arrival time. The value is measured on an array beam or a single channel filtered in an appropriate frequency band.

Traditionally, the relation (1) is defined only for the time window corresponding to a detected seismic event. We will now consider the righthand side of (1) as a continuous function of time. Define the "threshold parameter" $a_{ij}(t)$ as follows:

$$a_{ij}(t) = \log S_{ij}(t) + b_j(\Delta, h) \quad (2)$$

The equation (2) represents a function which can be considered as a continuous representation of the upper magnitude limit for a hypothetical seismic event at a given geographical location (target region). It coincides with the event magnitude estimate if an event occurs at that site. The function is, by definition, tied to a specific station and a specific phase.

Using a statistical approach, and assuming statistical independence of the observations, we can now proceed as described by Ringdal and Kværna (1989). After time-aligning the threshold traces to correspond to the target area, we obtain a network-based representation of the upper magnitude limit by considering the function:

$$g(m, t) = 1 - \prod_{i,j} \left(1 - \Phi \left(\frac{(m - a_{ij}(t))}{\sigma_{ij}} \right) \right) \quad (3)$$

where m is event magnitude, σ_{ij} is the standard deviation of the assumed magnitude distribution for the i -th station and j -th phase and Φ denotes the standard (0,1) normal distribution function.

The function $g(m, t)$ is the probability that a given (hypothetical) seismic event of magnitude m at time t would generate signals that exceed the observed noise values at at least one station of the network. For a given t , the function $g(m, t)$ is a monotonously increasing function of m , with values between 0 and 1. A 90% upper limit at time t is defined as the solution to the equation

$$g(m, t) = 0.90 \quad (4)$$

The solution is a function of t , which we will denote $n_{T90}(t)$. We call this the *threshold trace* for the network and target region being considered.

Calculating a "detection capability" trace

The *threshold trace* developed above is not directly related to the *detection capability* of the network in the usual sense. Nevertheless, the general method described above can easily be used to obtain a continuous estimate of the network n -station detection capability. In order to do this, we must add the required signal-to-noise ratio (SNR) to each individual station threshold trace and adjust the level to correspond to a probability level of 90% for phase detection at each station. Let us denote by T_{ij} the SNR (in log units) required for detection at the i 'th station and the j 'th phase, and denote by $d_{ij}(t)$ the corresponding station detection threshold (in magnitude units). Further, let σ_{ij} denote the assumed standard deviation of the (hypothetical) signal. We then obtain:

$$d_{ij}(t) = a_{ij}(t) + T_{ij} + \mu_{90} \cdot \sigma_{ij} \quad (5)$$

where $\mu_{90} = 1.282$ is the 90% quantile in the standard normal distribution function. In this particular connection, let us for simplicity consider only P-type phases (the extension to the general case is obvious). Eliminating the index j , we order the individual station detection thresholds so that:

$$d_1(t) \leq d_2(t) \leq \dots \leq d_N(t) \quad (6)$$

We define the M -station network detection threshold at time t as the magnitude value $d_M(t)$. For a hypothetical event at this magnitude we would then expect at least M stations to exceed their respective detection thresholds, thus allowing for a network detection of the hypothetical event.

We note that this formulation is quite different from the standard methods for network detection threshold estimation (Harjes, 1985) for several reasons:

- Standard methods assume a statistical distribution of noise and signal amplitude levels, while our approach covers the actually recorded seismic field continuously
- Standard methods employ a somewhat more complicated combinatorial technique, that we have simplified by ordering the individual station thresholds by increasing magnitude.

We can in fact apply a variant of the standard method to use the actually recorded seismic field instead of a statistical noise model. Define the detection probability $P_i(m)$ of the i th station by using the same notation as in (3), but without the time variable t and the phase index j :

$$P_i(m) = \Phi\left(\frac{(m - (a_i + T))}{\sigma_i}\right) \tag{7}$$

We assume that the probability of detection is statistically independent among the stations in the network. Setting for simplicity of notation $P_i = P_i(m)$, the probability $P(K/m)$ that exactly K out of the N station will detect the event (given its magnitude m) becomes:

$$P(K/m) = \sum_{(i_1 < i_2 < \dots < i_K)} (P_{i_1}) \cdot (P_{i_2}) \cdot \dots \cdot (P_{i_K}) \prod_{(j \neq i_1, i_2, \dots, i_K)} (1 - P_j) \tag{8}$$

By summing terms as above we will obtain the probability that at least M out of N stations detect the event. The 90% detection threshold for M -station detection is thus the solution of the equation:

$$1 - \sum_{K=0}^{M-1} P(K/m) = 0.90 \tag{9}$$

It would be feasible, given sufficient computer resources, to calculate the detection thresholds in this "combinatorial" way on a continuous basis by using the individual station threshold traces as input. We have found, however, by studying various examples, that our simplified calculation based on eq. (6) gives generally consistent results with such combinatorial calculations, and that the divergences are in practice in the range 0-0.2 magnitude units. This is well below the inherent uncertainties in either method. We therefore use the simplified method in presenting our continuous global network detection threshold estimates.

Applying distance-depth corrections

Let us first consider threshold monitoring of a specific target area of limited geographical extent. The size of the target area may vary depending upon the application, but typically such an area might be a few tens of kilometers in diameter. A basic assumption is that the target area is defined such that all seismic events within the area show similar wave propagation characteristics.

The distance-depth correction factors $b_j(\Delta, h)$ in (1) and (2) can either be determined by using "generic" values representative for a larger region, or by calibration to the specific target area. The latter method is the most accurate and is preferable, assuming that previous calibration events are available. We then obtain the necessary magnitude calibration factors from processing previous events with known magnitude, using the relation

$$\hat{b}_{i,j} = \hat{m}_j - \log(\hat{S}_{i,j}) \quad (i = 1, \dots, K; j = 1, \dots, L) \tag{10}$$

where $\hat{b}_{i,j}$ is our estimate of the magnitude correction factor for phase i and event j , \hat{m}_j is the estimate of the magnitude for event j (based on independent network observations), and $\hat{S}_{i,j}$ is our estimate of the signal level at the predicted arrival time of phase i for event j . K is the num-

ber of phases considered (there might be several stations and several phases per station), and L is the number of events.

The magnitude correction factor to be used for phase i is then given by

$$b_i = \frac{1}{L} \cdot \sum_{j=1}^L \hat{b}_{i,j} \quad (11)$$

Parameters such as window lengths for signal level estimation, travel-times of the different phases, filter frequency bands and steering delays for array beamforming are obtained on the basis of processing results for the calibration events.

Developing a global grid

In principle, global threshold monitoring can be achieved by conducting site-specific monitoring of a grid of target points covering the globe. The density of the grid and the interpolation technique applied will determine the quality of the results.

We have adopted the method described by Vinje et al (1992) to develop global grid point systems. This method applies triangulation of an icosahedron to construct regularly sampled wavefronts, and provides close to uniform geographical coverage of the globe at a specified grid density (Kværna, 1992).

The grid density to be used in practice is mainly a cost-performance trade-off. We have chosen a 2562-point grid for the initial version of a global threshold monitoring system. This grid is shown in Figure 1, and corresponds to a radius of approximately 2.7 degrees for the area covered by each grid point.

It is important to be aware that the density of the global grid is quite different from the beam deployment density for the arrays in the station network. For each array, a certain number of steering points will be selected (typically a few tens for a small or medium aperture array, and more than 100 for a large array). When calculating the threshold traces for a given global grid point, the closest beam steering point is selected. Thus, there will be a potential beam steering loss that must be taken into account when calculating the "representative" threshold for the area represented by the global grid point.

The beam steering loss is mainly a function of array aperture and signal frequency. An illustration for the ASAR array is given in Figure 2, showing 3 dB beam loss contours for the selected filter band for that array (1.0-4.5Hz). These loss contours are circles when shown in inverse velocity space, and the steering points therefore do not translate into equidistant geographical points. Thus, if mainly teleseismic distances are considered, the number of steering points for a given worst-case loss will be modest. In our calculations, we have set the beam density in such a way that the maximum expected missteering loss is 3dB.

Calibration and time/azimuth tolerances

Ideally, global threshold monitoring requires access to magnitude calibration statistics for each target point and each station/phase combination considered. In a practical situation it will usually be impossible to obtain the necessary number of calibration events for each target point in the grid, and a different approach is therefore required.

Our approach is to develop a set of "generic" attenuation models. This can be done as a two-step process. The first step is to divide the earth into regions that are relatively homogeneous with respect to wave propagation characteristics. Within each region, an attenuation model is then established on the basis of available calibration data.

Using this approach, the distance-depth correction factors $b(\Delta, h)$ in (1) can be determined individually for each seismic phase, by applying a standard global attenuation model, in combination with region-specific station corrections.

In threshold monitoring there is a trade-off between the size of the target area and the tolerances of the parameter values used in the threshold computations. With a given grid, it is necessary to make the tolerances of each aiming point compatible with the grid spacing.

An illustration of the time and azimuth tolerances is given in Kværna et. al. (1994). For example, if we increase the time windows over which we measure the signal levels, this has the effect of broadening the target area for the aiming point. At the same time, some of the resolution in the regional threshold variation will be lost. The necessary time window corresponding to a typical teleseismic distance is of the order of ± 1 minute. A similar consideration applies to azimuth and slowness tolerances.

Parameter settings

General considerations

The basic components in global threshold monitoring are the stations in the network and the set of grid points. A station can be an array, a three-component station or a single-component station. The type of seismometer, digitizer, sampling rate and response function can vary, although for the purpose described here we will restrict ourselves to the short period processing band (typically 0.5 Hz and higher). A grid point is an aiming point in geographical space.

In global threshold monitoring, the number of grid points and their density and distribution may vary according to the available network, the monitoring requirements and the computing facilities available.

For each station, the following information is required:

- Latitude, longitude, height
- Types and deployments of sensors
- System response
- Sampling rate
- Number of beams
- Beam steering points and filter bands
- STA lengths and update rates

For each station/grid point combination, the following information is required:

- Latitude, longitude, depth
- Grid spacing
- A phase type indicator for each phase used
- Pointers to the nearest beams

- Station-site specific corrections if available (magnitude, travel-time etc.)

Beam deployment

The beam deployment is made taking into account the need for regional characterization (for non-arrays as well as arrays) and the allowable worst-case beam loss for the appropriate regional coverage. The beam configurations are set so as to obtain the optimum SNR for the actual beam in the frequency band used. The SNR is defined as the signal strength relative to the normal noise conditions.

Filter bands

The filter bands are set for each grid point-station-phase combination and should be designed for optimum SNR for all events of interest in the area covered by the grid point. Initially, we use a set of generic, wide-band filters, typically 0.8-4.5 Hz, but usually with higher frequency bands at local and regional distances (Kvørna, 1996). Furthermore, the selection of filter band also depends upon the typical signal and noise spectra at the station. The filter bands will be refined on an individual station basis as experience accumulates.

STA calibration

Since STA values are used instead of A/T as a basis for magnitude estimates, it is necessary to introduce a conversion formula. From experiments with different short-period instrument types, we have found that such a relation can be well parameterized in the following way:

$$\log(A/T) \approx \log((\pi/2)STA \times cal_{1,0}) + c(resp, filter) \quad (12)$$

where $cal_{1,0}$ is the instrument calibration factor at 1 Hz, and c is a constant that is dependent on the instrument response and the filter band used to calculate the STA value (Kvørna, 1996). The constant c is derived empirically for each instrument and the filter band, as illustrated in Figure 7.1.3.

Initial IDC implementation

The initial IDC implementation comprises the following main features:

- Continuous global detection capability map
- 2562 grid points
- 10 seconds update rate
- 7-day diskloop of STA values and capability maps
- Hourly summaries of station availability and background noise levels
- Hourly average and worst-case global capability maps

Provision for extracting site-specific traces will be implemented as a future option. It should be noted that such site-specific traces will initially be represented by the trace of the closest global grid point. "Optimum" site-specific traces could later be generated for regions where sufficient calibration information is available, as we will show in an example later.

Analysis results

Based on the raw data, three sets of results are generated by the automatic global threshold monitoring system on an hourly basis. These quantify both the network detection capability of the primary seismic network for monitoring the CTBT, and provide information on factors causing a possible degradation of this detection capability. A set of results from the TM system, describing the network detection capability for the one-hour interval 1998/05/11 10:00 to 11:00 is given in the following:

- The first set of results, (see example in Section 7.2, Figure 7.2.2), provides information on the data availability and interfering events for the particular 1-hour interval. The color of the station symbols provide information on the availability of data for a particular 1-hour interval (1998/05/11 10:00 to 11:00). The arrays are marked by circles and three-component stations by triangles. Notice that for the interval reported, several of the stations were out of operation for all or part of the time. The locations of events in the Reviewed Event Bulletin (REB) during the actual time interval are plotted, and the event information is given below the map. Notice the occurrence of the Indian nuclear explosion (m_b 5.0)
- The second set of results (see example in Section 7.2, Figure 7.2.3) is an overview of the background noise level and the observed signals at each of the primary stations during the data interval (1 hr 22 min 20 s) used for assessing the detection capability of the 1 hour interval. The traces shown are continuous log (A/T) equivalents derived from the STA traces. Notice in particular the signals from the m_b 5.0 event in India (origin time 10:13:44) seen at most stations of the primary network. The percentages of successfully recorded and processed data are also given for each station, and the intervals with gaps in data processing are indicated in red above the time axis.
- The third set of results (see example in Section 7.2, Figure 7.2.4), is a periodic capability map. The upper map of the figure shows the average network detection capability for the 1-hour interval (1998/05/11 10:00 to 11:00). Variation from hour to hour of the average detection capability is primarily caused by longer station or processing outages, by increased background noise levels at the different stations, or by signals of long duration from large seismic events. The lower map shows the worst-case detection capability for the analyzed hour. Differences from the average capability are primarily caused by signals from seismic events, short outages and data quality problems. Notice that the m_b 5.0 event in India temporarily causes a degradation of the detection capability all over the world, and in particular in the vicinity of the actual event location.

Both types of maps shown in Section 7.2, Figure 7.2.4 provide important information on the capability of the primary seismic network to detect events in different parts of the world, and the information provided in Section 7.2, Figures 7.2.2 and 7.2.3 will help to explain the variations in the global event detection capability.

The sets of results provided by the global threshold monitoring system are in this way useful for assessing the performance of the International Monitoring System, and also by giving a warning in the case of lowered monitoring capability, e.g., caused by station outages, communication problems, data processing problems or extremely high seismic activity.

Figure 7.1.4 illustrates the two different approaches to describe the global seismic field using as an example a snapshot of the threshold levels during a time without significant seismic activity:

- *Global threshold level:* The top part of Figure 7.1.4 displays the “global threshold level” for the time instance considered. We recall that this level describes the “background seismic field”, with no allowance made for station detection thresholds and no requirement for station detection. The map thus shows the actually observed seismic field as seen by the network.
- *Global detection capability:* The bottom part of Figure 7.1.4 corresponds to the 3-station detection capability for the time instance considered. Note that the levels are considerably higher than in the top part of the figure, with the difference exceeding one full magnitude unit in some cases. This shows that the two approaches, although quite similar in many aspects, complement each other and provide information that could be useful in different ways.

Figure 7.1.5 illustrates the variation in global detection capability before and during a large earthquake. Four snapshots of the global detection capability of the network are shown, using a requirement of at least 3 detecting stations. There is a significant increase in the threshold levels at the time of the event, first locally and later spreading out to cover the entire world. After about 30 minutes (not shown in the figure), the levels are back to “normal”.

Figure 7.1.6 shows an example of how the site-specific threshold monitoring technique can be used to supplement the global monitoring during a large earthquake followed by a large aftershock sequence. The figure shows threshold traces steered toward the Novaya Zemlya Test Site using the four IMS arrays ARCES, NORES, FINES and SPITS for the day 5 December, 1997. That day, a large (MS 7.7) earthquake occurred near E. coast of Kamchatka, followed by a very large aftershock sequence (at least 200 aftershocks during the first 12 hours detected teleseismically). There were also many “foreshocks” preceding this event. The plot shows the individual P-phases (STA traces) for each of the four arrays, with the combined network threshold monitoring trace on top. The network trace includes P and S on SPITS and ARCES, P for FINES and P for NORES. The individual arrays have large numbers of peaks corresponding to these aftershocks, whereas the network threshold trace is almost unaffected by the aftershock sequence. This shows that, when using the threshold monitoring technique, the Novaya Zemlya monitoring capability remains about the same if a large earthquake sequence occurs at a place far from the test site. We should note, however, that such good performance would not have been achieved if the sequence had taken place near the target area to be monitored.

We also add that the excellent capability of the site-specific technique as demonstrated above is due, to a large part, to our emphasis on high-frequency passbands in the regionally based site-specific monitoring. In fact, the advantages of our approach can be seen as being caused by three main factors:

- Large earthquakes tend to have predominantly low frequency energy. The resulting increase in the background “seismic field” is therefore much larger at frequencies around 1 Hz than at frequencies in the range 4 Hz and above. This means that stations recording high-frequency signals will be less affected by the interfering signals from such earthquakes.

- The coda of a large earthquake tends to last for several minutes in the short period band (and much longer for long period (20 seconds) signals), thus degrading the global detection capability for an extended period of time. The coda dropoff is much faster at higher frequencies, as shown by an example in Figure 7.1.7. This adds to the effect described above as far as improving the event detection capability in the earthquake coda is concerned.
- High-frequency arrays as used in our example from Novaya Zemlya have the added advantage of suppressing the noise (or signal coda) from interfering events, and retain signal coherency even at high frequencies. This further adds to the capability of detecting small events in the background of a large earthquake.

Discussion

The continuous threshold monitoring technique represents a new approach toward achieving reliable seismic monitoring. The method is well suited to supplement the traditional methods in monitoring potential test sites for the purpose of verifying a comprehensive nuclear test ban treaty. The method may equally well be used to monitor earthquake activity at low magnitudes for sites of special interest, and could also be useful for monitoring earthquake aftershock sequences. The system described here is intended to demonstrate how the concept is used in practice to enable threshold monitoring on a global basis, with applications to real-time displays.

The fact that the coda of a large earthquake tends to last for several minutes in the short period band, and much longer for long period (20 seconds) signals, has traditionally caused a significant degradation of the global detection capability of existing global networks (Bache and Bratt, 1985). While this problem cannot be entirely eliminated, we have shown that the threshold monitoring technique holds promise to reduce the adverse effects on the global detection capability. Further improvements might be achievable by extensive calibration, systematic utilization of regional networks and emphasis on the high-frequency passbands.

In principle, the global method, given enough calibration data and computer resources, could be expanded to approach the capability of the site-specific method for each target point. However, in practice, there will be a need to apply both methods in day-to-day monitoring. Another consideration here is that the site-specific method could be further optimized e.g. by considering different filter bands in parallel and applying specially generated digital filters to search for signals conforming to predetermined characteristics. We are currently investigating the feasibility and benefits of this type of optimization.

It is important to be aware that the main purpose of the threshold monitoring method is to call attention to any time instance when a given threshold is exceeded. This will enable the analyst to focus his efforts on those events that are truly of interest in a monitoring situation. He will then apply other, traditional analysis tools in detecting, locating and characterizing the source of the disturbance. Thus, the threshold monitoring method is a supplement to, and not a replacement of, traditional methods. There are four main factors that cause variations in the event detectability of the primary seismic network. These are:

- Fluctuations with time in the background noise level
- Changes in data quality at the IDC caused by communications problems, station outages or other data errors like spikes and gaps

- Temporary deficiencies in the IDC data processing
- Signals from interfering seismic events around the world.

Traditional methods for assessing the network detection capability use statistical models for the noise and signal distributions to calculate the detection thresholds as a function of the number of phase detections required for defining an event (Sykes & Evernden 1982; Harjes, 1985; Hannon 1985; Ringdal 1986; Sereno & Bratt, 1989). The noise models used in these capability assessments are not able to accommodate the effect of interfering signals, such as the coda of large earthquakes, which may cause the estimated thresholds to be quite unrealistic at times. Neither can these methods include effects like communication problems and data processing deficiencies.

The threshold monitoring approach incorporates all of the effects listed above, and will provide a valuable supplement to conventional techniques in the assessment of the detection capability of a global seismic network.

As discussed by Ringdal and Kværna (1992), continuous threshold monitoring offers a valuable supplement to traditional seismic techniques used in nuclear test ban monitoring. The method may also be useful for monitoring earthquake activity at low magnitudes for sites of special interest, as well as for monitoring earthquake aftershock sequences.

We will be continuing this study in order to characterize the long-term capabilities of the TM method for global and site-specific monitoring. At the same time, we are working on a streamlining and optimization of the technique, that should improve the performance further. These efforts will be documented in detail in a separate paper.

Acknowledgement

This research has been sponsored by the Nuclear Treaty Programs Office of the U.S. Department of Defense and monitored by the Air Force Technical Applications Center under contract no. F08650-96-C-0001.

Tormod Kværna
Frode Ringdal

References

- Bache, T.C. and S.R. Bratt (1985): High frequency P-wave attenuation and degradation of detection capability by large earthquakes, *Report No. AFGL-TR-85-0211*, SAIC, San Diego, California.
- Hannon, W. (1985): Seismic verification of a comprehensive test ban, *Science*, 227, 251-257.
- Harjes, H.-P. (1985): Global seismic network assessment for teleseismic detection of underground nuclear explosions, *J. Geophys.*, 57, 1-13.

- Kværna, T. (1991): Initial development of generic relations for regional threshold monitoring, *Semiannual Tech. Summ.*, 1 Apr - 30 Sep 1990, NORSAR Sci. Rep. 1-90/91, NORSAR, Kjeller, Norway.
- Kværna, T. (1992): Initial results from global Generalized Beamforming, *Semiannual Tech. Summ.*, 1 Apr - 30 Sep 1992, NORSAR Sci. Rep. 1-92/93, NORSAR, Kjeller, Norway.
- Kværna, T. (1996): Tuning of processing parameters for Global Threshold Monitoring at the IDC, *Semiannual Tech. Summ.*, 1 Apr - 30 Sep 1996, NORSAR Sci. Rep. 1-96/97, NORSAR, Kjeller, Norway.
- Ringdal, F. (1986): Study of magnitudes, seismicity and earthquake detectability using a global network, *Bull. Seism. Soc. Am.*, 76, 1641-1659.
- Ringdal, F. & T. Kværna (1989): A multichannel processing approach to real time network detection, phase association and threshold monitoring, *Bull. Seism. Soc. Am.*, 79, 1927-1940.
- Ringdal, F. & T. Kværna (1991): Continuous threshold monitoring using "regional threshold displays", *Semiannual Tech. Summ.*, 1 Oct 90 - 31 Mar 91, NORSAR Sci. Rep. 2-90/91, NORSAR, Kjeller, Norway.
- Ringdal, F. & T. Kværna (1992): Continuous seismic threshold monitoring, *Geophys. J. Int.*, 111, 505-514.
- Sereno, T.J. & S.R. Bratt (1989): Seismic detection capability at NORESS and implications for the detection threshold of a hypothetical network in the Soviet Union, *J. Geophys. Res.*, 94, 10397-10414.
- Sykes, L. & J. Evernden (1982): The verification of a comprehensive nuclear test ban, *Sci. Am.*, 247, 47-55.
- Vinje, V., E. Iversen, H. Gjøystdal & K. Åstebøl (1992): Traveltime and amplitude estimation using wavefront construction. Abstract of paper presented at the 54th Meeting and Technical Exhibition of the European Association of Exploration Geophysicists, Paris, France, 1-5 June 1992.

2562 grid points

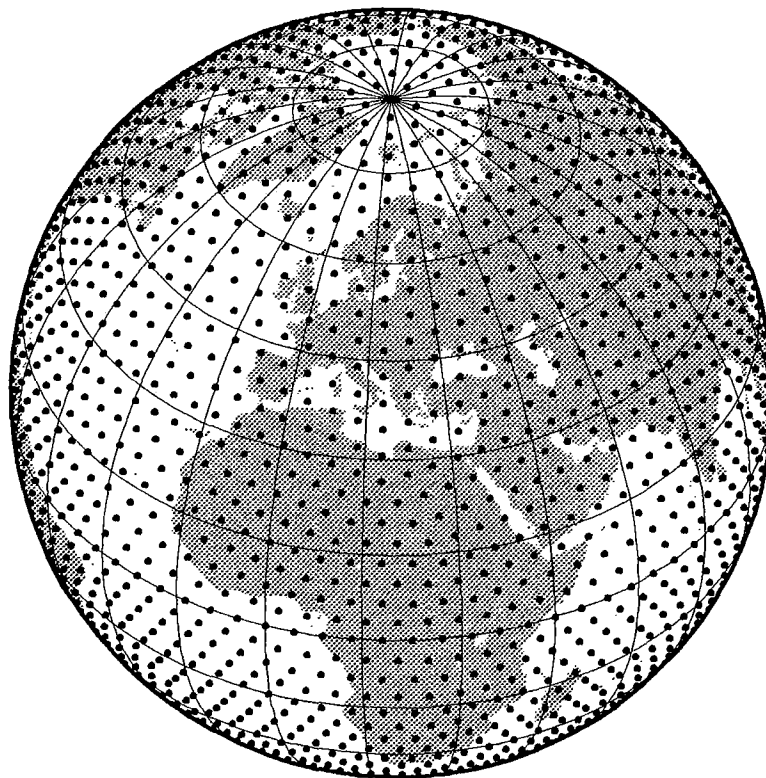


Fig. 7.1.1. The global threshold monitoring is based on a grid of 2562 target points projected upon an azimuthal orthographic projection of the earth. The grid was obtained by a four-fold triangulation of the icosahedron, and each grid point represents a target region of 2.7 degrees radius.

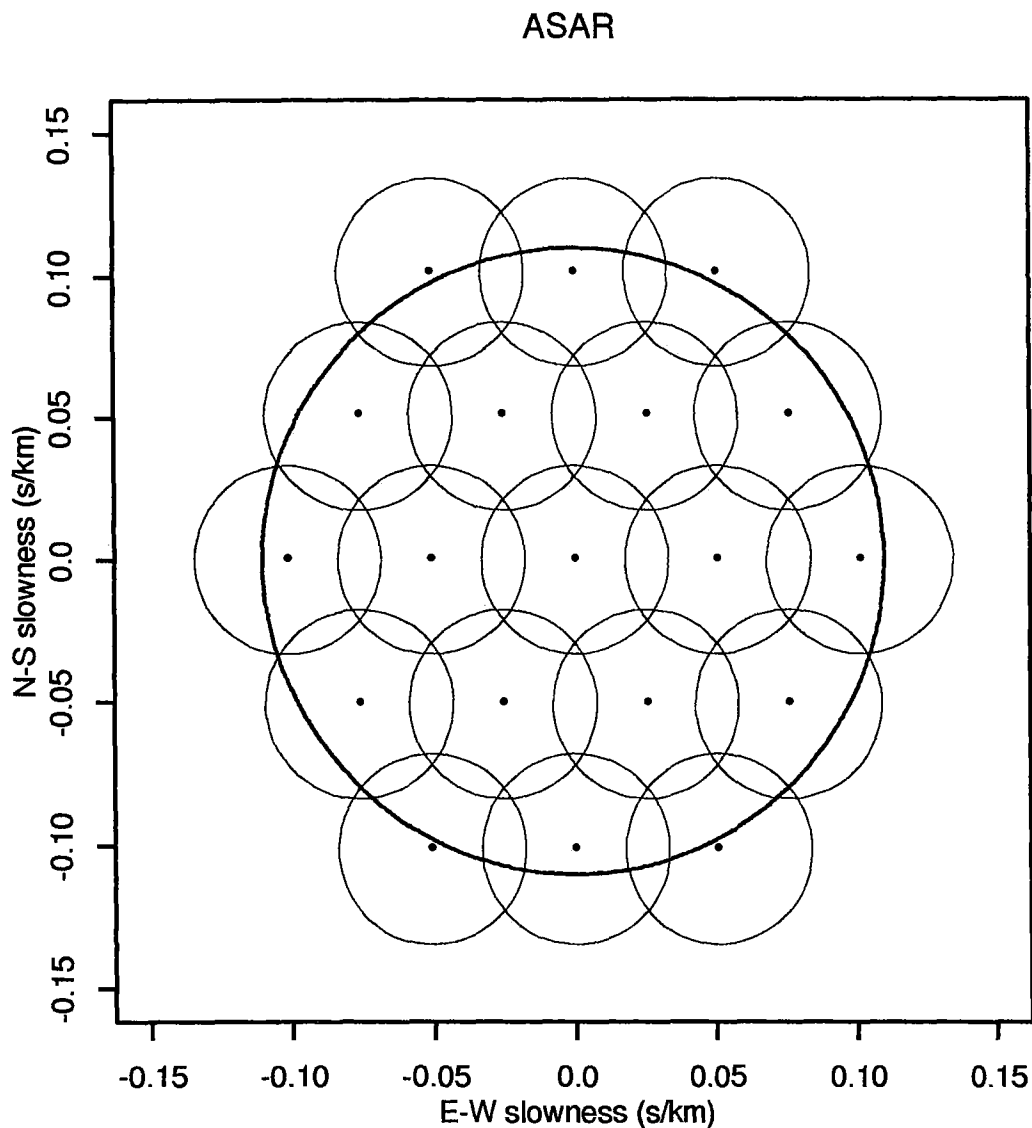


Fig. 7.1.2. Beam deployment for the ASAR array used in the threshold monitoring calculations. The circles around each beam point correspond to 3 dB beam loss contours. The beam density has been determined based upon a reference data set filtered in the frequency band 1.0-4.5 Hz.

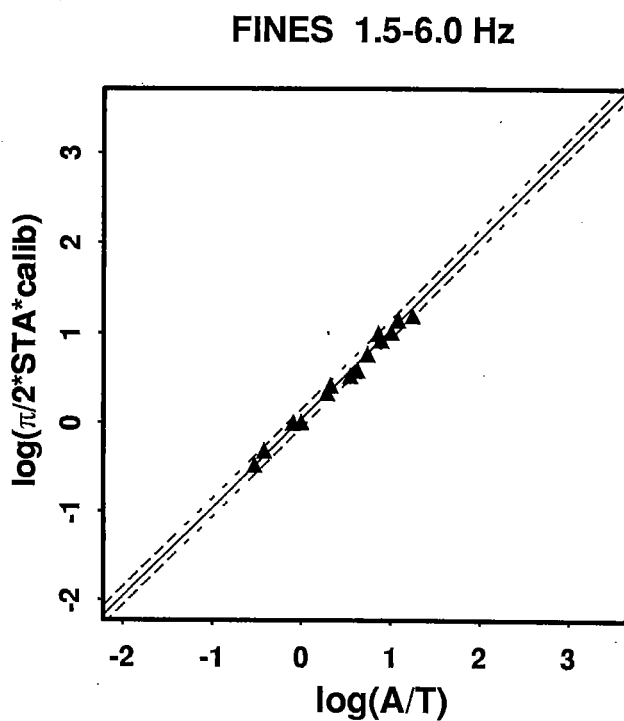
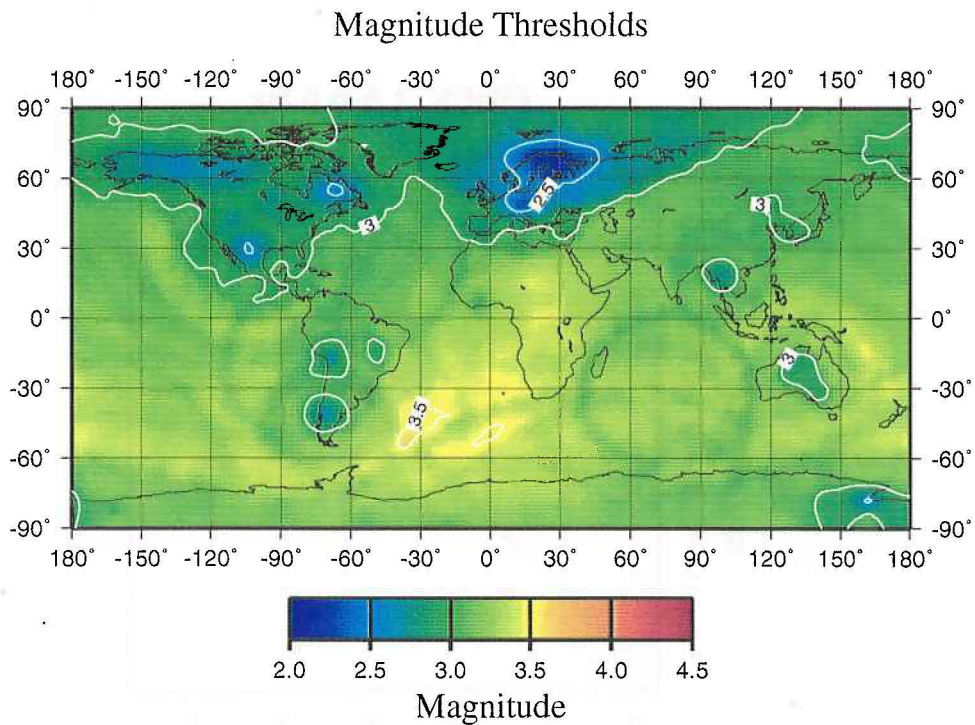
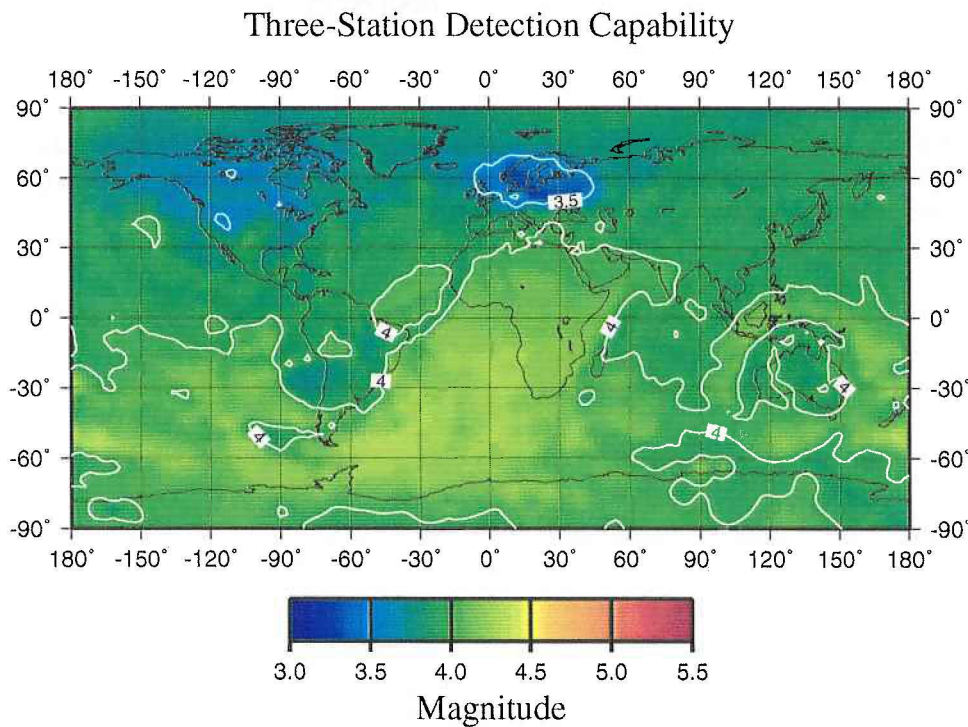


Fig. 7.1.3. Illustration of the linear relation between $\log(A/T)$ and $\log(STA(calibrated))$ for the IMS station FINES. The straight line has been fitted with a restricted slope of 1.0, and shows an excellent correspondence with the data points.



a)



b)

Fig. 7.1.4. Snapshots of the network global thresholds (top) and 3-station detection capability (bottom) during a time without significant seismic activity. The global threshold map shows levels about one magnitude unit lower than the detection capability map (note the difference in color codings). The bottom figure is comparable to the traditional 3-station global capability maps, since it essentially represents detection capability during noise conditions.

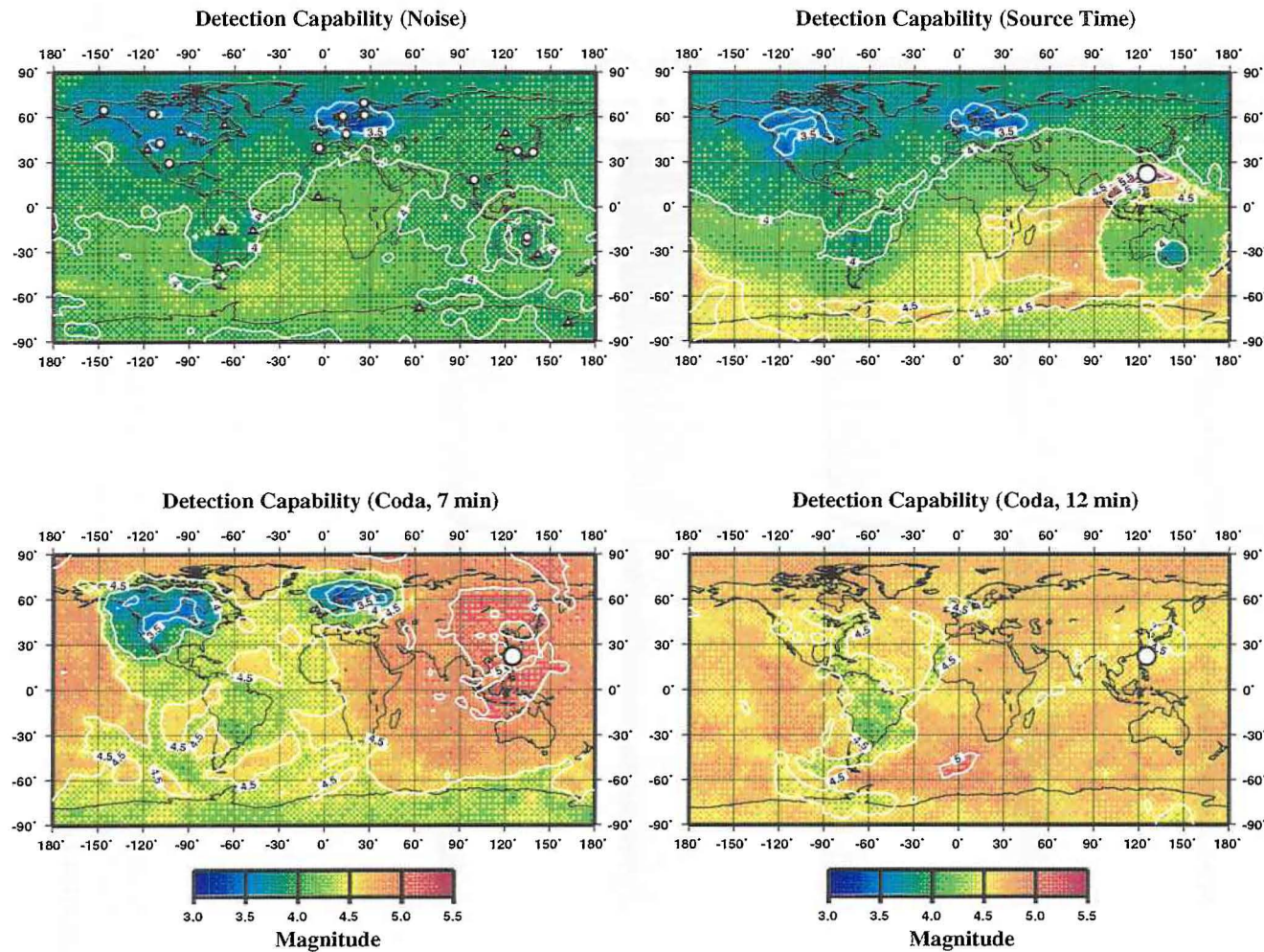


Fig. 7.1.5. Snapshots of the global detection capability display before and during a large earthquake. At the time of the earthquake, the thresholds are increased in the vicinity of the epicenter. After about 7 minutes, the threshold increases in many parts of the world, except that the P-wavefront from the earthquake has not yet reached northern Europe and North America. After 12 minutes, there is a threshold increase globally.

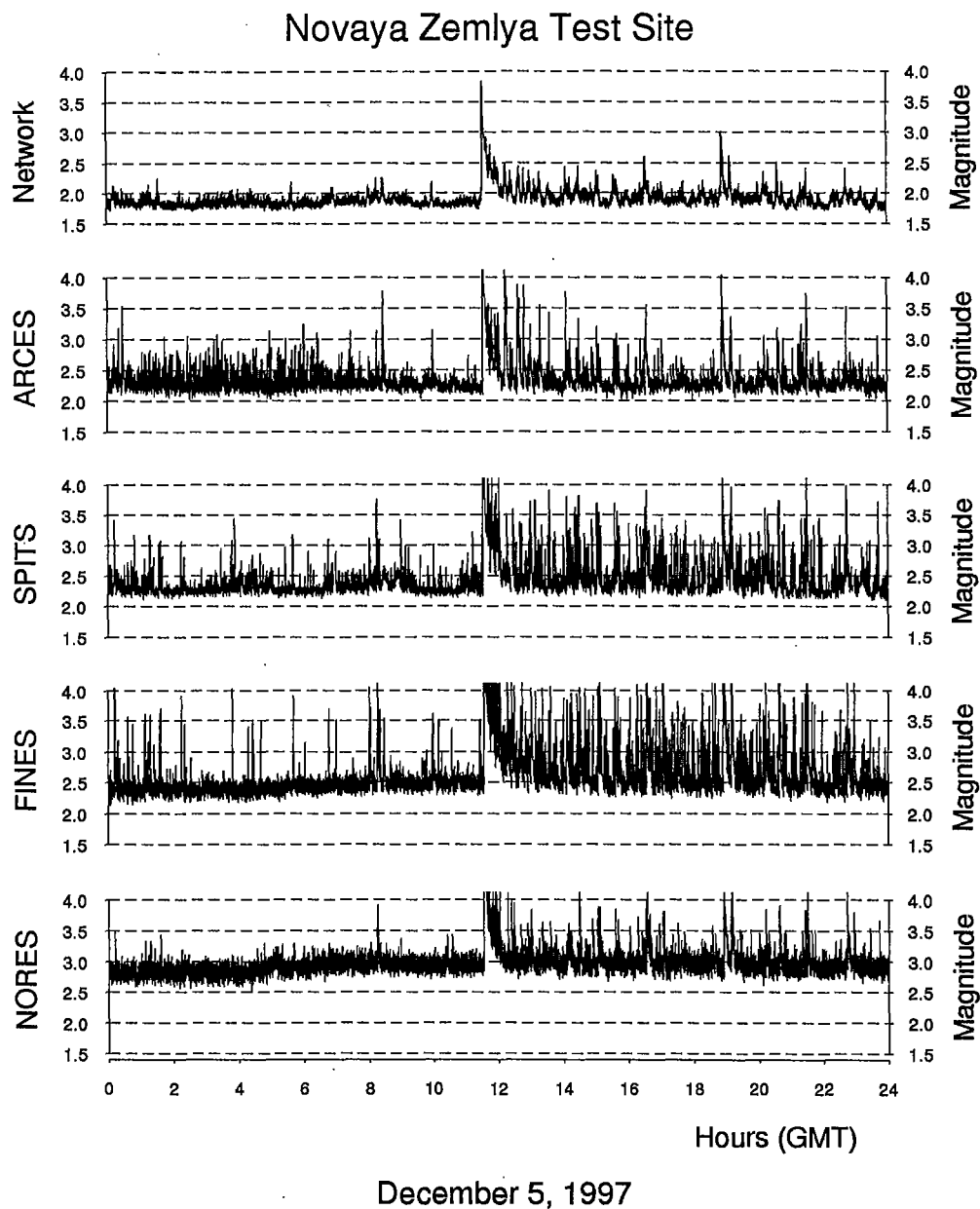


Fig. 7.1.6. Example of site-specific threshold display of the Novaya Zemlya test site for the day 5 December 1997, during which a large earthquake occurred in the Kamchatka Peninsula. See text for detailed explanation.

NORSAR recording of Kamchatka event, 5 Dec, 1997

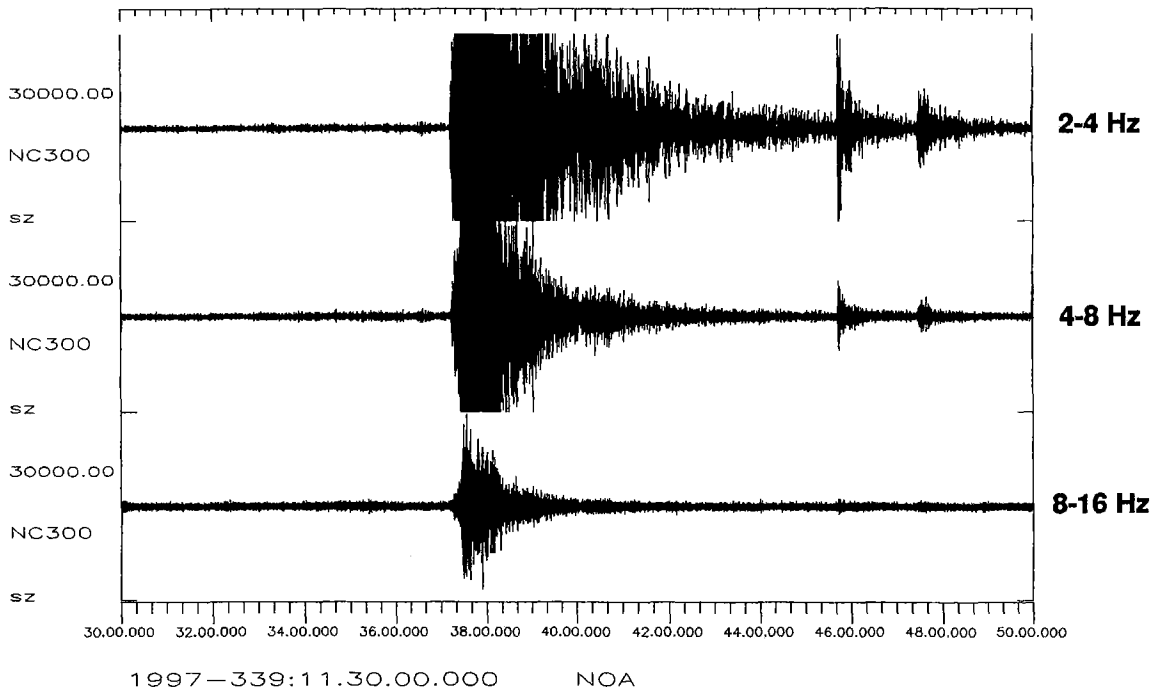


Fig. 7.1.7. Earthquake coda pattern as a function of filter frequency for the Kamchatka earthquake on 5 December 1997. The data, which have been "clipped" in the plot for illustration purposes, are from the NORSAR array, located at a teleseismic distance from the event. Note the significantly faster decrease in the coda level at the highest frequencies. Also note that the two aftershocks seen clearly on the low-frequency top trace are essentially invisible in the highest frequency band.

7.2 Threshold Monitoring: Summary of pipeline processing

Introduction

The Threshold Monitoring software and operations manual have been completed and are in use at the International Data Center (IDC) in Arlington, Virginia. This report is a summary of the pipeline processing discussed in the manual, which describes the TM system.

The Threshold Monitoring (TM) system is intended for continuous assessment of the detection capability of the International Monitoring System's Primary Seismic Network, in support of Comprehensive Nuclear Test Ban Treaty. It accomodates temporary problems which traditional methods based on statistical models may not account for. This includes background noise fluctuations, data quality variations, processing deficiencies, and unrelated seismic events (*e.g.*, large earthquakes).

Software and data files

The TM software resides in a directory structure which also contains the static data files required for processing, such as target lists, beamforming recipe files, *etc.* Scripts for defining TM environment variables are included. The directory structure and the files therein are thoroughly explained in the Operations Manual.

Although some of the software consists of Bourne shell scripts, most of the programs are written in C, with C and FORTRAN subroutines. Arguments for the C programs can be stored in a parameter file rather than entered on the command line. This system makes it easier to run the software.

The input and output files used by TM are binary files which are organized with respect to a reference time T_r . Data observed at time T will begin at the file position corresponding to the remainder of $(T - T_r)/L$, where L is the file size in seconds. Since data will wrap around from the end of the file back to the beginning, these files are referred to as *disk loops*. Raw data are stored in disk loops which are large enough to hold seven days' worth of data. These disk loops are updated continuously.

TM processing

TM produces statistics for every hour of data. The sequence of events is shown below, with program names in bold face.

- **CreateTMSession**: creates the working directory and initializes files.
- **DFX** (Detection and Feature Extraction, Wahl 1996a,b): generates STA (short term average) traces from the raw data.
- **TMthreshold**: calculates thresholds for predetermined targets from the STA data..
- **TMmap**: generates a single disk loop containing merged, resampled threshold data for plotting.
- **TMprod**: generates hourly plots showing station availability, STA data, and worldwide thresholds.
- **TMBulletin**: reads Reviewed Event Bulletin.

- **replotuptime**: adds seismic event information to the station availability plot.

Before TM processing commences, a working directory structure with initialized output files must be created with `CreateTMSession`. This is done once. Processing is performed continuously in the so-called Alpha and Delta pipelines (see the flowchart in Fig. 7.2.1).

Quality control, beamforming, bandpass filtering, and short-term-average calculations are performed by `DFX` for each station. These "STA" data are written to new disk loops. `DFX` processes each ten minute segment of raw data as soon as it becomes available. It runs in the Alpha pipeline, as described in the International Data Center Operations Manual (CTBT/PC/V/WGB/TL/44/Rev.2, 1998). The remaining steps are performed in the Delta pipeline, currently ten hours behind real time.

Network detection thresholds for each of 2562 targets distributed around the globe are calculated by `TMthreshold` and written to a third set of disk loops. These threshold data are interpolated and resampled by `TMmap`, which writes the results to a final disk loop. This disk loop is organized with respect to time and is used to generate the threshold maps described below.

The following statistics are generated by `TMprod` for each hour for which data are available:

- Map showing the location and percent availability of each station (see Fig. 7.2.2).
- Plots of STA traces for each station in the primary network, allowing the user to see the background noise levels, observed signals, and processing gaps (see Fig. 7.2.3).
- Maps showing the average and worst-case detection thresholds for the world (see Fig. 7.2.4).

Finally, `TMbulletin` reads the Reviewed Event Bulletin, and this information on interfering seismic events can then be included on the station availability map by the script `replotuptime`.

L. Taylor

References

CTBT/PC/V/WGB/TL/44/Rev.2 (1998): Initial Draft of the Operational Manual for the International Data Centre. Preparatory Commission for the Comprehensive Nuclear-Test-Ban Organization, Vienna, 19-30 January 1998.

Wahl, D. (1996a): User's Manual for the Detection and Feature Extraction program (DFX). SAIC-96/1098.

Wahl, D. (1996b): Programmer's Guide for the Detection and Feature Extraction program (DFX). SAIC-96/1069.

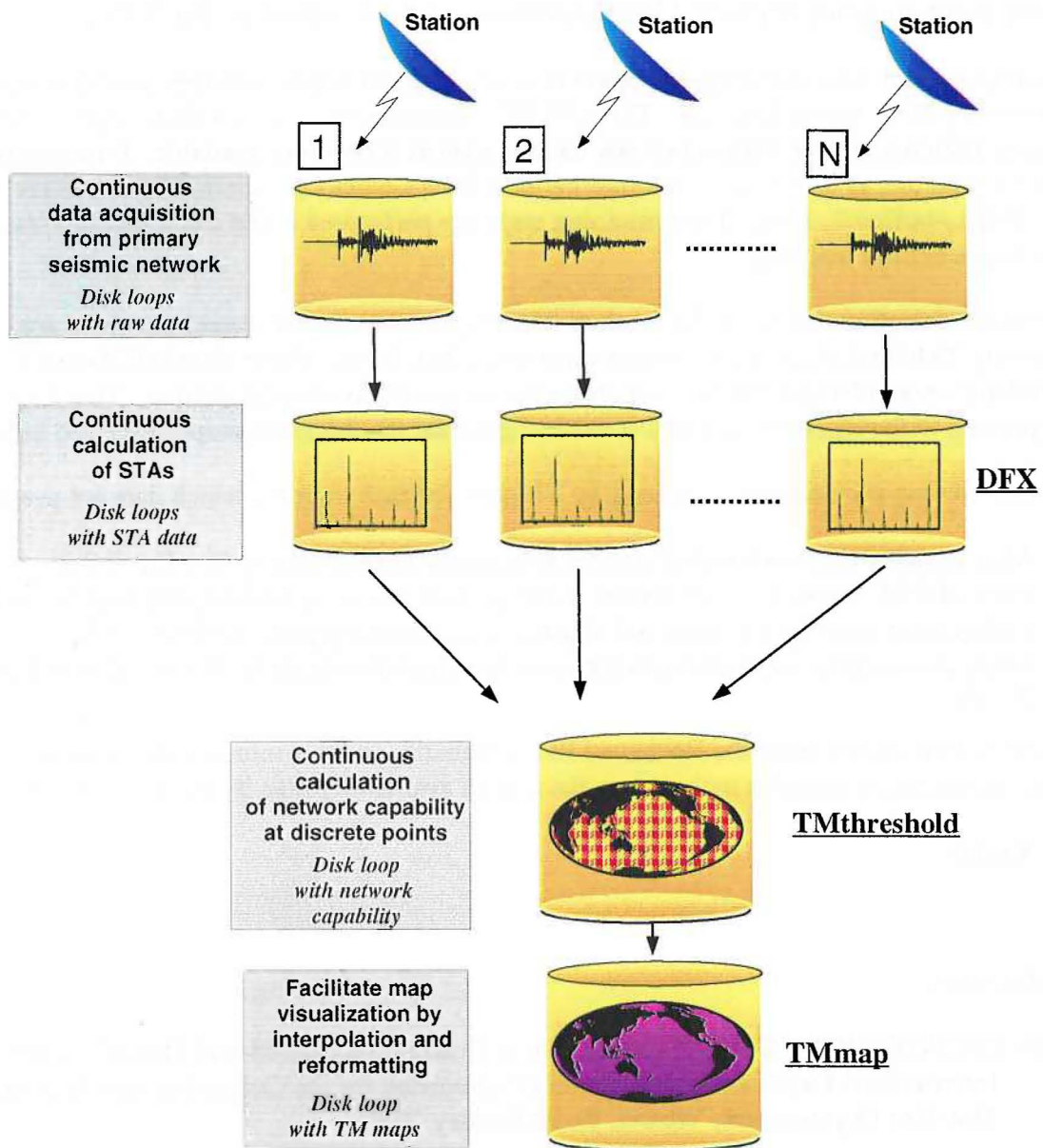
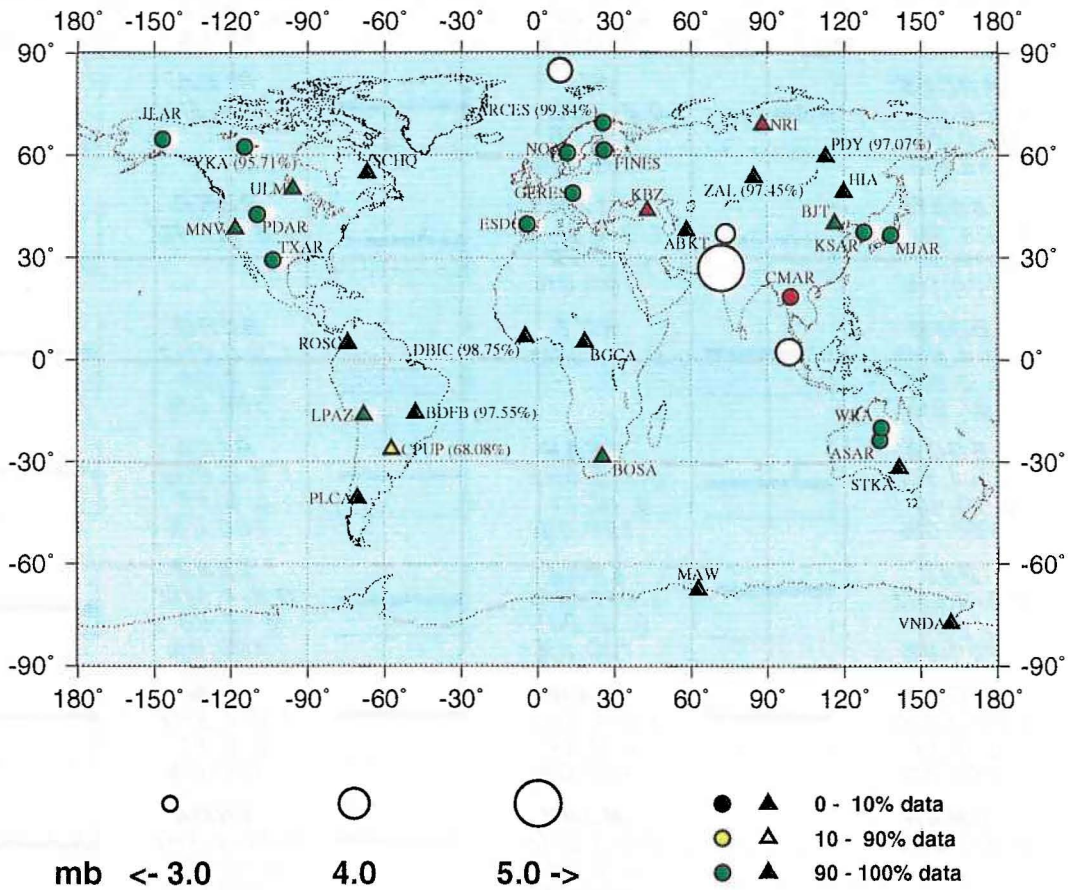


Fig. 7.2.1. Flowchart of processing within the TM system. Text in sans serif typeface describes each process, whereas text in italics describes the results and the type of storage. The names of the programs used at each step are underlined in the figure.

1998/05/11 10:00:00 - 1998/05/11 11:00:00



○ ○ ○ ● ▲ 0 - 10% data
 mb <- 3.0 4.0 5.0 -> ● ▲ 10 - 90% data
 ● ▲ 90 - 100% data

IDC REB

Orid	Time	Lat	Lon	Depth	mb	ndef
1408557	10:13:44	27.07	71.76	0.0	5.00	72
1393281	10:26:08	84.86	8.72	0.0	3.59	10
1393288	10:50:46	37.07	73.53	338.5	3.28	6
1393290	11:10:23	2.19	98.37	0.0	3.76	4

Fig. 7.2.2. Station availability map created by TMprod. The colors of the station symbols indicate the percent availability for detecting events occurring during the time period indicated (11 May 1998, between 10:00 and 11:00 GMT). Three component stations are marked by triangles; the circles represent arrays. When the Reviewed Event Bulletin is complete, the locations of seismic events occurring within or shortly after the given time interval are added to the map. The event with mb=5.0 represents the three simultaneous nuclear tests conducted in India at 10:13:44 GMT.

1998/05/11 10:00:00 - 1998/05/11 11:22:20

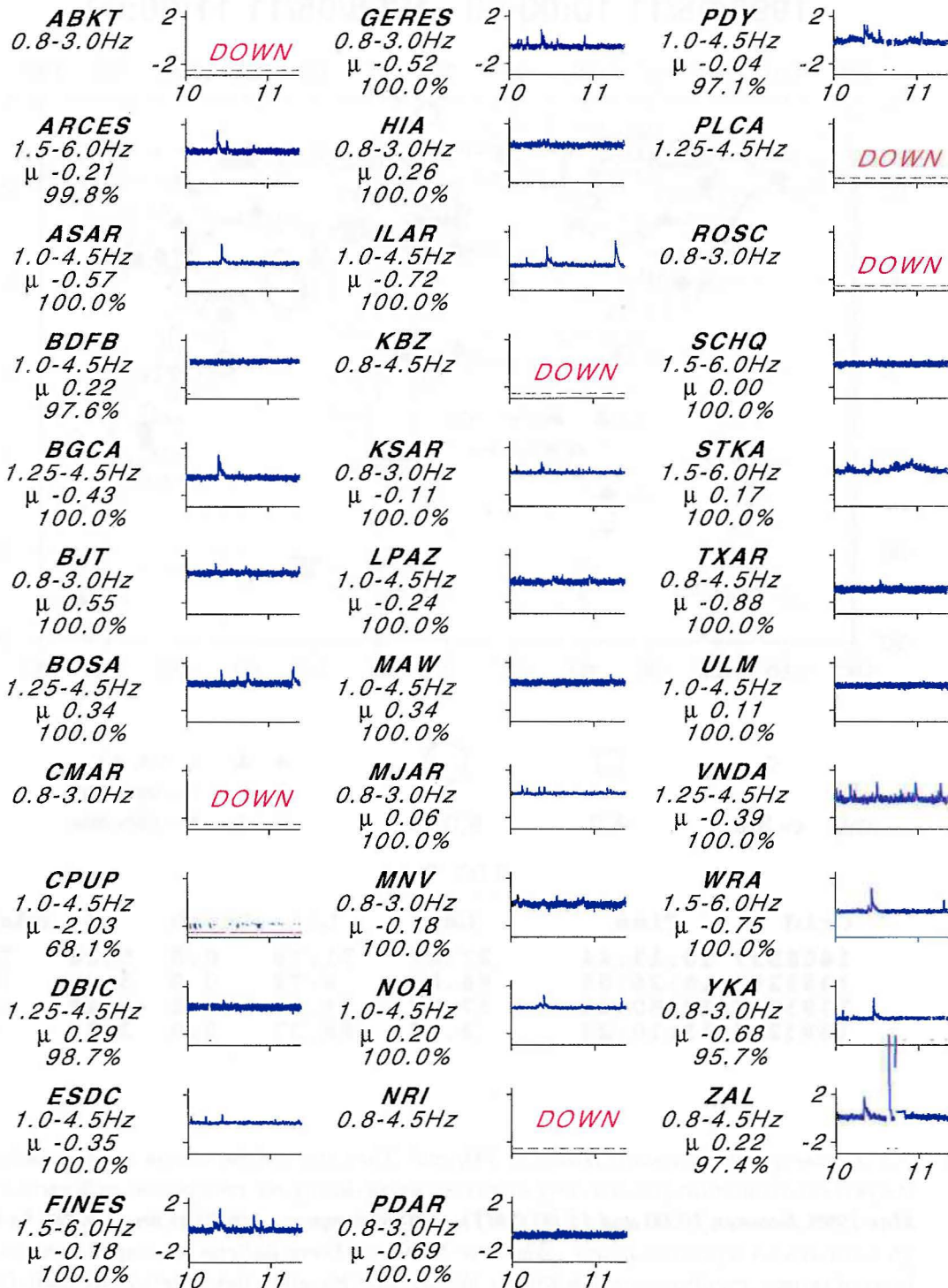


Fig. 7.2.3. Continuous log (A/T) equivalentents derived from STA traces are shown in blue for each station in the primary network. Periods of down time are shown in red. The data interval is extended beyond the hour to allow for the travel times of events originating near the end of the hour. The station name, filter cutoffs, average values, and percent availability are shown next to each trace.

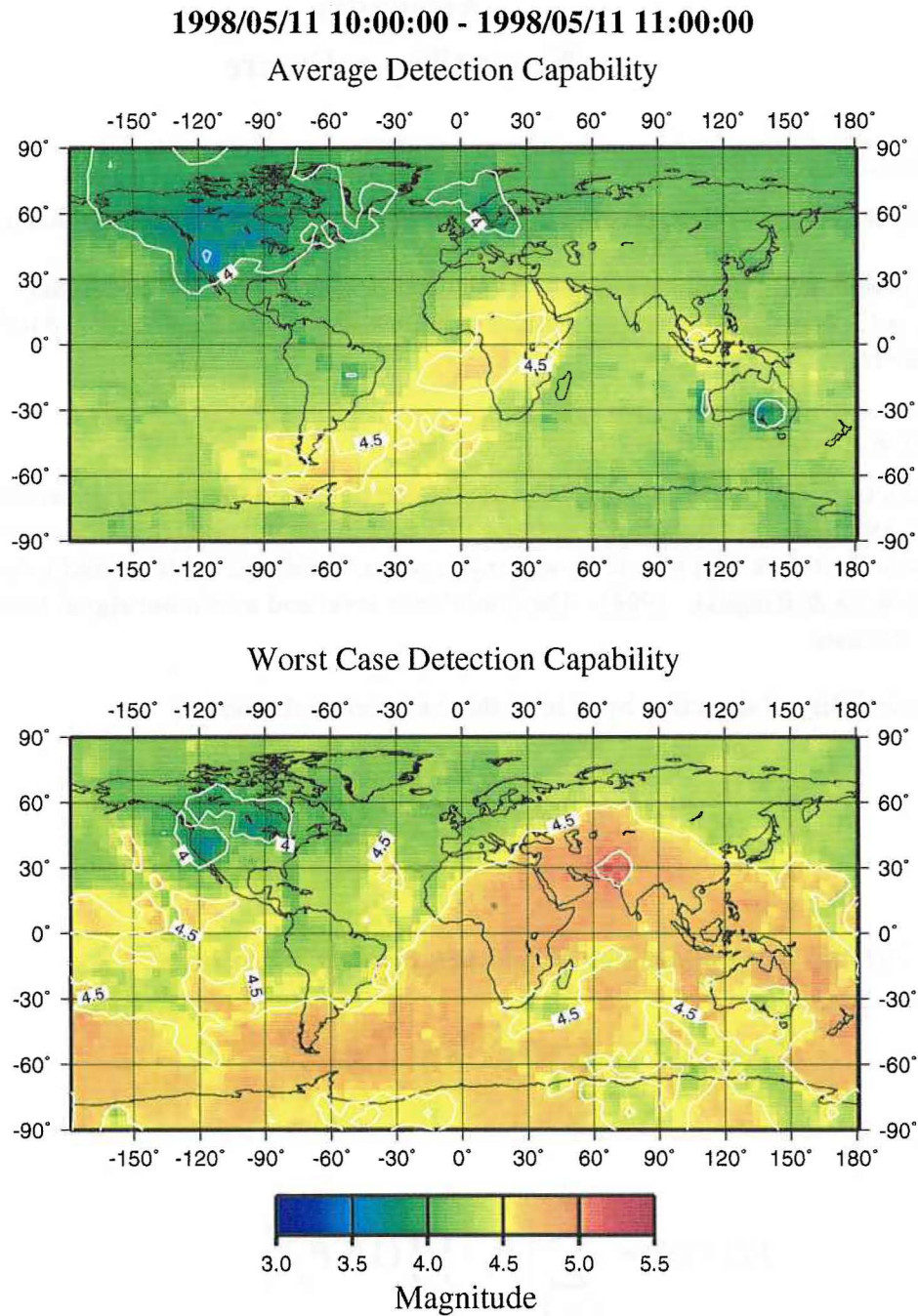


Fig. 7.2.4. Detection capability maps for the given one hour interval. The average capability (top) may vary from hour to hour depending on lengthy station outages, fluctuating background noise levels at different stations, and large long-duration seismic signals. The nuclear explosions in India temporarily lowered the capability over much of the world, as shown in the worst case map.

Appendix

New utility software

Introduction

This report discusses two software modules that have been written during this reporting period:

- **detprob3**, a C function designed to calculate network detection thresholds.
- **wf**, a C program which creates tables of information related to the IDC database waveform headers.

Detection probability

This function (detprob3) calculates the magnitude threshold for which it is assumed that events will be detected by at least three stations. Thresholds calculated for the observed noise levels in a global network will be a time-varying function similar to the threshold monitoring output (see Kværna & Ringdal, 1998). The confidence level and minimum signal to noise ratio are set by the user.

The probability of detection by at least three stations is defined as

$$F(\mu) = 1 - P(0/m) - P(1/m) - P(2/m)$$

where $P(k/m)$ is the probability of detection by exactly k stations:

$$P(0/m) = \prod_{i=1}^N (1 - P_i)$$

$$P(1/m) = \sum_{i=1}^N \left[P_i \cdot \prod_{j \neq i} (1 - P_j) \right]$$

$$P(2/m) = \sum_{i=1}^{N-1} \sum_{j=i+1}^N \left[P_i \cdot P_j \cdot \prod_{k \neq i, j} (1 - P_k) \right]$$

The probability of detecting an event of magnitude μ at station i is given by the error function:

$$P_i = \Phi\left(\frac{\mu - m_i - t}{\sigma}\right)$$

where σ^2 is the assumed signal variance, t is the signal to noise level specified by the user, and the m_i are the observed magnitudes. The probability function F is calculated for μ ranging from $m_3 + \text{lowlim}$ through $m_3 + \text{uplim}$, where m_3 is the third smallest magnitude observed at any station, and the limits are set by the user. $F(\mu)$ is then linearly interpolated to the desired confidence level, and the corresponding magnitude is returned to the user.

Usage

The function requires two arrays containing the observed magnitudes and sigmas, as well as the signal to noise ratio, the confidence level, the lower and upper limits to be added to the test magnitude, and the step size.

A main program (magthresh.c) has been written which will read the magnitudes and sigmas from an ASCII file before calling detprob3. The first line of the file should contain the number of magnitudes; two columns should follow which contain the magnitudes and sigmas, respectively. Other inputs can be entered in a par file (default values are shown):

file=<datafile>

snrthresh=0.4

conflev=0.9

step=0.1

lowlim=-1.0

uplim=1.0

To execute: magthresh file=<filename> par=<parfile> tkfr verbose

There is an option to use $m_3 + t + 1.258 \cdot \sigma_3$ as the test magnitude by including "tkfr" in the calling sequence. If not present, m_3 is the default.

Examples

The default values shown above are used, and the test magnitude (using the "tkfr" option) $m_3 + 0.4 + 1.258 \cdot \sigma_3$ is 4.78 for each case. There are a total of 50 stations.

Case 1: Values for three stations equal 4.0 and the remaining 47 are effectively infinite. We get a magnitude threshold of 4.952.

Case 2: Values for eight stations equal 4.0, two are $-\infty$, and the remainder are ∞ . The magnitude threshold is 4.203.

Case 3: Same as Case 2, but with only four stations having values of 4.0. The result is 4.359.

The difference relative to the test magnitude for these extreme cases ranges from -0.58 to +0.17 magnitude units.

Waveform headers

This software (wf) creates new versions of the IDC site, sitechan, sensor, and instrument tables. Information that is pertinent to a set of online waveforms is extracted from the ASCII versions of these tables. Response files listed in the instrument table will also be copied to the output directory.

These four tables contain the following information:

IDC Table	Contents
sensor	Calibration information for specific sensor channels.
site	Station location information.
sitechan	Channel information for each station.
instrument	Calibration information for each instrument.

The wfdisc (waveform header) table contains descriptive information about data which are stored on disk. Entries in the four tables discussed above are copied verbatim to new tables if the station and channel are found in the wfdisc table. The starting and ending times for each entry must overlap with those found in wfdisc.

The instrument table lists the paths for the response files. These are replaced with "." in the output file. Otherwise, the entries in the output files are identical to those in the original tables.

The arguments for wf may be entered in a parameter file:

```
infile=</path/name>
tabledir=</path/tablename>
outdir=<outputdirectory>
```

To execute: wf par=<parfile> verbose

/path/name (the wfdisc table) is read, and the program searches for matching entries in /path/tablename.site, /path/tablename.sensor, etc.

L. Taylor
F. Ringdal

References

Carter, J. A. & J. R. Bowman (1997): IDC Database Schema, Tech. Rep. CMR-97/28.

Kværna, T. & F. Ringdal, (1998): Seismic Threshold Monitoring for continuous assessment of global detection capability, *Semiannual Tech. Summ. 1 October 1997 - 31 March 1998*, NORSAR Sci. Rep. 2-97/98 , NORSAR, Kjeller, Norway.

7.3 Development of a regional database for seismic event screening

Introduction

Efforts have started to create a database of regional seismic recordings to be used in a subsequent research effort to study the seismic event screening problem (see the Protocol to the Comprehensive Nuclear Test-Ban Treaty for the concept of event screening). This contribution gives an account of the event and station selection criteria, the approach adopted to arrive at a list of events, and the current status of the effort of compiling this database.

Event and station selection criteria

The database will mainly be composed of recordings that are obtainable from NORSAR's historical archive of recordings from the NORSAR teleseismic array, the Fennoscandian regional (high-frequency) arrays (NORESS, ARCESS, and the Spitsbergen array in Norway, FINESS in Finland, and the Apatity array on the Kola peninsula of northwestern Russia), and the GERESS array in Germany. Since the database is to represent regional wave propagation, the source region will thus be centered on Fennoscandia. An additional objective is to choose events in such a way that all propagation paths are contained within a relatively homogeneous region, geologically speaking. To achieve this, it was decided to limit the region to that part of the Eurasian plate that is encompassed by the Urals to the east, the Mid-Atlantic Ridge to the west and the Alps and the Carpatians to the south. More specifically, the selected source region is composed of one large rectangle [10°W-60°E] x [47°N-70°N] to cover most of the area, and a smaller rectangle [13°E-70°E] x [70°N-82°N] to cover relevant parts of the Arctic region (see Fig. 7.3.1 for a map of the area under consideration).

As to the size of events to be included in the database, it was decided to initially consider events for which at least one agency had reported a magnitude (of some sort, e.g., m_b or m_l) exceeding 3.5. If it is decided at some future time to extend the database to include events of lower magnitude, there will be a multitude of events of magnitudes lower than 3.5 to choose from. The initial event selection is also made with a view to include special events with magnitudes below 3.5 (see next paragraph).

For events that occurred prior to 1984, only data for the NORSAR teleseismic array are available in NORSAR's archives. The regional arrays in Fennoscandia (and GERESS) all became operational during 1984-1992. It was thus decided that the database should primarily consist of events from the period 1984-1997. Again, exceptions are made in order to include data for the NORSAR teleseismic array from events of particular interest that occurred prior to 1984.

As to the length of the data segments, it was decided to extract 30 minutes of data for each station for all events, with segment start time 10 minutes prior to the expected P arrival time. This is considered to provide a sufficient amount of pre-signal noise data for various possible future purposes, and is at the same time an appropriate length to accommodate all phases of interest, including surface waves, for the distance intervals considered here.

Approach adopted to generate a list of events

The main approach for selecting events for this database has been a search of available bulletins. At our disposal for this purpose were the PDE and ISC bulletins, the REBs (Reviewed Event Bulletins) of the Prototype International Data Center, as well as a number of regional seismic bulletins issued by various agencies, e.g., the University of Helsinki in Finland and the LDG in France.

We started the bulletin search by selecting those events that matched the criteria described in the previous paragraph, and that in addition were defined by three or more of the bulletin agencies. This resulted in a total of 82 events. Of these, 56 were selected for the database in such a way as to maximize the geographical coverage. A bulletin search for events listed by two agencies only resulted in an additional 56 events, out of which 30 were added to the list of events for this database, based on their occurrence in regions not well covered by the initial 56 events. Finally, 17 events were added that were either defined by one agency only, or were special events that did not meet the criteria in the above paragraph. Among these special events were a couple of shots conducted in connection with seismic refraction experiments, a calibration shot in a mine, the recordings of the sea-bottom impact resulting from the accidental sinking of a concrete oil production platform, a dynamite explosion aboard a wrecked ship and a lightning-triggered explosion of an array of underwater mines.

The locations of the 103 events selected so far for this database are plotted in Fig. 7.3.1. Two other databases involving regional seismic recordings are planned to be constructed at NORSAR. One of these involves recordings of events in the Novaya Zemlya region (therefore events in this region are not shown in Fig. 7.3.1), and the other is a compilation of recordings of PNEs conducted in the European part of the Soviet Union before 1984. The merging of these two databases with the one considered here will contribute to an improvement of the event coverage shown in Fig. 7.3.1.

For the Novaya Zemlya and PNE databases, the recordings are being stored in the CSS3.0 format, which will also be used for the database described in this contribution. In this way, all three databases will be consistent (also with respect to the length of each data segment), and the databases will eventually be merged into one database of regional seismic recordings.

Current status of effort and remaining work

As of the date of this report, data have been copied from the archive for about 80 of the 103 events selected for the database. The copying effort started with the oldest data, and what remains are events from the period 1993-1997. Taking into consideration that the most recent events have the highest number of stations contributing data, it is our assessment that 60-70% of the copying effort for these 103 events has now been completed. The recovery of data from the archive has met with a high degree of success, as very few intervals have been irretrievable. Station downtimes have affected the database construction to a small degree only. For each data segment copied, standard plots have been produced and arranged in a binder, where also specific information that is available (e.g., newspaper and other reports on special events) has been compiled.

When all waveform data have been entered into the database, it remains to add the metadata (e.g., station coordinates, station transfer functions, etc.). When all this is in place, we will consider copying the database on to CD-roms, as the primary medium for external distribution.

The next progress report on this effort will include a listing of all events in the database, along with an indication of which stations have contributed data for each event.

S. Mykkeltveit

B.Kr. Hokland

B. Paulsen

Database events

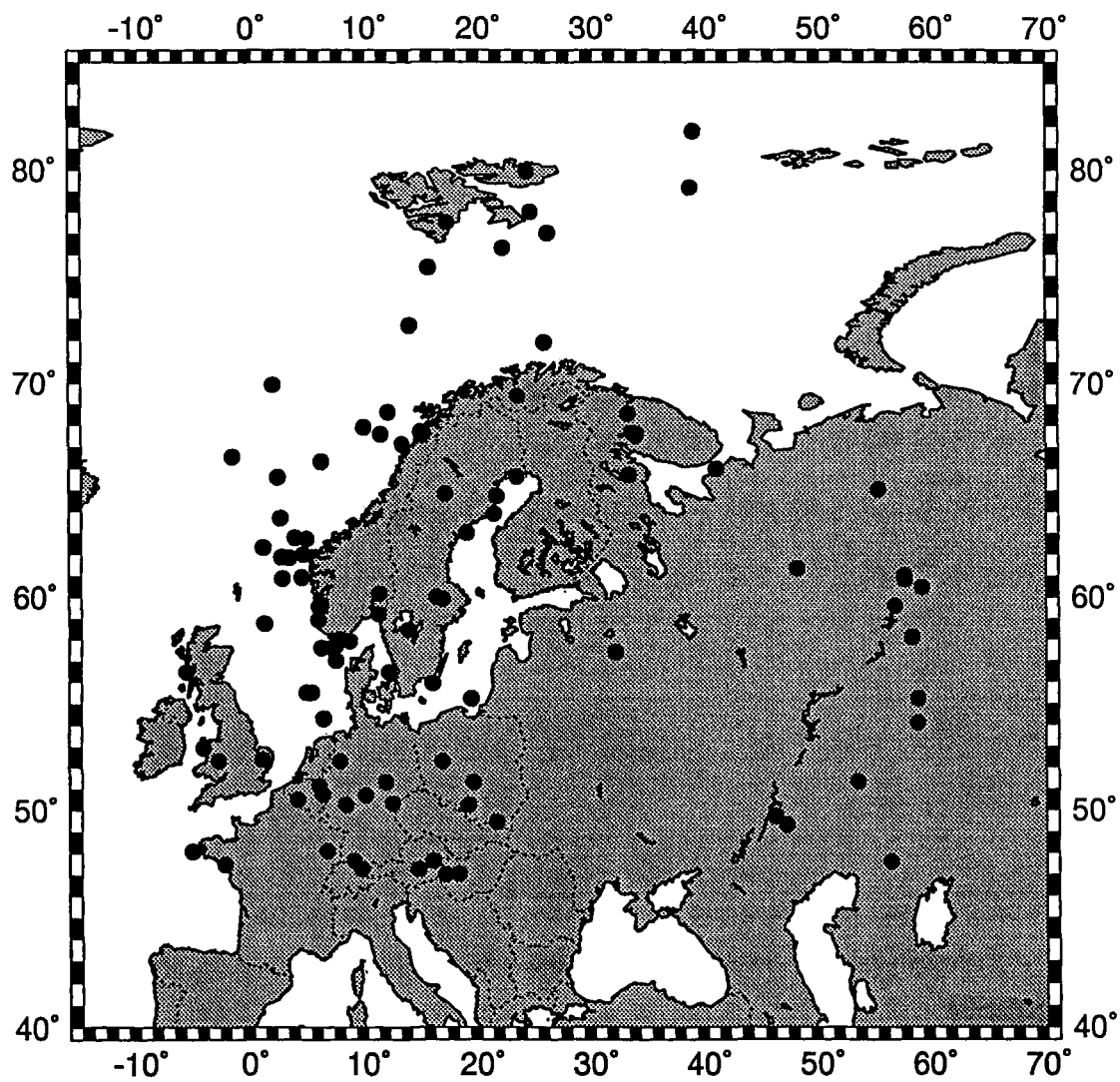


Fig. 7.3.1. The map shows the 103 events so far selected for the regional database described in this report.

7.4 Monitoring seismic events in the Barents/Kara Sea region

Introduction

NORSAR has for many years been cooperating with the Kola Regional Seismological Centre (KRSC) of the Russian Academy of Sciences in the continuous monitoring of seismic events in North-West Russia and adjacent sea areas.

KRSC began its seismic network processing in 1982. Initially, this was done primarily by processing data from the KRSC network of seismological stations (see Table 7.4.1), but in recent years the analysis has been supplemented with data from IRIS stations (KBS, LVZ, KEV, ARU, ALE, NRI etc.) and the Scandinavian seismic arrays (ARCESS, SPITS, FINESS, HFS, NORESS) for analyzing of the most interesting events.

As the result of KRSC's operations and research activities a large amount of information has been collected. It comprises seismic bulletins and catalogues, waveforms from digital stations, digitized seismograms for selected interesting seismic events recorded by the analog stations in the network, results of spectral processing etc.

Because of industrial and other man-made activity in the Kola region a number of artificial seismic signals of different types has been registered, including open-pit, underground and underwater explosions, explosions followed by acoustic signals etc. This provides a good basis to make attempts to work out some criteria for discrimination between various source types and for evaluating previously proposed discriminants.

This paper describes briefly the KRSC seismic network and the approaches to data processing and event location implemented at the KRSC data center. We will also describe some of the most interesting seismic events occurring in the region in recent years. We will demonstrate by examples that the S/P ratio is a highly questionable discriminant for regional events, even at high frequencies.

Kola regional seismic network

Before 1992 KRSC applied data from analog seismic stations only in the regular analysis. All of the analog stations have been equipped with SKM-3 short-period seismometers with identical amplitude-phase response (amplification 50000 in frequency range 1.25-2 Hz). In addition the Apatity station has included three-component long-period seismographs of type SKD ($T_s=25$ sec).

Seismograms from all the stations (excluding KHE) are stored in Apatity. Data from KHE has been transferred to KRSC by telex in the form of daily bulletins.

In 1991 an extensive cooperative research program between KRSC and NORSAR (Norway) was initiated. Part of this cooperation involved the installation in NW Russia of three modern digital seismic stations, two of which are arrays.

One array (aperture 1 km) comprising 11 short-period sensors (Geotech S-500) is situated about 17 km to the west of Apatity. In the town of Apatity there is a 3-component broad band

digital station (Guralp GMG-3T). A micro-array with aperture about 150 m was installed in Amderma in 1993. The array is situated in an underground fluorite mine and comprises 3 vertical sensors and 3-component station in the centre. The sampling rate is 40 measurements per second.

Table 7.4.1. Kola seismic network

Name	Latitude (N)	Longitude (E)	Type	Worked since	Until
APA	67.558	33.442	Analog	1956	now
PLQ	66.410	32.750	Analog	1985	now
BRB	78.073	14.197	Analog	1982	1990
PYR	78.659	16.216	Analog	1983	1987
AMD	69.744	61.648	Analog	1983	1995
KHE	80.600	58.200	Analog	?	1990
APA	67.558	33.442	Digital 3-C	1991	now
AP0	67.603	32.994	Array	1992	now
AMD	69.744	61.648	Micro-array	1993	now

Seismicity

The seismicity of the Barents/Kara sea region is quite low as discussed by Ringdal (1997). This is illustrated in Fig. 7.4.1 which shows the epicenters in northern Europe and adjacent areas determined in the Revised Event Bulletin of the GSETT-3 IDC during 1995-1996. Because of the high-quality coverage of regional arrays in Fennoscandia, a large number of seismic events (mostly mining explosions) are detected in this region. The seismic event occurrence is also very high in the Spitsbergen area and offshore Norway (to the north and west). These events are presumably mostly earthquakes.

On the other hand, the figure shows that there are almost no recorded events in the region comprising the eastern part of the Barents sea, the Kara Sea, Novaya Zemlya and the northern part of Russia (excluding Kola). While the GSETT-3 network has a lower detection capability in this region compared to Fennoscandia, its capability is nevertheless around magnitude 3.0-3.5 and it is thus clear that seismic events of such magnitudes or larger occur rather infrequently in the region specified above.

Event location

Since the IASPEI-91 model is not suitable for Barents region (Ringdal et al, 1997), it has been necessary to study local travel-time curves using data from a set of strong explosions with

known locations. In addition, an underground calibration explosion has been carried out in the Khibiny Massif (29.09.1996, 350 ton), see Ringdal et al (1996).

We have attempted to fit a one-dimensional velocity model to agree with these results. This has resulted in the compilation of a model which is a combination of the NORSAR model for smaller depths (up to 200 km) and IASPEI-91 at greater depths. To validate the model we have re-located several previous seismic events (see Table 7.4.2). As can be seen from this table, and further illustrated in Figure 7.4.2, the locations by the regional network are within 5-10 km of the locations obtained by joint hypocentral determination (JHD) using world-wide data.

Table 7.4.2. Location comparison - regional versus global network

Date	KRSC location	JHD location	Comment
18.08.83	73.289 N, 54.893 E	73.358 N, 54.943 E	
01.08.86	72.945 N, 56.549 E	73.031 N, 56.726 E	Marshall et.al. (1989)
02.08.87	73.298 N, 54.398 E	73.324 N, 54.597 E	
07.05.88	73.275 N, 54.436 E	73.314 N, 54.557 E	
24.10.90	73.304 N, 54.634 E	73.317 N, 54.803 E	

The model therefore seems to be satisfactory for event location in the Barents region. In addition, the documented consistency with precise global network locations is especially important since we are able to use the network to locate regional events far smaller than those which can be detected teleseismically. For example, the KRSC network was the only network with sufficient data to locate reliably the smallest recorded nuclear explosion on the Novaya Zemlya test site ($m_b=3.8$) on August 26, 1984 (Michailov et. al., 1996). The result is shown in Fig.7.4.3. Our estimated epicentral coordinates of this explosion are 73.326N, 54.763E, thus placing the event within the group of explosions shown in Fig. 7.4.2. While we have no other network solution with which to compare our result, we believe this explosion to be rather accurately located.

Data analysis

The KRSC detection and location software is based on a specially developed algorithm which is very close to the generalized beamforming approach (Ringdal and Kverna, 1989). It operates well when data from several seismic stations are available.

The Amderma station is far from all the other seismic stations in the network so we have to locate weak events near this station using only one-station data. The small aperture makes it difficult to use beamforming or some other array-based procedure to determine backazimuths. Moreover, strong industrial noise (probably due to construction work) occurs quite regularly in this place.

Under such circumstances a completely automatic processing often results in wrong phase association (true phases may be associated with noise bursts, etc.). To avoid this we use a semi-automatic routine. We first run a detector to identify segments of the recording which contain seismic energy above a given threshold. The analyst then marks approximately those parts of the recording which may contain phases of real seismic events and a new automatic procedure is executed for these parts. (For the Amderma station this automatic process includes filtering, STA/LTA detection and joint polarization analysis for P and S phases). Although the accuracy of this method is limited, it is often sufficient to obtain preliminary location with reasonable accuracy (see examples below).

To carry out this automatic analysis we have developed a variant of site-specific monitoring (SSM), as described in the Appendix. It scans pairs of detected phases and for each pair assumes a hypothesis that the first phase is P-wave and the second one is S-wave from an event occurring somewhere inside a given region. The validity of this hypothesis is estimated by joint polarization analysis for P and S phases and application of several additional criteria such as frequency and amplitude compatibility. Those pairs for which a resulting rating function is greater than some predefined threshold are assumed to correspond to possible real seismic events.

Naturally, such an automatic process will occasionally result in false alarms, but their number is within reasonable limits. We will illustrate this by an example. During the day 16 August 1997, five real seismic events occurred near the Amderma station. Two of them were very similar events of unknown nature occurring at the same point in the Kara sea (distance from Amderma about 320 km). The waveforms are shown in Fig. 7.4.4. Two others were explosions near Vorkuta (about the same distance but to the south-west from Amderma) and one event was too weak to locate.

The result of site-specific monitoring for this day is shown in Fig.7.4.5. The SSM procedure has detected and located the Kara events and the two Vorkuta explosions. False alarms are also shown (the total number of false alarms for this day was five). The results of the semi-automatic location process for two of the events, the smallest Kara sea event (16.07.1997, 6.20 GMT) and one Vorkuta explosion (16.07.1997, 7.02 GMT) are shown in the insertions.

The problem of event discrimination

As mentioned above the network often registers seismic events of a nature which cannot be determined by traditional criteria like spectral characteristics or P/S ratios. For example, the numerous explosions at Vorkuta recorded by Amderma have much lower dominant frequencies for P and S waves than the 16 August 1997 Kara sea events, which some investigators have characterized as earthquakes, even though the epicentral distances are the same (about 300 km).

As another example, the 1 August 1986 Novaya Zemlya event, generally assumed to be an earthquake, had essentially the same S/P characteristics at the Barentsburg station (distance 10 degrees) as the 26 August 1984 nuclear explosion. Admittedly, because we had only analog recordings available at this time, we are unable to compare the characteristics at very high frequencies, but the picture is very clear in the 1-3 Hz band.

An event occurring on February 9, 1998 near Murmansk (69.18 N, 32.63 E, origin time 16.51:07) was recorded by the seismic arrays ARCESS and SPITS with very different signal characteristics. The S-wave amplitude for SPITS was much less than the P-wave amplitude regardless of which bandpass filter was used. On the other hand, ARCESS recordings showed a strong S-wave and even Lg and Rg phases.

The most striking example of the variations in P/S ratios was observed for an event which occurred on April 18, 1998 in Norwegian Sea near Bear Island. The waveforms (recordings by APA, ARCESS and SPITS) together with our estimated location are shown in Fig.7.4.6.

The nearest station is SPITS (about 470 km) and its recording contains no noticeable S phase in any frequency band. In contrast, ARCESS (670 km) has recorded strong S-waves, whereas APA (1020 km) registered P-waves only in the band 8-12 Hz. This illustrates that attempts to use the P/S ratio of a single station to discriminate between various source types can give rather contradictory results, depending on the radiation pattern and path attenuation.

Conclusions

The combined regional networks of the Kola Regional Seismological Centre and NORSAR is capable of locating even very low magnitude events with high accuracy in the Barents/Kara sea region. Studies of historic recordings in the past 15 years have revealed that there are almost no seismic events in this area exceeding magnitude 2.5, except for in the western part between Norway and Spitsbergen.

Case studies, some of which are discussed briefly in this paper, have demonstrated that traditional regional discriminants are not effective for separating between seismic source types at low event magnitudes in this region. In particular, we conclude that the S/P ratio, even at high frequencies, is rather unstable and should not be relied upon for regional event discrimination.

With regard to the two Kara sea events on 16 August 1997, we respectfully disagree with those scientists who have claimed that these events can be positively identified as earthquakes on the basis of seismological evidence. On the other hand, neither is there any seismological evidence to confidently classify these events as explosions. In our opinion, the source type of these two events remains unresolved.

V.E. Asming, KRSC

E.O. Kremenetskaya, KRSC

F. Ringdal, NORSAR

References

Kvcerna T. and F.Ringdal (1996). Generalized beamforming, phase association and threshold monitoring using a global seismic network. In: E.S.Husebye and A.M.Dainty (eds), *Monitoring a Comprehensive Test Ban Treaty*. 1996, 447-466. Kluwer Academic Publishers. Netherlands.

- Marshall, P.D., R.C. Stewart and R.C. Lilwall (1989): The seismic disturbance on 1986 August 1 near Novaya Zemlya: a source of concern? *Geophys. J.*, 98, 565-573.
- Mikhailov, V.N. et.al. (1996): USSR Nuclear Weapons Tests and Peaceful Nuclear Explosions, 1949 through 1990, RFNC - VNIIEF, Sarov, 1996, 63 pp.
- Ringdal, F. (1997): Study of Low-Magnitude Seismic Events near the Novaya Zemlya Test Site, *Bull. Seism. Soc. Am.* 87 No. 6, 1563-1575.
- Ringdal, F., E.Kremenetskaya, V.Asming, Y.Filatov (1997). Study of seismic travel-time models for the Barents region. *Semiannual Technical Summary 1 October 1996 - 31 March 1997*, NORSAR Sci. Rep. 2-96/97, Kjeller, Norway.
- Ringdal F., Kremenetskaya E., V.Asming, I.Kuzmin, S.Evtuhin, V.Kovalenko (1996): Study of the calibration explosion on 29 September 1996 in the Khibiny Massif, Kola Peninsula. *Semiannual Technical Summary 1 April - 30 September 1996*, NORSAR Sci. Rep. 1-96/97, Kjeller, Norway.
- Ringdal, F. and T. Kvaerna (1989), A multi-channel processing approach to real time network detection, phase association and threshold monitoring, *Bull. Seism. Soc. Am.* 79, 1927-1940.
- Ringdal F. and T.Kværna (1992). Continuous seismic threshold monitoring. *Geophys. J. Int.* 111, 505-514.

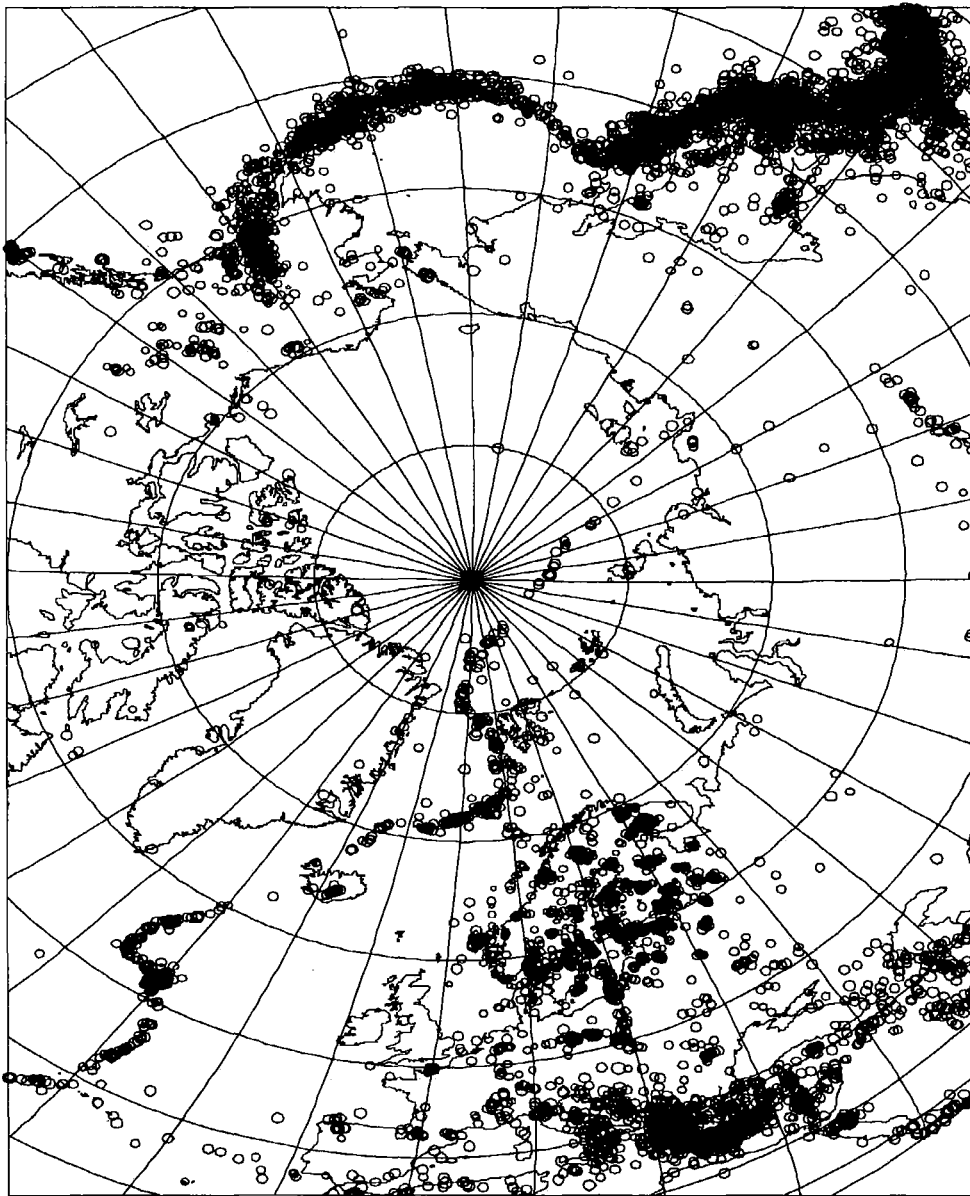


Fig. 7.4.1. Epicenters in northern Europe and adjacent areas determined in the Revised Event Bulletin of the GSETT-3 IDC during 1995-1996. Note the large number of seismic events (mostly mining explosions) in Fennoscandia and the high seismicity in the Spitsbergen area and offshore Norway (mostly earthquakes). Also note the low observed seismicity in the Barents/Kara sea region.

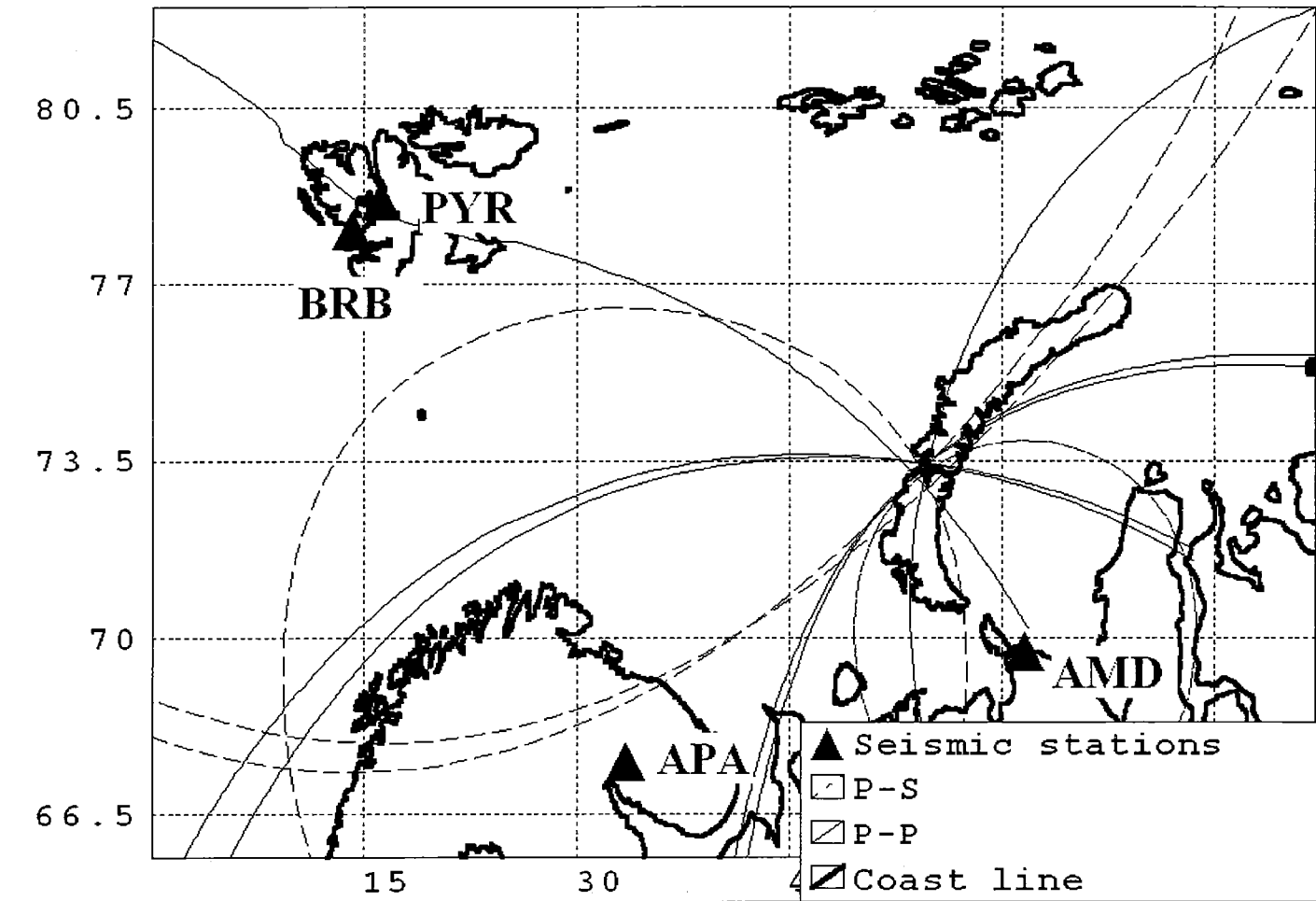


Fig. 7.4.2. Location of the smallest recorded Soviet nuclear explosion (26 August 1984, $m_b=3.8$) at Novaya Zemlya using data by the stations PYR, BRB, APA and AMD.

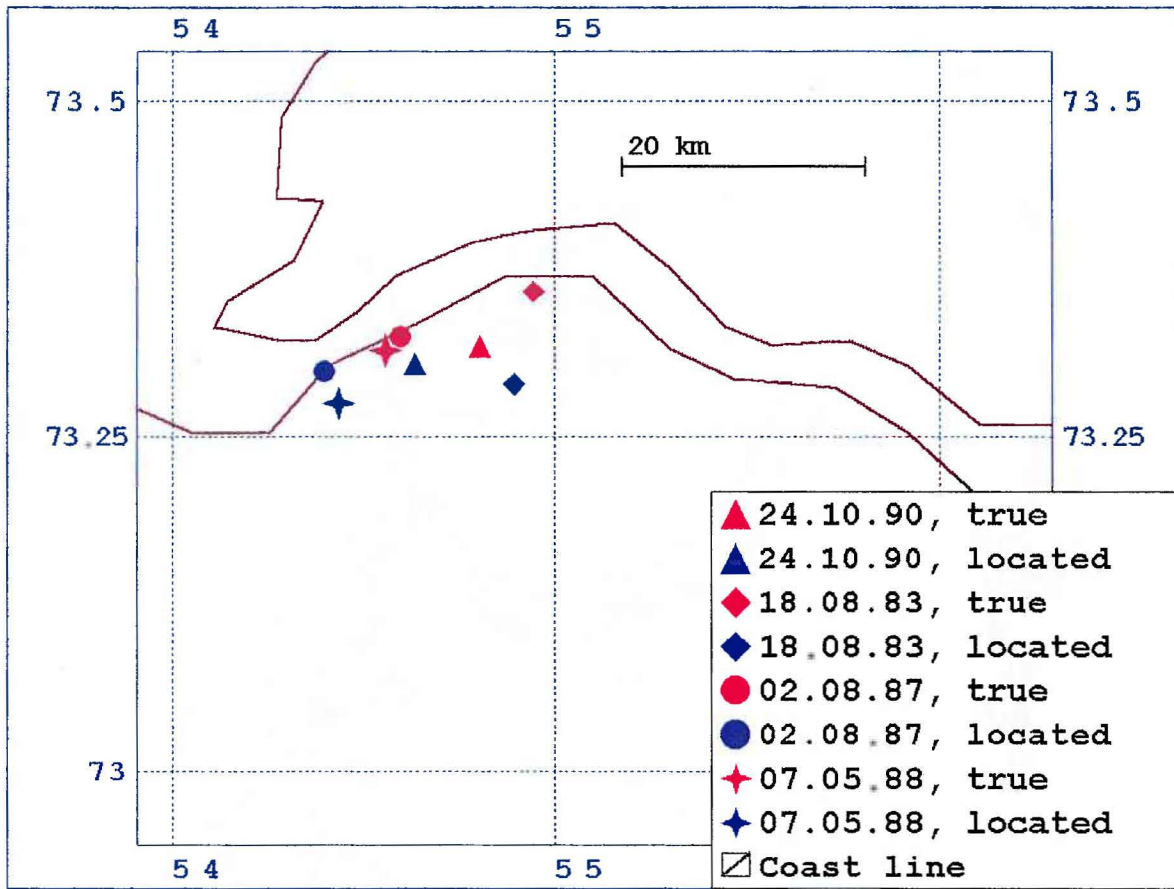


Fig. 7.4.3. Comparison of the locations of well-recorded seismic events at Novaya Zemlya using joint hypocentral determination from a global network with the same events located using only the data by the stations PYR, BRB, APA and AMD in the KRSC regional network. Note the excellent consistency.

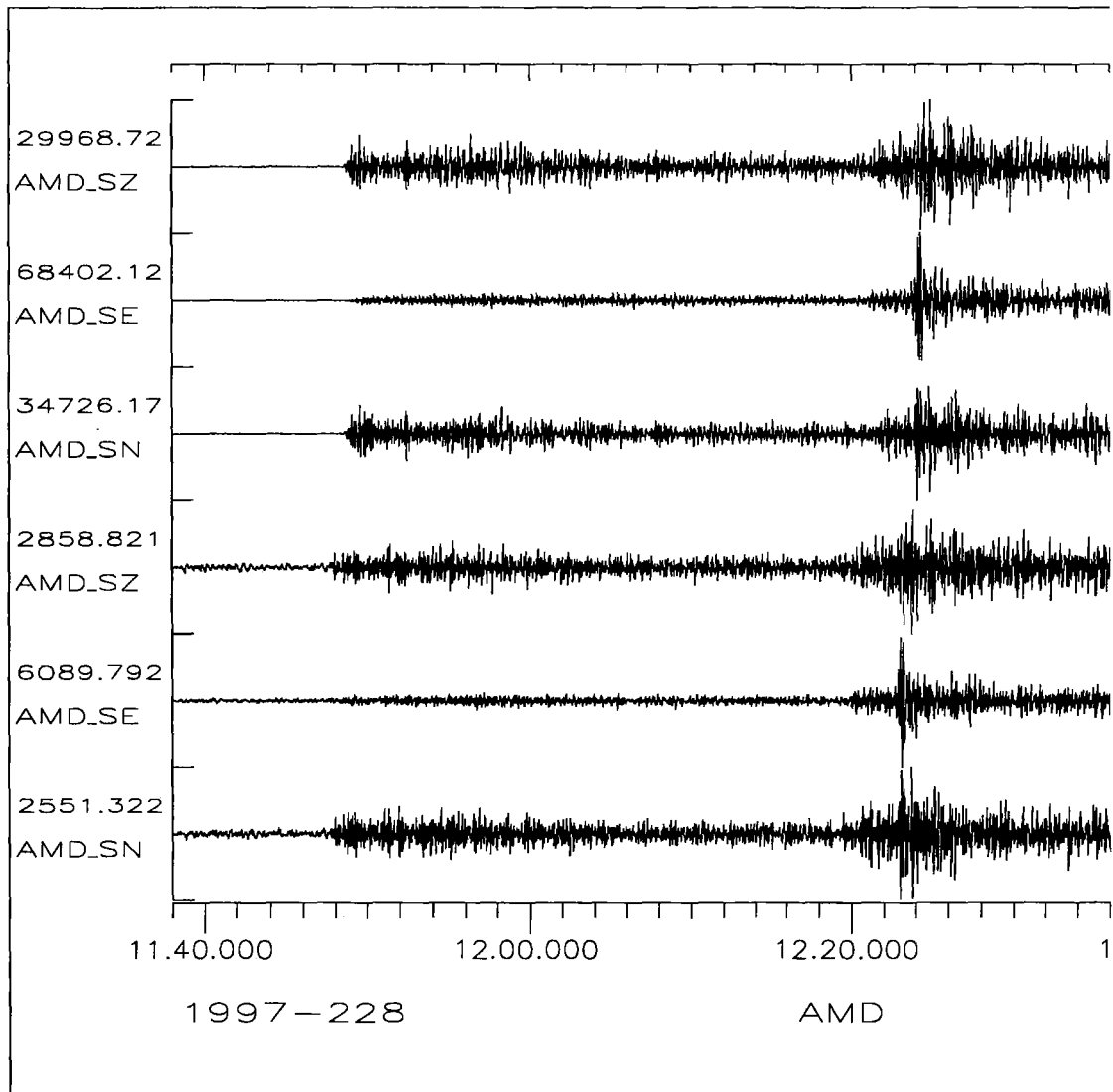


Fig. 7.4.4. Recordings by the Amderma 3-component center station of the two seismic events on 16 August 1997. The upper three traces are three-component data for the first event ($m_b=3.5$), and the lower three traces correspond to the second event ($m_b=2.5$). The traces are filtered in the 2-16 Hz band. The scaling factors in front of each trace is indicative of the event size. Note the similarity between the two event recordings.

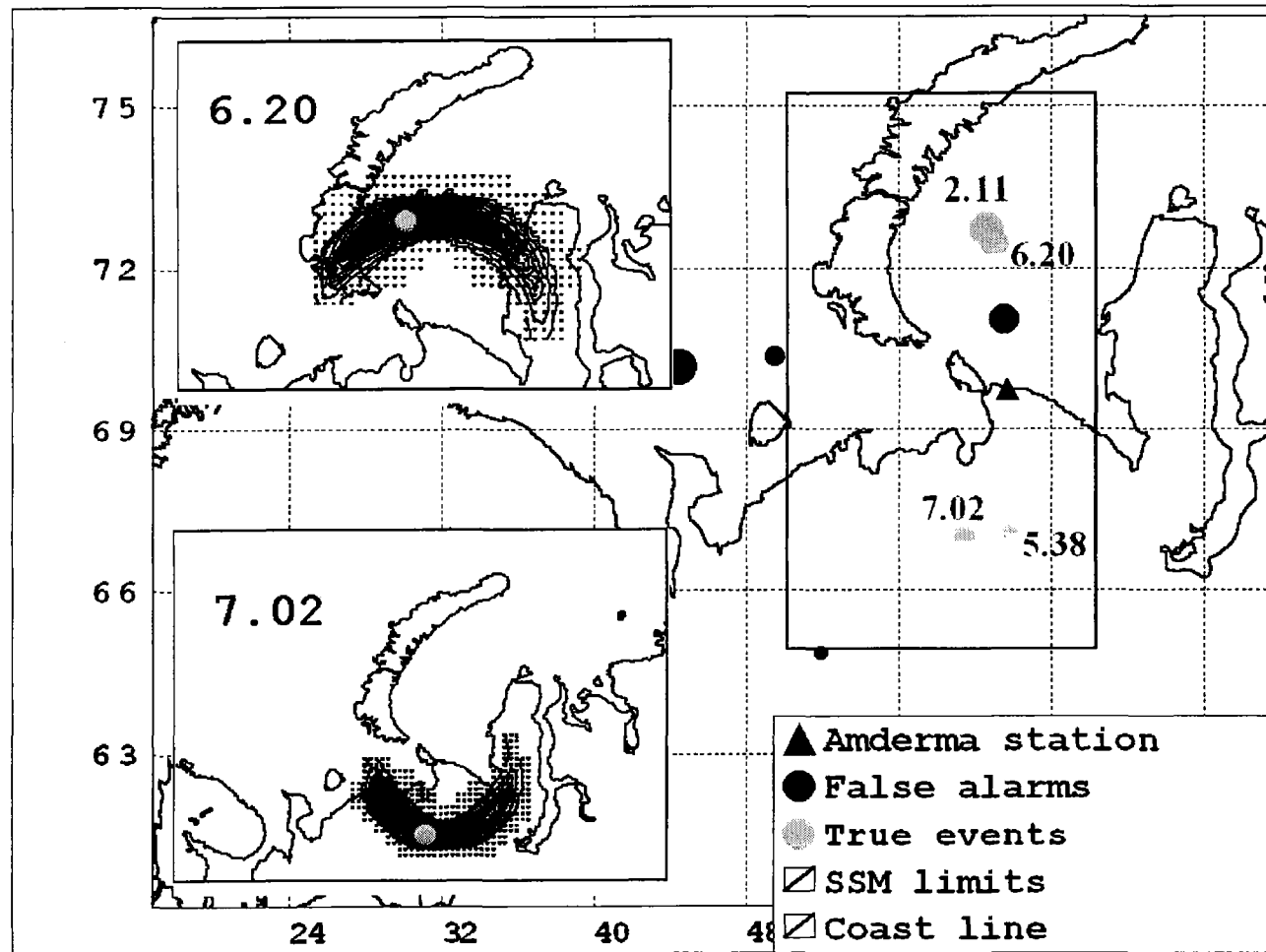


Fig. 7.4.5. Results of site-specific monitoring using the Amderma station for the day 16.08.1997. Examples of semi-automatic location (iso-lines of rating functions and their maxima corresponding to epicentres) are shown in the insertions.

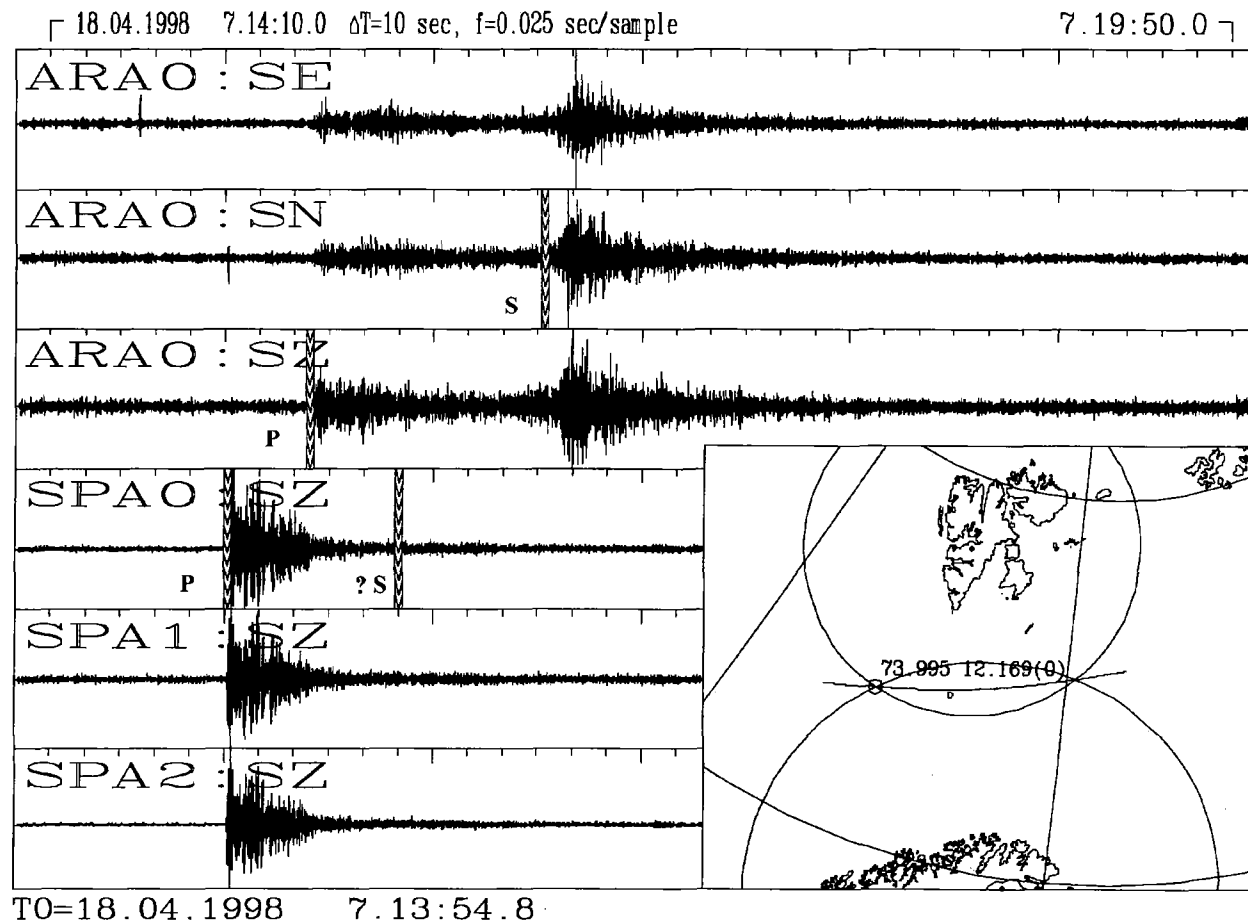


Fig. 7.4.6. Waveforms together with KRSC's location of the event near Bear Island on 18.04.1998. The symbols "? S" mark places of expected S-onsets. Note the large variation in P/S ratios for the stations shown.

Appendix

Site-specific monitoring (SSM) applied to the Amderma station

The Amderma station is situated far from other seismic stations in the KRSC network, so we need to locate weak events near this site using single-station data only. We have developed a variant of site-specific monitoring (SSM). It scans pairs of detected phases and for each pair assumes a hypothesis that the first phase is a P-wave and the second phase is an S-wave from an event occurring somewhere inside a given region. This hypothesis is validated by computing a rating function based on joint polarization analysis for P and S phases and several additional criteria such as frequency and amplitude compatibility. Those pairs for which the rating value is greater than a predefined threshold are considered as candidates for real seismic events.

1. Polarization analysis.

In this study we use the traditional mathematical coordinate system: X to the right (east), Y upward (north) and calculate angles from the X counterclockwise (to recalculate such angles into seismological backazimuths one have to substitute A by 450-A).

For each direction we calculate a function representing a projection of horizontal motion in this direction :

$$S(\alpha) = \sum_j |E_j \cos(\alpha) N_j \sin(\alpha)| \quad (13)$$

where E_j and N_j represent samples of East-West and North-South channels respectively.

To normalize this function we introduce:

$$R(\alpha) = [S(\alpha) - S(\alpha + 90^\circ)] / [S(\alpha) + S(\alpha + 90^\circ)] \quad (14)$$

This function assumes values within [-1,+1] and is maximized for P-waves when α equals the event's backazimuth (or the backazimuth +180), and for S-waves when α is perpendicular to the true backazimuth.

However, the function does not enable us to calculate the sign and real type of polarization (linear or circular). We introduce one more function which calculates the correlation between horizontal and vertical motion for a given angle:

$$CZ(\alpha) = \text{Corr}(E \cos(\alpha) + N \sin(\alpha), Z) \quad (15)$$

where E , N and Z represent samples of East, North and vertical channels respectively. If α is a true backazimuth, this function should be maximized for P-waves. On the other hand, $CZ(\alpha + 90^\circ)$ should be about zero for S-waves because S is polarized circularly.

Finally, we introduce backazimuth-dependent polarization criteria for P and S :

$$P_p(\alpha) = (1 + R(\alpha))(1 + CZ(\alpha))/4 \quad (16)$$

$$P_s(\alpha) = (1 + R(\alpha + 90^\circ))(1 - |CZ(\alpha + 90^\circ)|)/2 \quad (17)$$

Both of these functions range within $[0,1]$. $(1+R)$ instead of R is used to soften the criteria : the polarization is often not seen clearly and negative weights are more difficult to analyze.

2. Calculating detection lists for Amderma station.

An ordinary analysis using a set of bandpass filters and STA/LTA criterion is carried out for each Amderma recording. When STA/LTA exceeds a fairly low threshold (now 2) the phase is considered to be detected and the polarization weights P_p and P_s are calculated using the band where STA/LTA has its maximum value. Thus, for each detected phase the detection list contains the corresponding best frequency band, the maximum STA/LTA and associated P_p and P_s estimates.

3. Site-specific monitoring.

A region for SSM is specified by ranges of angles for Amderma backazimuths (α_1, α_2) and distances (R_1, R_2) between Amderma and possible epicenters of an event. From the distance range the SSM program calculates a range of corresponding time differences between P and S onsets :

$$\Delta t_1 = [T_s(R_1) - T_p(R_1)] \leq t_s - t_p \leq \Delta t_2 = [T_s(R_2) - T_p(R_2)] \quad (18)$$

Subsequently the program scans the pairs of phases for which the time difference is within the limits $(\Delta t_1, \Delta t_2)$ and for each such couple (denote the first phase "A" and the second one "B") assumes the hypothesis that A is a P-wave and B is an S-wave. Then the program has to assess the likelihood of this hypothesis.

It is intuitively clearly that the following features should be taken into account :

- values of STA/LTA for both the phases;
- joint polarization.

We assume that the pair of phases correspond to the same event so that an angle maximizing the product of P_p for A and P_s for B should be found. To take into account the

STA/LTA value we use some monotonously increasing, but bounded function $F(\text{STA}/\text{LTA})$. The choice for F is rather arbitrary and now the system uses:

$$F(x) = 1 - \exp(-x/(x_0)) \quad (19)$$

where x_0 is a constant (some typical STA/LTA for strong events).

We use a bounded function to obtain compatible ratings for events which are strong enough, although their STA/LTA values may differ considerably.

Finally, the rating function RV_{AB} is defined as:

$$RV_{AB} = F((\text{STA}/\text{LTA})_A)F((\text{STA}/\text{LTA})_B)\max\{P_{PA}(\alpha)P_{SB}(\alpha)(1 - |P_{PB}(\alpha)|)\} \quad (20)$$

$$\alpha \in (\alpha_1, \alpha_2)$$

The terms $(P_{PA}(\alpha))$ and $(P_{SB}(\alpha))$ are weights indicating the likelihood that A is a P-wave and that B is an S-wave. Note that the Amderma station often records significant long-duration industrial noise. Such noise often contains segments looking like event phases but with identical polarization for the two hypothesized phases.

On the other hand, the criteria $(P_{PA}(\alpha))$ and $(P_{SB}(\alpha))$ are not too strict, so that possible errors in the polarization calculations may be accepted. Thus the program could associate even identically polarized phases if their STA/LTA are large enough. That is the reason why the term $(1 - |P_{PB}(\alpha)|)$ was added. It is designed to suppress cases where the B phase is a continuation of A, i.e., has the same polarization.

When the rating function appears greater than some threshold the SSM program declares a possible event and determines its preliminary coordinates. The distance between the station and the event is determined by the time difference between the phases and the angle which maximizes the rating :

$$\alpha = \text{Argmax}\{P_{PA}(\alpha)P_{SB}(\alpha)(1 - |P_{PB}(\alpha)|)\} \quad (21)$$

$$\alpha \in (\alpha_1, \alpha_2)$$

Examples of the SSN in practical application are shown in the main body of this paper.

7.5 The Indian nuclear explosions of 11 and 13 May 1998

Introduction

This contribution describes observations made at our institution for the announced Indian nuclear explosions on 11 and 13 May this year. Some comparisons are also made with the PNE at the same site on 18 May 1974.

The nuclear explosion of 11 May 1998

The explosion (which were in fact announced as three separate explosions, but which apparently were conducted at the same time) took place near Pokhran on 11 May 1998, with origin time 10:13:44 GMT. Table 7.5.1 lists the basic parameters of the event as provided by various sources. The m_b magnitudes range from 5.0 to 5.3. The most accurate location is provided by the REB bulletin, which uses a world-wide network for location purposes. The solution by the NORSAR regional network after analyst processing and locating with HYPOSAT (Schweitzer, 1997) and using the IASP91 travel-time tables (Kennett and Engdahl, 1991), is also listed. The NORSAR array automatic solution is included in the table and the NORSAR automatic detection/event processor output is shown in Fig. 7.5.1.

Figs. 7.5.2 shows plots of the P-onset beams at each regional array. The trace plots of Fig. 7.5.2 are based on single channels for the seven arrays Apatity, ARCESS, FINESS, GERESS, Hagers, NORESS, and Spitsbergen and the beam parameters velocity and back-azimuth are the results from the automatic processing. Table 7.5.2 summarizes these parameters for the seven regional arrays. The ARCESS and Spitsbergen arrays show outstanding signal-to-noise ratios (SNR). The velocity/azimuth estimates are within the expected uncertainty for all arrays.

We were also able to retrieve data from the station Nilore (NIL), Pakistan for this event. NIL, which is providing data through a satellite link installed and operated by NORSAR, is the closest digital broad-band station to the Indian test site. Fig. 7.5.3 shows all three components of the original broad-band STS-2 seismograms and the same data filtered in two different frequency bands: once band-pass filtered between 3. and 8. Hz and once low-pass filtered at 1 Hz and afterwards band-pass filtered between 0.04 and 0.08 Hz. Note the different P-to-S amplitude ratios for the different frequency bands. The SNR is quite high on all traces, and it is clear that the station NIL is by far the best IMS station for monitoring the Indian test site. Fig. 7.5.4 show the vertical component after reconstructing the ground movement from the STS-2 trace. Note the complex Pn onset with a relative long period first onset. Whether this Pn phase shows details of the three subevents of the explosion cannot be decided as long as the upper mantle and crustal structure between the test site near Pokhran and the station in Nilore is unknown.

Estimating M_s for the nuclear explosion of 11 May 1998

The only station with a surface wave that could be confidently detected was Nilore (NIL): The broad-band channel NIL-sz was low-pass filtered at 1 Hz and then band-pass filtered between 0.04 and 0.1 Hz (see Fig. 7.5.3, trace NIL-Z2). A maximum amplitude of 523.97 nm with a period of 11.95 s was measured at 10:18:20.8. The observed surface wave magnitude in a distance of 6.6 degrees is $M_s = 3.31$.

No M_s values were possible to calculate from stations in Fennoscandia and Europe. We carried out an intensive study to calculate such values, but without success. In the following we list estimated upper limits for M_s values from observations at arrays of different apertures and at several single stations. The time window in which surface waves for this event can be expected in Northern and Central Europe is influenced by the direct phases and surface waves from an earthquake North of Svalbard which occurred about 12 minutes after the Indian explosions (REB source parameters: 11 May 1998, 10:26:08.4, 84.86 N, 8.72 E, m_b 3.6). If this event is not taken into account, M_s measurements for the Indian nuclear test can easily be overestimated.

German Regional Seismic Network (GRSN): the broad-band stations of the GRSN were analyzed as part of an huge array with an aperture of about 300 km. The vertical traces of the stations BFO, BRG, BSEG, BUG, CLZ, FUR, and MOX were used to calculate a theoretical beam (velocity 3.2 km/s; back-azimuth 94 degrees) after filtering (at first with a low-pass at 1 Hz and afterwards with a band-pass between 0.04 and 0.08 Hz) all data equally. An upper limit for M_s was estimated by measuring on the beam at 10:39:05.3 a maximum amplitude of 14.30 nm with a period of 12.96 s. For the reference station MOX (delta 50.8 degrees) we obtained $M_s \leq 3.18$.

Gräfenberg Array (GRF): This array has an aperture of about 100 x 40 km. The data were processed as for the GRSN stations and a theoretical beam (velocity 3.2 km/s, back-azimuth 93 degrees) was calculated for the reference station GRA1 (delta 51 degrees). The maximum amplitude was measured two times: at 10:35:22.5 (and at 10:40:53.0) with an amplitude of 11.52 (and of 16.15) nm and a period of 18.14 (and of 17.98) s. This gave an estimate for M_s of ≤ 2.94 (or 3.09).

NORSAR array: We can use the 7 broad-band channels of the NORSAR array to form a beam for an array with an aperture of about 50 km. As reference station NAO01 was used, with an epicentral distance of 52.6 degrees. The data were processed as explained above and a theoretical beam was calculated for a velocity of 3.2 km/s and a back-azimuth of 101.3 degrees. Whether this case we also measured the maximum amplitude two times: at 10:37:24.78 (and at 10:39:31.49) with an amplitude of 8.03 (and of 23.76) nm and a period of 13.31 (and of 21.50) s. This gave an estimate for M_s of ≤ 2.94 (or 3.20). The second measurement is clearly influenced by the surface waves of the Svalbard event.

For the following stations only one broad-band or long-period channel is available to measure long-period amplitudes and therefore no enhancement of the SNR due to beam forming could be applied:

Apatity array: The broad-band channel APZ9-bz was filtered as above and a maximum amplitude of 103.52 nm with a period of 20.83 s could be measured at 10:37:04.6. The M_s estimate for a distance of 46.8 degrees is: $M_s \leq 3.77$.

GERESS array: The broad-band channel GEC2-hz was filtered as above and a maximum amplitude of 16.68 nm with a period of 11.36 s could be measured at 10:38:57.5. The M_s estimate for a distance of 49.4 degrees is: $M_s \leq 3.28$.

ARCESS array: The long-period channel ARE0-lz was band pass filtered between 0.04 and 0.08 Hz. A maximum amplitude of 49.23 nm with a period of 19.97 s could be measured at 10:35:48.0. The M_s estimate for a distance of 50.3 degrees is: $M_s \leq 3.52$. The maximum amplitude is clearly influenced by the event North of Svalbard!

Hagfors array: The long-period channel FSC2-lz was band pass filtered between 0.04 and 0.08 Hz. A maximum amplitude of 21.22 nm with a period of 15.63 s could be measured at 10:40:31.7. The M_s estimate for a distance of 51.2 degrees is: $M_s \leq 3.27$.

The M_s 3.31 measured at the near-by station NIL is reasonably consistent with the upper limit measurements for this explosion at the European arrays and stations.

The nuclear explosion of 13 May 1998

This explosion (or two explosions, according to the Indian authorities), took place on 13 May 1998, with an announced origin time 06:51 GMT. No signals were detected by any of the IMS stations. We retrieved data from the NIL station for this event as well, and were not able to find any signal in a large time window around the expected onset time. The upper limit of detectability of this station is approximately $mb=2.5$, as seen by scaling the original signal with a SNR of 714 down towards the noise value. The upper limit for the M_s is, by the same algorithm, obtained by measuring the noise before the observed event. Using the same filters as above, the maximum noise amplitude is 55.29 nm for a period of 10.13 s (see the beginning of trace NIL-Z2 in Fig. 7.5.3). This would correspond with a noise $M_s = 2.41$.

Comparison with a previous event at the Indian test site

In the following we make a brief comparison between the first explosion dealt with above and the test conducted at the same test site on 18 May 1974.

The 11 May 1998 and the test conducted at the same test site on 18 May 1974 have very similar magnitudes and wave forms. This similarity is illustrated in Fig. 7.5.5, which shows the NORSAR P-wave recordings for both events. The data were band-pass filtered between 1. and 3. Hz and all traces were aligned visually and sorted by the NORSAR sites. The upper trace shows always data from the 11 May 1998 test and the lower trace the data from the 18 May 1974 explosion, respectively.

Because we can assume different source functions for the two events, the pulse-form similarity at each NORSAR site is an indication that these observed pulses are mostly formed by path effects rather than by the test devices. The main conclusion from this similarity is that the two tests took place at a very close distance.

The similarity of the recordings, taken 24 years apart, also demonstrate that the NORSAR instrumentation has remained stable, and confirms that even after the recent refurbishment of the seismometers and digitizers the recordings can be successfully used for comparisons with historical archives.

J. Schweitzer
F. Ringdal
J. Fyen

References

Kennett, B.L.N. & Engdahl, E.R., 1991. Travel times for global earthquake location and phase identification, *Geophys. J. Int.* 105, 429 - 466.

Schweitzer, J. 1997. HYPOSAT - a new routine to locate seismic events. In: NORSAR Semiannual Tech. Summ. 1 April - 30 September 1997, NORSAR Sci. Rep. 1-97/98, Kjeller, Norway, 94-102.

Reference	Origin time	Latitude	Longitude	m_b
REB	10:13:44.2	27.07	71.76	5.0
NORSAR array (automatic)	10:13:44.02	25.22	70.49	5.1
NORSAR- regional arrays	10:13:44.97	27.08	71.45	
PDE-Q	10:13:41.78	27.09	71.91	5.3

Table 7.5.1: Location estimates by various systems of the 11 May 1998 nuclear explosion. One of the estimates (NORSAR array solution) was made automatically. The solution NORSAR-regional arrays was calculated with P observations at Apatity, ARCESS, FINESS, GERESS, Hagfors, NORESS and SPITS and PcP observations at FINESS, GERESS and Hagfors (inverted were re-measured values of onset time, azimuth and slowness for all phases).

Array	Onset time	STA/ LTA	Velocity	Res	Azimuth	Res
Apatity	131:10.22.15.1	44.3	14.8	0.6	124.5	-6.3
ARCESS	131:10.22.41.0	193.6	15.3	0.7	123.8	1.0
FINESS	131:10.22.07.4	89.2	15.2	1.1	121.3	4.2
GERESS	131:10.22.34.8	40.3	15.5	0.2	97.2	3.2
Hagfors	131:10.22.47.3	48.9	19.7	4.9	124.6	21.3
NORESS	131:10.22.55.3	33.2	14.8	-2	107.5	5.7
NORSAR	131:10.22.57.4	47.1	15.2	0.2	104.3	3.0
SPITS	131:10.23.30.0	207.90	12.7	-2.9	112.0	-6.6

Table 7.5.2. Automatic detection list for the Indian nuclear explosion on 11 May 1998. The columns show array name, automatic EP-SigPro onset time, maximum signal-to-noise ratio (STA/LTA), apparent velocity (km/s), residual in km/s, back-azimuth in degrees, and back-azimuth residual. All residuals are relative to predictions using IASP91 tables and PDE-Q location.

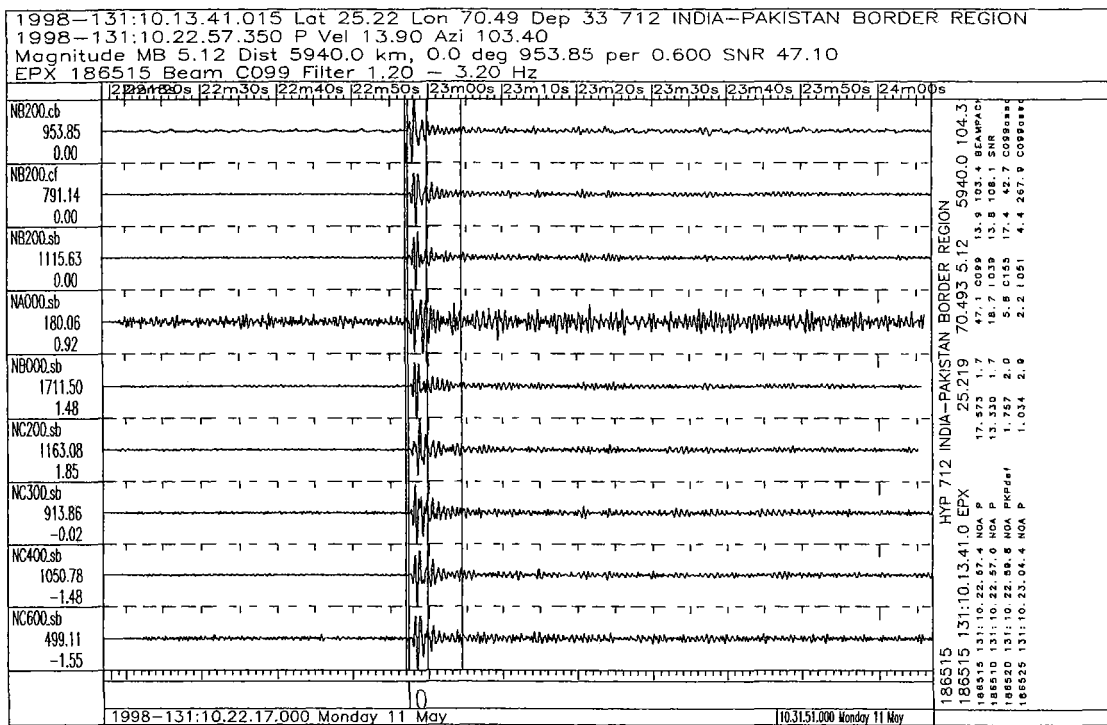


Fig. 7.5.1. Plot of the automatic NORSAR detection/event processor output for the Indian nuclear explosion on 11 May 1998.

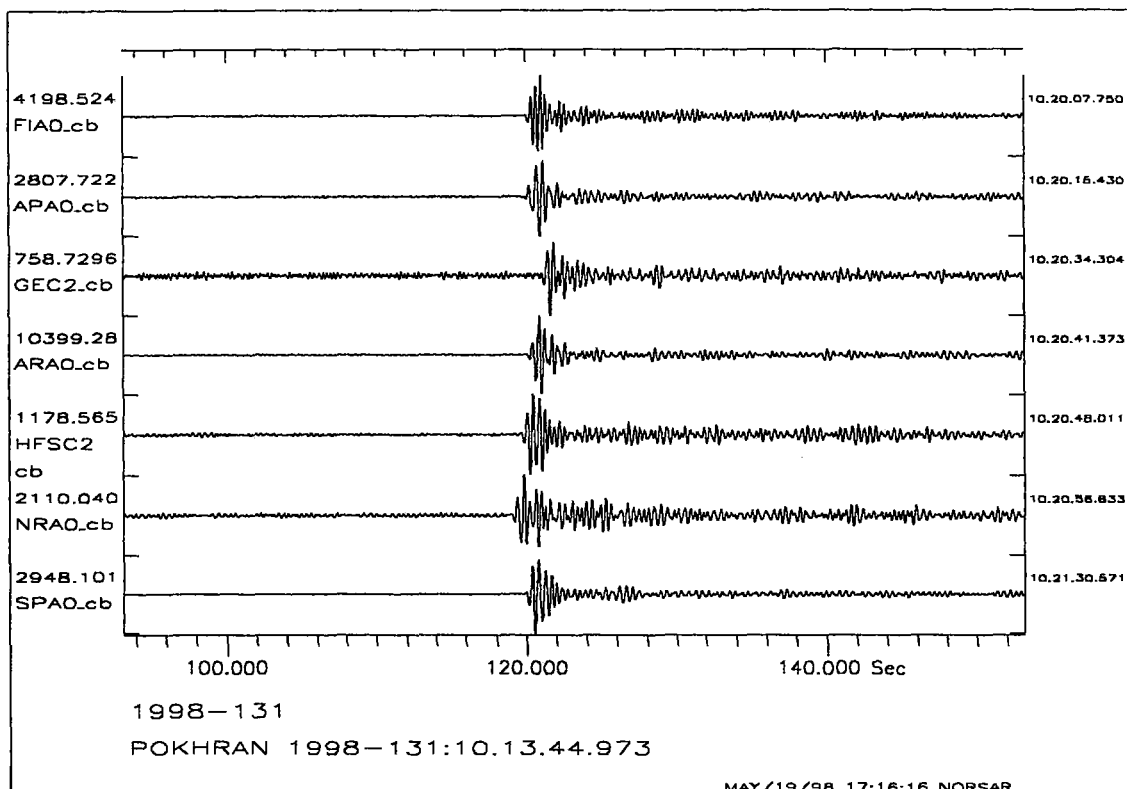


Fig. 7.5.2. Plot of the automatic beams at the regional arrays for the 11 May 1998 explosion at the Indian test site Pokhran. The traces are sorted by epicentral distance from top to bottom and shifted by the theoretical travel times from the IASP91 tables using the NORSAR regional array solution (see Table 7.5.2). Corrections for ellipticity of the Earth and station elevation were not taken in account for this plot but were accounted for the location program.

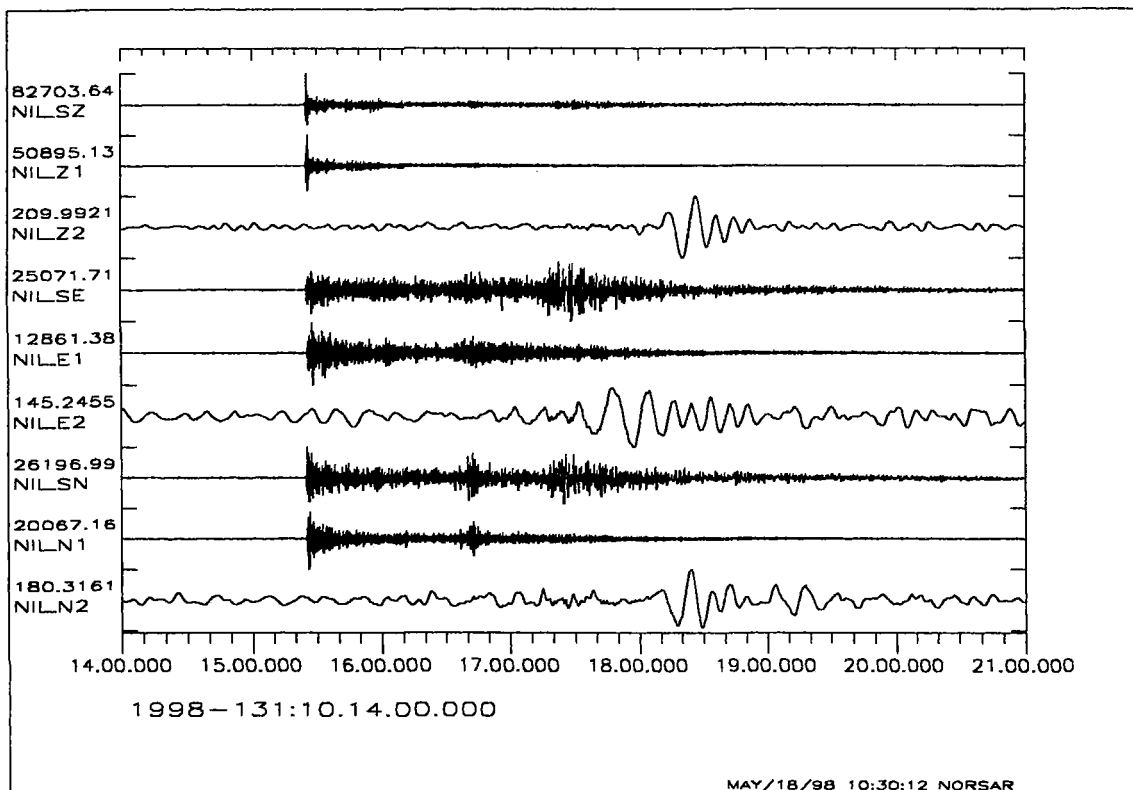


Fig. 7.5.3. The observations of the Indian nuclear explosion on 11 May 1998 at station NIL. Shown are the original broad-band data (traces SZ, SE, and SN), the 3 - 8 Hz band-pass filtered data (traces Z1, E1, and N1) and the 1 Hz low-pass and afterwards 0.04 - 0.1 Hz band-pass filtered data (traces Z2, E2, and N2). All seismograms were normalized by the given amplitudes (in counts).

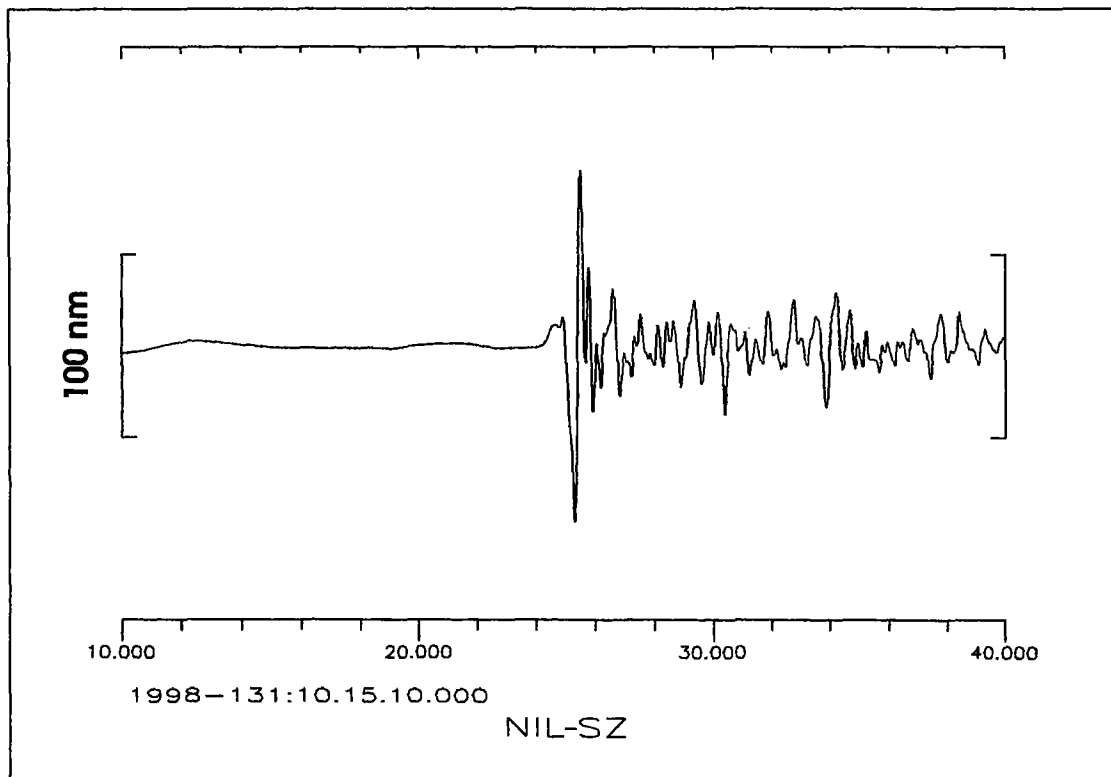


Fig. 7.5.4. Restitution of the ground movement from the STS-2 vertical component at NIL of the Indian nuclear test on 11 May 1998. The peak-to-peak amplitude of the Pn signal is 192.16 nm with a dominant period of 0.413 s. The length of the amplitude bar shown at the left scales corresponds to 100nm.

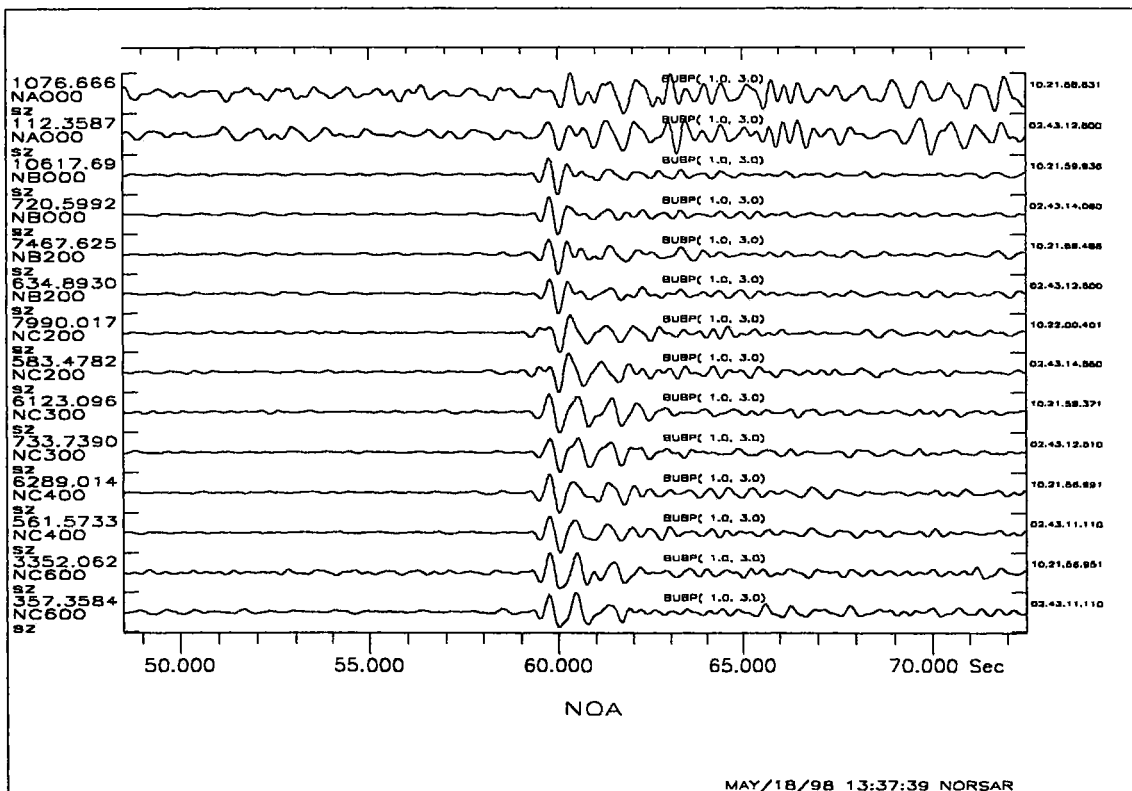


Fig. 7.5.5. Observations of the 18 May 1974 and of the 11 May 1998 explosions at the Indian nuclear test site. Shown are pairwise seismograms at single sites of NORSAR. The upper trace shows always the 11 May 1998 and the lower trace the 18 May 1974 explosion. All data were 1. - 3. Hz band-pass filtered, the traces were normalized with the given maximum amplitudes (in counts), and the traces were aligned visually to a common onset time.

7.6 Accurate location of seismic events in northern Norway using a local network, and implications for regional calibration of IMS stations

Introduction

A seismic network was installed in the Ranafjord area in June 1997 as part of the NEONOR (Neotectonics in Norway) project which is a multidisciplinary research project undertaken in cooperation with several other Norwegian institutions. The purpose of the network was to monitor seismic activity along the potential neotectonic Båsmoen fault. Of the total 260 seismic events located in the first nine months of operation, 180 are probable earthquakes located within the network. Data from the Norwegian national seismic station southeast of Mo i Rana was made available by the University of Bergen and used to improve event locations where possible. The magnitudes of the local events range from M_L 0.1 to 2.8, with depths mainly in the 4-12 km. range. Nine focal mechanism solutions have also been determined, seven of which are tightly clustered in the western part of the network. These solutions show a large, up to 90° , rotation of the direction of maximum horizontal compressive stress (σ_{Hmax}) with regard to the ridge-push dominated regional stress field. Eight of the events within the network were also located by the NORSAR GBF system, and these locations as well as NORSARs analyst reviewed locations have been compared to the local solutions.

Technical installation and data processing

Five of the six stations transmit data via radio links to a central station (the sixth is connected directly to the digitizer), where the data are digitized and sent over a permanent landline to NORSAR. The sampling frequency is 40 Hz, which unfortunately is somewhat low for studying source effects for events with the magnitudes encountered in the region. The station locations are shown in Fig. 7.6.1, along with the location of the Norwegian national station to the east of Mo i Rana, operated by the Institute of Solid Earth Physics, University of Bergen.

Event detection and processing is performed using NORSARs detection and event processing software. Event location, database management, seismic modelling etc. are performed using the Seisan software from the University of Bergen

Historic seismic activity

The offshore and onshore parts of Northern Norway have long been considered an area of elevated seismic activity with regard to the rest of the Baltic shield and margin areas, albeit not particularly high as compared to other passive continental margins globally (Byrkjeland et al., in prep.). The largest known onshore earthquake in Fennoscandia occurred in the Ranafjord area on August 31, 1819, with an estimated magnitude of M_S 5.8-6.2 (Muir Wood, 1989). Although an exact hypocenter location is unavailable, a large number of reports concerning rockfalls, standing waves and difficulties standing exist in the western and parts of the area (Fig. 7.6.2). A landslide was also triggered near Utskarpen by the Rana fjord.

Local seismic activity

Of the 260 events located by the network, 220 are located in the immediate vicinity of the network, 40 of these are explosions and probable explosions, leaving 180 probable earthquakes. Magnitudes range from M_L 0.1 to 2.8, with most events in the M_L 1.0 to 1.5 range. Hypocenter

depths are shallow, mainly from 4 to 12 km. This is consistent with other reports of onshore seismic activity in Northern Norway (e.g Bungum et al., 1979; Atakan et al., 1994). Fig. 7.6.3 shows the seismic activity plotted according to magnitude (explosions removed). Four groups of events are visible in the western part of the network, three of these groups have well defined activity periods and hypocenter depths. A time vs. magnitude plot for the local events is shown in Fig. 7.6.4. The largest events within the network occurred within the two westernmost groups, which are also located in the vicinity of many of the reported phenomena concerning the 1819 earthquake (Fig. 7.6.2). The easternmost (red) group has hypocenter depths predominantly around 4-6 km, while the other groups have depths mainly in the 10-12 km range.

Focal mechanism solutions and stress data

Nine earthquake focal mechanism solutions have been determined using data from the network (in combination with data from the University of Bergen where available), shown in Fig. 7.6.5 with corresponding σ_{Hmax} directions. One is a composite solution based on first motion polarities only, the rest are selected on a basis of available first motion polarities combined with full waveform modelling using Herrmann code (Havskov, 1997). A sample synthetic and real trace from the modelling is shown in Fig. 7.6.6.

While seven of the nine solutions are for earthquakes located within the network, there is also one solution around 50 km south of the network, and one offshore to the west. The solutions are mainly oblique-normal to strike-slip. The seven local solutions all show an approximately N-S trending direction of maximum horizontal compression, in contrast to the ridge-push dominated regional stress field which has a WNW-ESE σ_{Hmax} direction (Hicks et al., in prep.). This implicates a strong local stress influence on the seismic activity in the area.

Calibration of IMS stations

Eight of the earthquakes occurring within or close to the network from July 1997 to April 1998 were of sufficient size to also be detected by NORSARs automatic GBF system. The magnitudes for these events range from M_L 2.0 to 2.8 (Table 7.6.2). The detection threshold appears to be around M_L 2.0-2.1 for this area. Two events with magnitudes over 2.0 were not detected by the GBF system, an M_L 2.1 on 26.12.97 and an aftershock (M_L 2.0) of the M_L 2.8 event 09.02.98.

The eight GBF events are excellent candidates for a study on calibration with regard to local crustal effects, to verify the NORSAR GBF system as it operates at present, and in general with regard to the capabilities of the international monitoring system. The locations of the eight events are shown in Fig. 7.6.7, with the GBF grid points superimposed. The smallest event has a difference in location of approx. 175 km (based on only four phases), and the westernmost event has a discrepancy of around 75 km (7 phases). The GBF locations for the remaining six events are within 50 km of the local solutions (6 to 11 phases). This is an excellent result for a fully automatic system considering the magnitudes and distances to the stations involved (closest station is ARCESS at ~580 km), but shows that further improvements to the system should be possible.

The seven NORSAR analyst reviewed events are listed in Table 7.6.3 and plotted (along with the corresponding local solutions) in Fig. 7.6.8. The analyst reviewed locations are all within

~25 km of the local solutions, which again is excellent considering the distances involved. The NORSAR solutions do appear to have locations systematically to the east/southeast of the local solutions, which could be an indication of a local crustal anomaly, and should be studied more closely.

E. Hicks

References

- Atakan, K., C. D. Lindholm & J. Havskov (1994): Earthquake swarm in Steigen, Northern Norway: an unusual example of intraplate seismicity. *Terra Nova*, 6, 180-194.
- Bungum, H., B. K. Hokland, E. S. Husebye & F. Ringdal (1979): An exceptional intraplate earthquake sequence in Meløy, Northern Norway, *Nature*, 280, 32-35.
- Byrkjeland, U., H. Bungum & O. Eldholm (in prep): Seismotectonics of the Norwegian margin.
- Havskov, J. (ed.) (1997): *The seisan earthquake analysis software for the IBM PC and Sun Version 6.0*, Univ. of Bergen, Norway, 236 pp.
- Hicks, E., H. Bungum & C. D. Lindholm (in prep): Crustal stresses in Norway and Surrounding areas as derived from earthquake focal mechanism solutions and in-situ stress measurements.
- Muir Wood, R. (1989): The Scandinavian Earthquakes of 22 December 1759 and 31 August 1819, *Disasters*, 12, 223-236.

Date	Lat.	Lon.	Depth	Mag.	P-trn	P-plng	T-trn	T-plng
Comp.1	66.31	13.32	5 km	N/A	167	48	270	11
97.11.21	66.41	13.22	7 km	2.3	208	29	302	7
97.11.25	66.50	12.40	11 km	2.7	77	29	343	7
97.11.28	66.32	13.14	11 km	1.7	74	58	299	23
97.11.28	66.32	13.15	11 km	1.8	74	58	299	23
97.12.26	66.32	13.11	11 km	1.8	176	1	268	67
98.01.08	66.37	13.13	13 km	2.2	27	33	284	19
98.02.09	66.39	13.09	11 km	2.8	351	22	257	11
98.03.09	65.85	13.53	7 km	2.8	115	13	225	57

Table 7.6.1. Earthquake focal mechanism solutions determined using data from the network. The composite solution is determined using first motion polarities only, the remaining eight are determined through a combination of first motion polarities and full waveform modelling

Date	Time	NEONOR				GBF			
		Lat.	Lon.	Mag	Depth	Lat.	Lon.	Mag	Nph
97.11.21	18:00:09	66.41	13.22	2.3	6.3	66.65	12.85	2.2	10
97.11.25	22:24:17	66.50	12.40	2.7	11.0	66.35	14.35	2.4	7
98.01.08	08:04:46	66.37	13.13	2.2	12.8	66.65	12.85	2.0	8
98.01.11	20:01:18	66.37	13.11	2.2	12.3	66.65	12.85	2.1	7
98.02.04	14:31:40	66.38	13.09	2.3	10.6	66.35	14.35	2.2	6
98.02.09	12:59:05	66.39	13.09	2.8	10.7	66.35	14.35	2.7	11
98.02.28	16:53:26	66.70	13.32	2.0	11.6	66.65	17.37	1.6	4
98.03.09	14:19:57	65.85	13.53	2.8	6.6	65.75	14.30	2.9	11

Table 7.6.2. Events located by the local network and at the same time by the NORSAR GBF system. All GBF solutions use at least two stations. Nph refers to number of phases used in the solution.

		NEONOR				NORSAR (analyst reviewed)		
Date	Time	Lat.	Lon.	Mag	Depth	Lat.	Lon.	Depth
97.11.21	18:00:09	66.41	13.22	2.3	6.3	66.39	13.24	10.3
97.11.25	22:24:17	66.50	12.40	2.7	11.0	66.43	12.71	20.2
98.01.08	08:04:46	66.37	13.13	2.2	12.8	66.34	13.39	0
98.01.11	20:01:18	66.37	13.11	2.2	12.3	66.34	13.46	0
98.02.04	14:31:40	66.38	13.09	2.3	10.6	66.28	13.41	13.6
98.02.09	12:59:05	66.39	13.09	2.8	10.7	66.30	13.54	8.9
98.03.09	14:19:57	65.85	13.53	2.8	6.6	65.85	13.65	3.4

Table 7.6.3. Events located by the local network and at the same time reviewed and located by the NORSAR regional system. The events are the same as in Table 7.6.2, except for the smallest event (98.02.28) which was not reviewed.

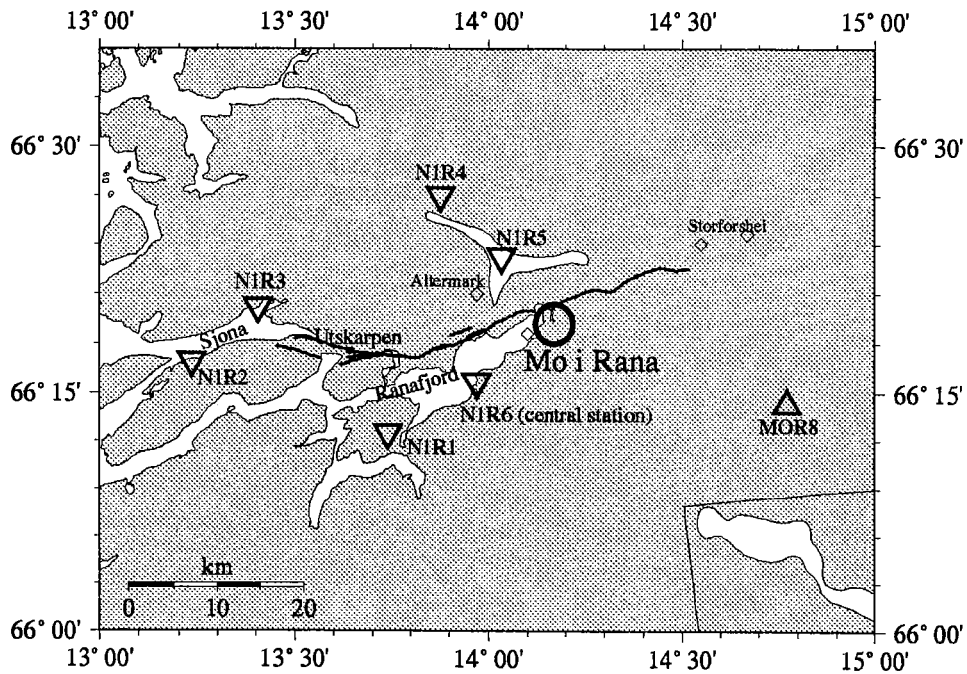


Fig. 7.6.1. The six NEONOR stations (inverted triangles) and the MOR8 station operated by the University of Bergen. The thick black line represents the Båsmoen fault. Diamonds represent mines.

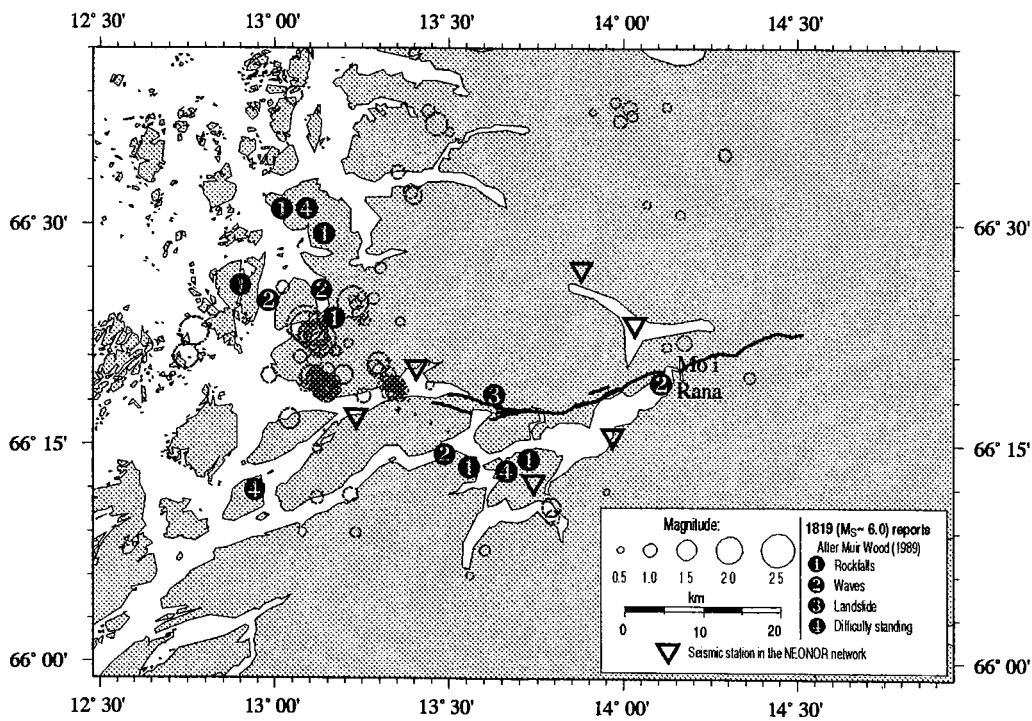


Fig. 7.6.2. Reported effects from the August 31, 1819 M_S 5.8-6.2 earthquake. Earthquakes located by the NEONOR network are plotted according to magnitude as grey circles.

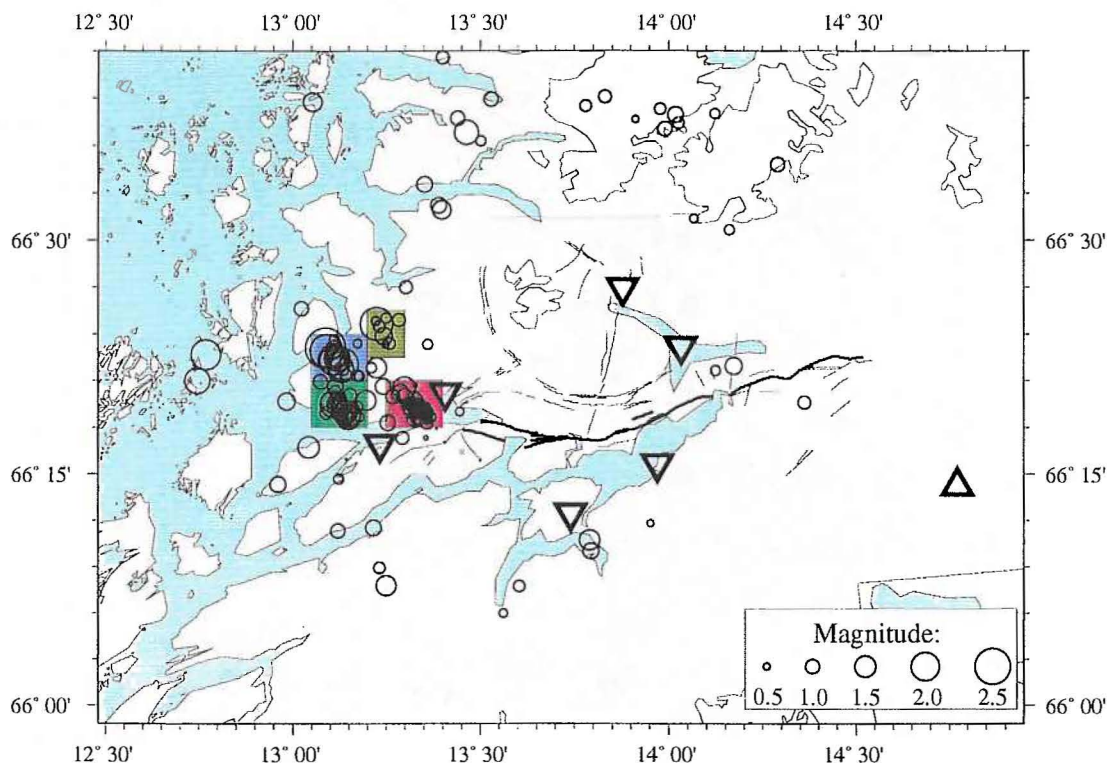


Fig. 7.6.3. Local earthquakes plotted according to magnitude (explosions and probable explosions removed). Events within the colored boxes correspond to the colored bars in Fig.7.6.4.

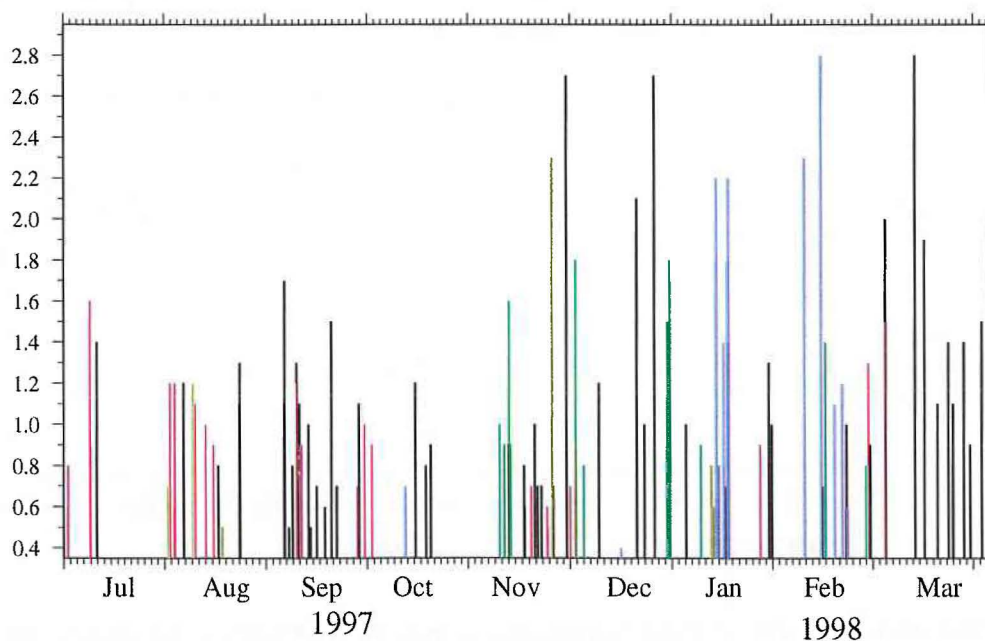


Fig. 7.6.4. Event magnitudes plotted vs. time. The colors indicate events within the colored boxes in Fig. 7.6.3.

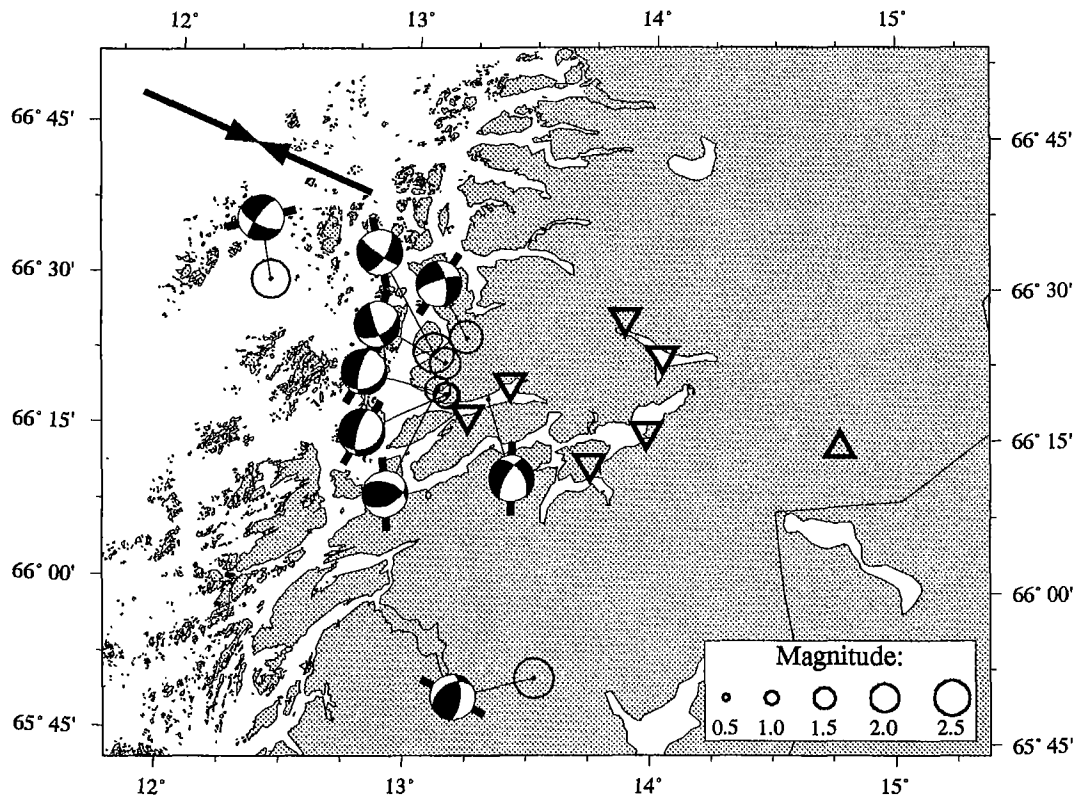


Fig. 7.6.5. Earthquake focal mechanism solutions determined using data from the network. The bars indicate the σ_{Hmax} stress direction for each solution. The large arrows represent the approximate direction of the regional ridge push dominated stress field.

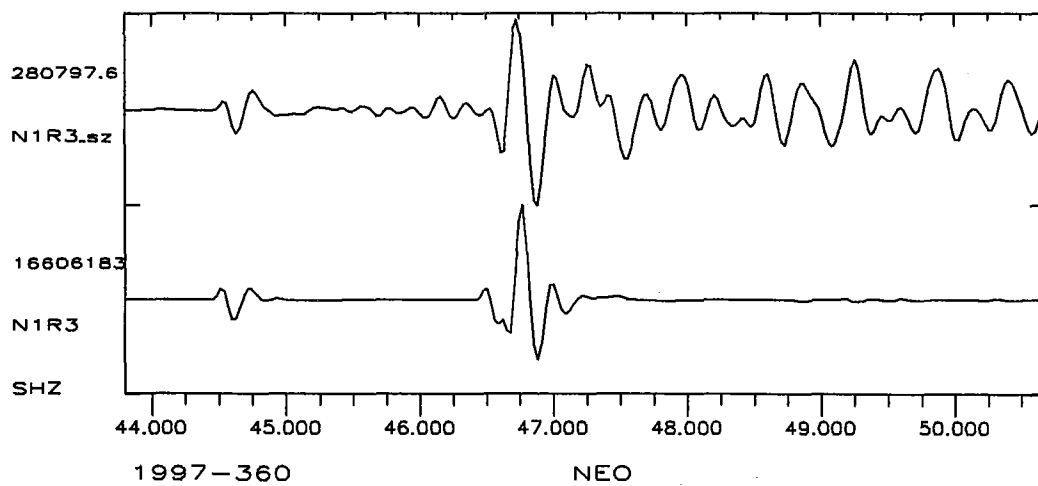


Fig. 7.6.6. Real (top) and synthetic (bottom) traces from the NIR3 station for the selected focal mechanism solution for the 26 December 1997 M_L 1.8 earthquake.

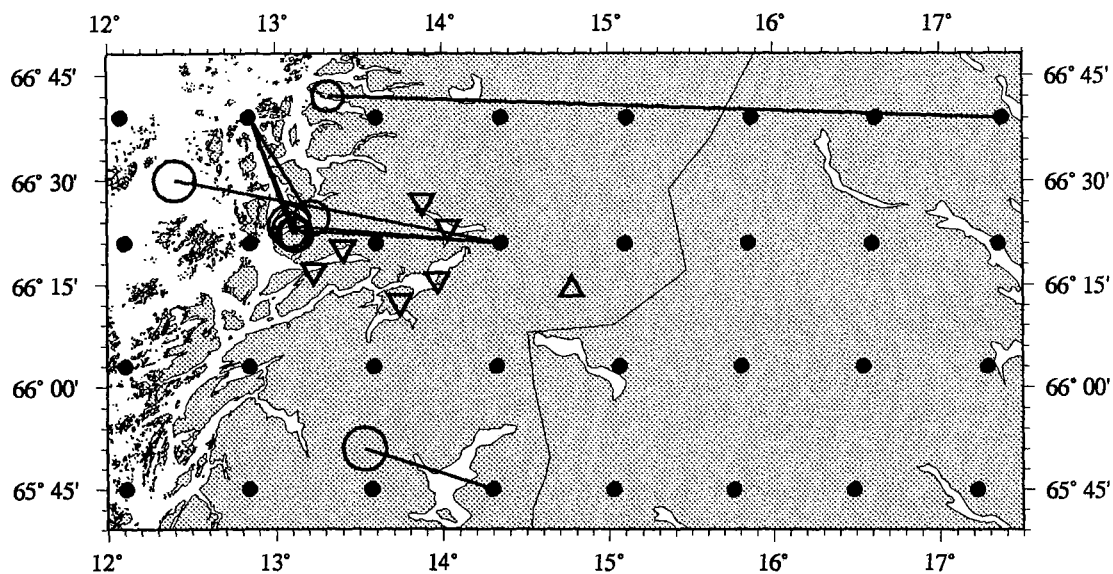


Fig. 7.6.7. Locations of the 8 common detected events (circles). The GBF grid points are represented by dots, the grid interval is 33 km. Lines join the GBF locations to the corresponding local event locations.

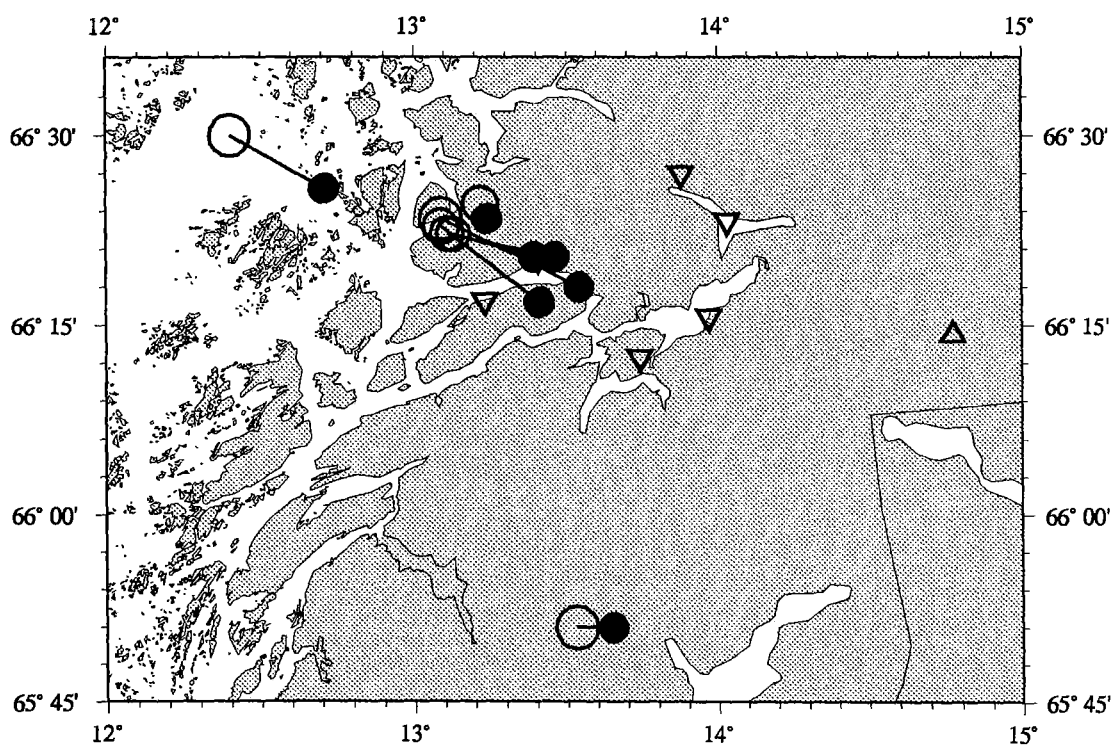


Fig. 7.6.8. Locations of the 7 reviewed events (filled circles) and the corresponding local solutions (open circles).

7.7 Status Report: Norway's participation in GSETT-3

Introduction

This contribution is a report for the period October 1997 - March 1998 on activities associated with Norway's participation in the GSETT-3 experiment, which is now being coordinated by PrepCom's Working Group B. This report represents an update of contributions that can be found in the previous four editions of NORSAR's Semiannual Technical Summary.

Norwegian GSETT-3 stations and communications arrangements

During the reporting interval 1 October 1997 - 31 March 1998, Norway has provided data to the GSETT-3 experiment from the four seismic stations shown in Fig. 7.7.1. The NORSAR array (station code NOA) is a 60 km aperture teleseismic array, comprised of 7 subarrays, each containing six vertical short period sensors and a three-component broadband instrument. ARCES and NORES are 25-element regional arrays with identical geometries and an aperture of 3 km, whereas the Sptisbergen array (station code SPITS) has 9 elements within a 1-km aperture. ARCES, NORES, and SPITS all have a broadband three-component seismometer at the array center.

Data from these four stations are transmitted continuously and in real time to NOR_NDC. The NOA and NORES data are transmitted using dedicated land lines, whereas data from the other two arrays are transmitted via satellite links of capacity 64 Kbits/s and 19.2 Kbits/s for the ARCES and SPITS arrays, respectively. From the NOR_NDC, relevant data (see below) are forwarded to the prototype IDC (PIDC) in Arlington, Virginia, USA, via a dedicated fiber optical 256 Kbits/s link between the two centers.

The NORES array has been used in GSETT-3 as a temporary substitute for the NOA teleseismic array, awaiting the completion of a technical refurbishment of the latter. This effort has been completed, and data from the NOA array have been transmitted since 30 August 1996 to the PIDC for Testbed processing. The purpose of the PIDC Testbed is to facilitate integration testing and therefore minimize disruption to the operational system. Results of NOA Testbed processing are given in Fyen and Paulsen (1997). Following approval by the PIDC Configuration Control Board in December 1997, processing of the NOA data was moved to the PIDC operational pipeline, and the NOA data are now fully used in the PIDC bulletin production. This changeover from NORES to NOA in the PIDC operational processing was effective on 7 January 1998.

The NOA and ARCES arrays are primary stations in the GSETT-3 network, which implies that data from these stations are transmitted continuously to the PIDC with a delay not exceeding 5 minutes. The SPITS array is an auxiliary station in GSETT-3, and the SPITS data are available to the PIDC on a request basis via use of the AutoDRM protocol (Kradolfer, 1993; Kradolfer, 1996). The Norwegian stations are thus participating in GSETT-3 with the same status (primary/auxiliary seismic stations) they have in the International Monitoring System (IMS) defined in the protocol to the Comprehensive Nuclear Test-Ban Treaty.

Uptimes and data availability

Figs. 7.7.2 - 7.7.4 show the monthly uptimes for the Norwegian GSETT-3 primary stations ARCESS (period 1 October 1997 - 31 March 1998), NORESS (1 October 1997 - 6 January 1998), and NOA (7 January - 31 March 1998), respectively, given as the hatched (taller) bars in these figures. These barplots reflect the percentage of the waveform data that are available in the NOR_NDC tape archives for each of these three stations. The downtimes inferred from these figures thus represent the cumulative effect of field equipment outages, station site to NOR_NDC communication outages and NOR_NDC data acquisition outages.

Figs. 7.7.2-7.7.4 also give the data availability for these three stations as reported by the PIDC in the PIDC Station Status reports. The main reason for the discrepancies between the NOR_NDC and PIDC data availabilities as observed from these figures is the difference in the ways the two data centers report data availability for arrays: Whereas NOR_NDC reports an array station to be up and available if at least one channel produces useful data, the PIDC uses weights where the reported availability (capability) is based on the number of actually operating channels. As can be seen from these figures, these differences in the reporting practice in particular affect the results for the NORESS and NOA arrays.

Experience with the AutoDRM protocol

NOR_NDC's AutoDRM has been operational since November 1995 (Mykkeltveit & Baadshaug, 1996).

The PIDC started actively and routinely using NOR_NDC's AutoDRM service after SPITS changed its station status from primary to auxiliary on 1 October 1996. For the month of October 1996, the NOR_NDC AutoDRM responded to 12338 requests for SPITS waveforms from two different accounts at the PIDC: 9555 response messages were sent to the "pipeline" account and 2783 to "testbed". Following this initial burst of activity, the number of "pipeline" requests stabilized at a level between 5000 and 7000 per month. Requests from the "testbed" account show large variations.

The monthly number of requests for SPITS data for the period October 1997- March 1998 is shown in Fig. 7.7.5.

NDC automatic processing and data analysis

These tasks have proceeded in accordance with the descriptions given in Mykkeltveit and Baadshaug (1996). For the period October 1997 - March 1998, NOR_NDC derived information on 991 supplementary events in northern Europe and submitted this information to the Finnish NDC as the NOR_NDC contribution to the joint Nordic Supplementary (Gamma) Bulletin, which in turn is forwarded to the PIDC. These events are plotted in Fig. 7.7.6.

Data forwarding for GSETT-3 stations in other countries

NOR_NDC continues to forward data to the PIDC from GSETT-3 primary stations in several countries. These currently include FINESS (Finland), GERESS (Germany) and Sonseca (Spain). In addition, communications for the GSETT-3 auxiliary station at Nilore, Pakistan, are

provided through a VSAT satellite link between NOR_NDC and Pakistan's NDC in Nilore. The PIDC obtains data from the Hagfors array (HFS) in Sweden through requests to the AutoDRM server at NOR_NDC (in the same way requests for Spitsbergen array data are handled, see above). Fig. 7.7.7 shows the monthly number of requests for HFS data from the two PIDC accounts "pipeline" and "testbed".

Future plans

NOR_NDC will continue the efforts towards improvements and hardening of all critical data acquisition and data forwarding hardware and software components, so as to meet future requirements related to operation of IMS stations to the maximum extent possible.

The PrepCom has tasked its Working Group B with overseeing, coordinating and evaluating the GSETT-3 experiment until the end of 1998. The PrepCom has also encouraged states that operate IMS-designated stations to continue to do so on a voluntary basis and in the framework of the GSETT-experiment until such time that the stations have been certified for formal inclusion in IMS. In line with this, and provided that adequate funding is obtained, we envisage continuing the provision of data from Norwegian IMS-designated stations without interruption to the PIDC, and later on, following certification, to the IDC in Vienna, via the new global communications infrastructure currently being elaborated by the PrepCom.

U. Baadshaug
S. Mykkeltveit
J. Fyen

References

- Fyen, J. & B. Paulsen (1997): NORSAR large array processing at the IDC Testbed. *Semiann. Tech. Summ.*, 1 April - 30 September 1997, NORSAR Sci. Rep. No. 1-97/98, Kjeller, Norway
- Kradolfer, U. (1993): Automating the exchange of earthquake information. *EOS, Trans., AGU*, 74, 442.
- Kradolfer, U. (1996): AutoDRM — The first five years, *Seism. Res. Lett.*, 67, 4, 30-33.
- Mykkeltveit, S. & U. Baadshaug (1996): Norway's NDC: Experience from the first eighteen months of the full-scale phase of GSETT-3. *Semiann. Tech. Summ.*, 1 October 1995 - 31 March 1996, NORSAR Sci. Rep. No. 2-95/96, Kjeller, Norway.

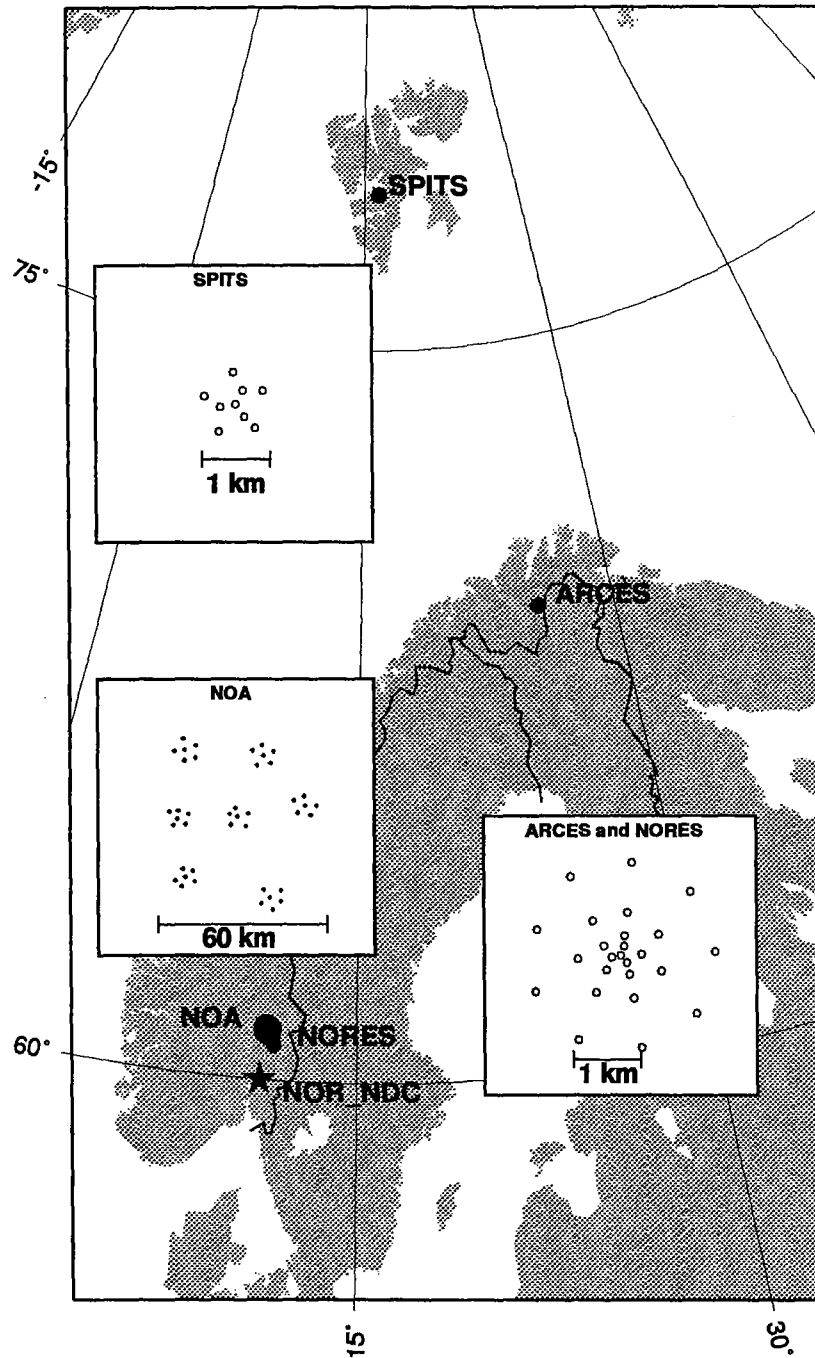


Fig. 7.7.1. The figure shows the locations and configurations of the four Norwegian seismic array stations that have provided data to the GSETT-3 experiment during the period 1 October 1997 - 31 March 1998. The data from these stations are transmitted continuously and in real time to the Norwegian NDC (NOR_NDC). The stations NOA, NORES and ARCES have participated in GSETT-3 as primary stations, whereas SPITS has contributed as an auxiliary station. On 7 January 1998, NOA replaced NORES in the PIDC processing pipeline.

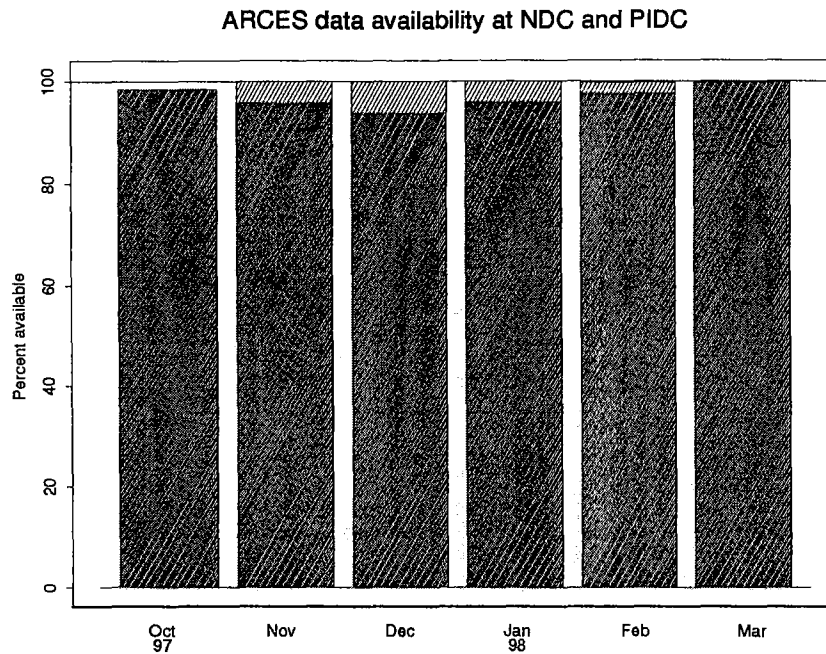


Fig. 7.7.2. The figure shows the monthly availability of ARCESS array data for the period October 1997 - March 1998 at NOR_NDC and the PIDC. See the text for explanation of differences in definition of the term "data availability" between the two centers. The higher values (hatched bars) represent the NOR_NDC data availability.

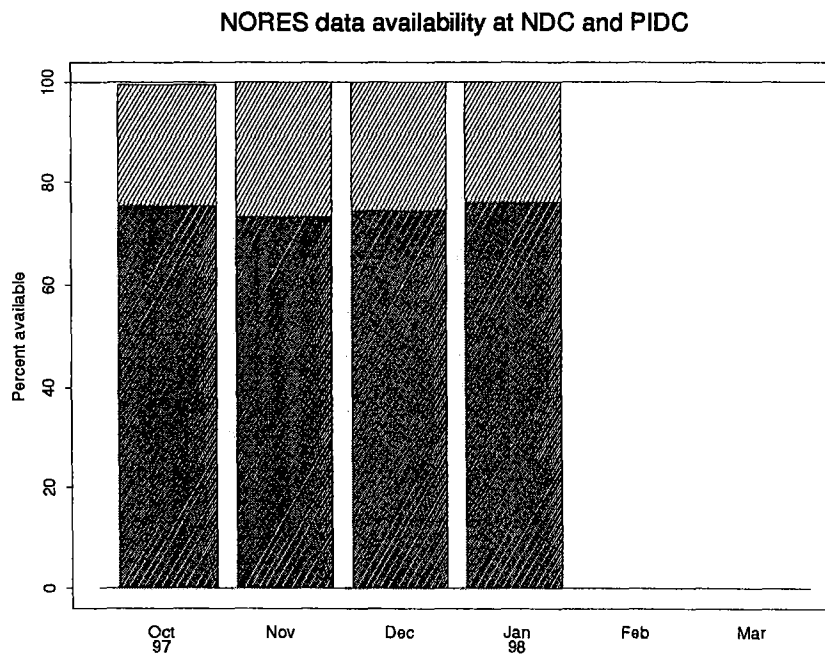


Fig. 7.7.3. The figure shows the monthly availability of NORESS array data for the period 1 October 1997 - 6 January 1998 (when NOA replaced NORES in the PIDC processing pipeline) at NOR_NDC and the PIDC. See the text for explanation of differences in the definition of the term "data availability" between the two centers. The higher values (hatched bars) represent the NOR_NDC data availability.

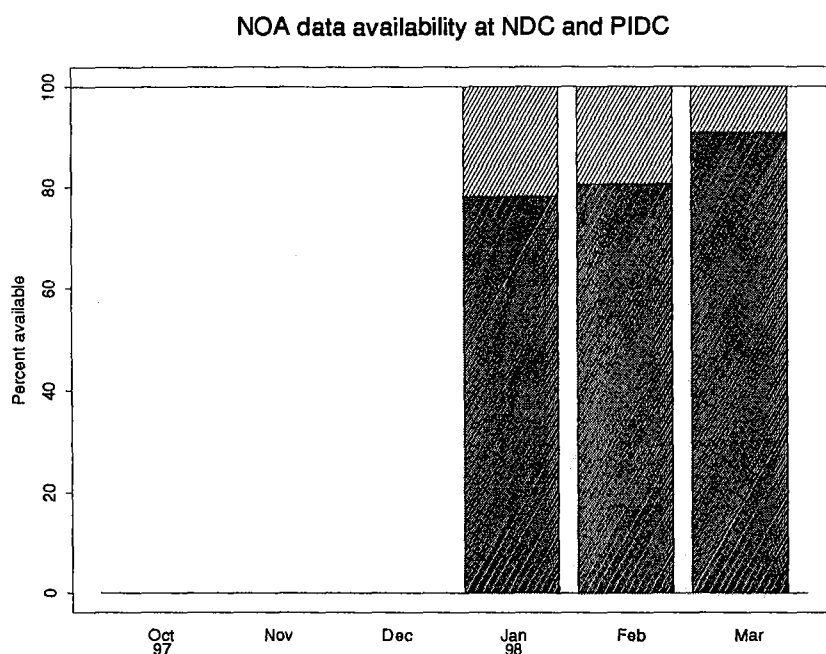


Fig. 7.7.4. The figure shows the monthly availability of NORSAR array data for the period 7 January - 31 March 1998 at NOR_NDC and the PIDC. See the text for explanation of differences in definition of the term "data availability" between the two centers. The higher values (hatched bars) represent the NOR_NDC data availability.

AutoDRM SPITS requests received by NOR_NDC from pipeline and testbed

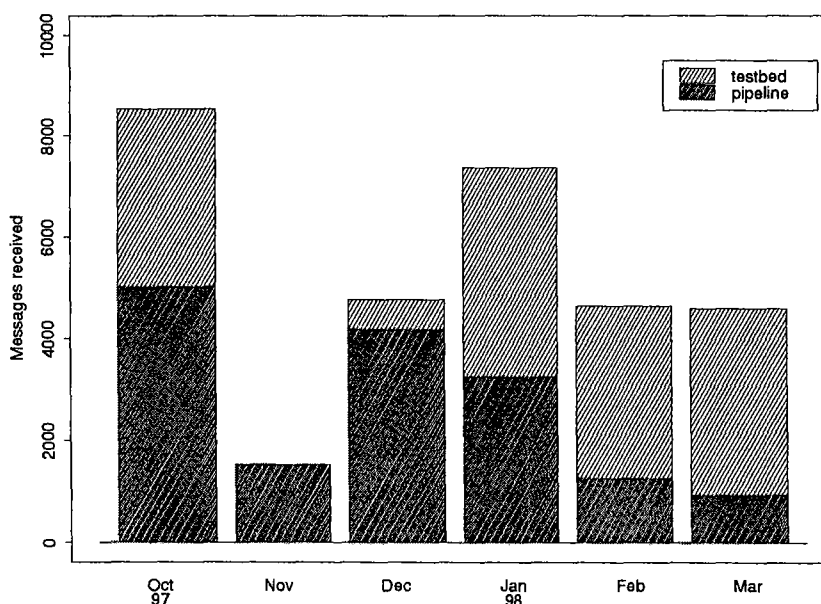


Fig. 7.7.5. The figure shows the monthly number of requests received by NOR_NDC from the PIDC for SPITS waveform segments. The numbers for the period 7 November - 25 November 1997 were lost when a logfile-disk filled up.

Reviewed Supplementary events

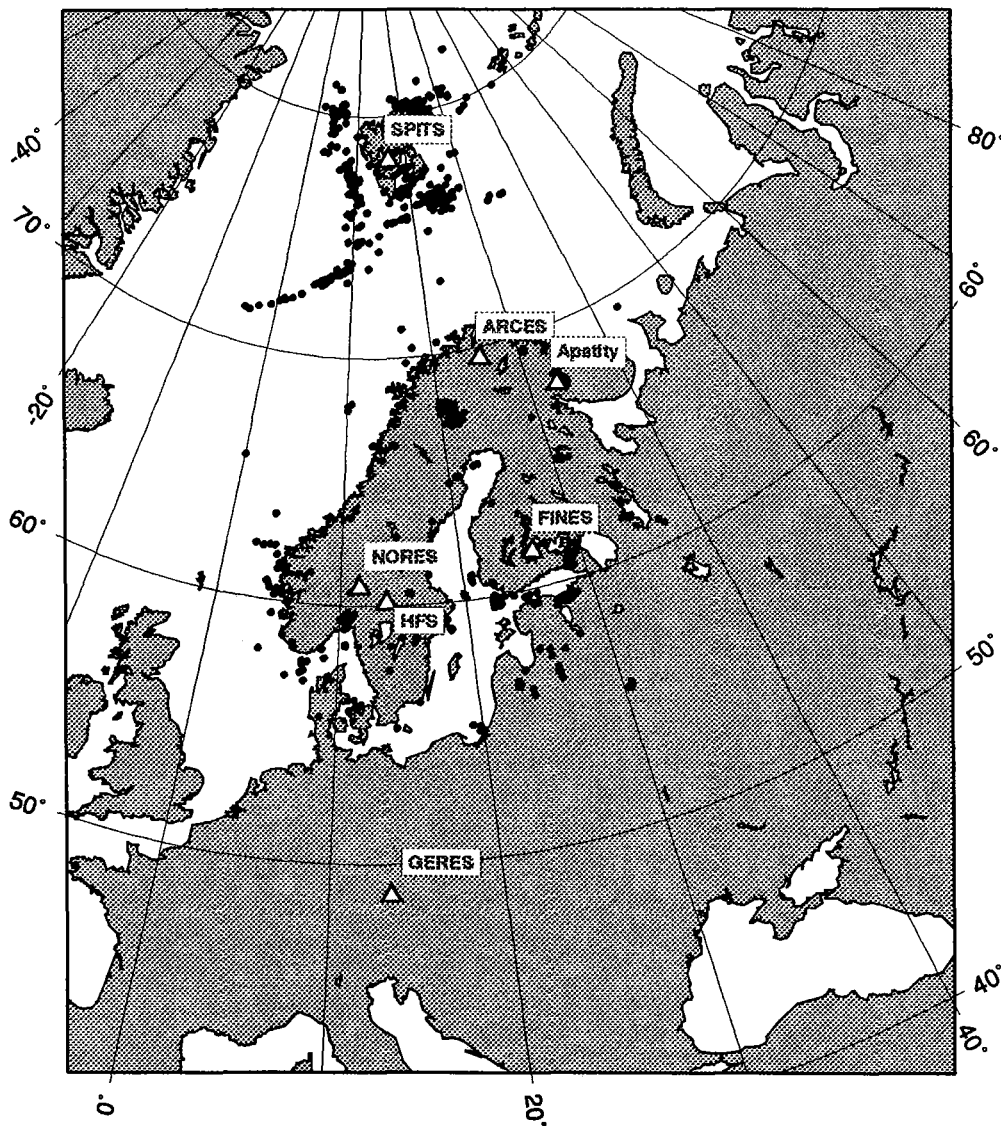


Fig. 7.7.6. The map shows the 991 events in and around Norway contributed by NOR_NDC during October 1997 - March 1998 as Supplementary (Gamma) data to the PIDC, as part of the Nordic Supplementary data compiled by the Finnish NDC. The map also shows the seismic stations used in the data analysis to define these events.

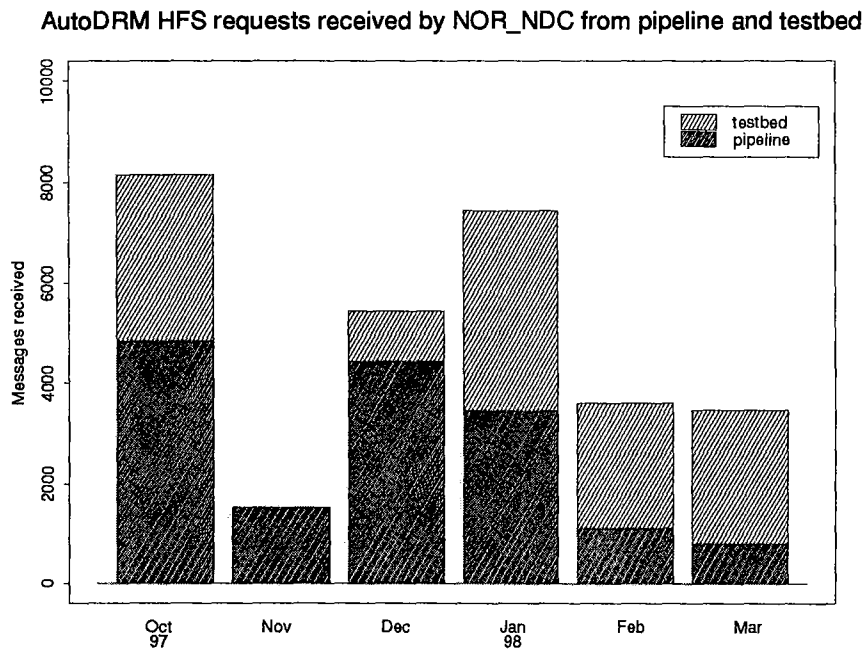


Fig. 7.7.7. The figure shows the monthly number of requests received by NOR_NDC from the PIDC for HFS waveform segments. The numbers for the period 7 November - 25 November 1997 were lost when a logfile-disk filled up.

